



## Piezotronics and Tribotronics of 2D Materials

Yifei Wang<sup>a,b</sup>, Qijun Sun<sup>a,b,c,\*</sup>, Zhong Lin Wang<sup>a,d,\*</sup>

<sup>a</sup> Beijing Institute of Nanoenergy and Nanosystems, Chinese Academy of Sciences, Beijing 101400, PR China

<sup>b</sup> School of Nanoscience and Engineering, University of Chinese Academy of Sciences, Beijing 100049, PR China

<sup>c</sup> Center on Nanoenergy Research, School of Physical Science & Technology, Guangxi University, Nanning 530004, PR China

<sup>d</sup> Georgia Institute of Technology, Atlanta, GA 30332, USA

### ARTICLE INFO

#### Keywords:

Two-dimensional materials  
Piezotronics  
Tribotronics  
Nanogenerator  
Field-effect transistors  
Moore's Law

### ABSTRACT

Two-dimensional (2D) materials, featuring superior electronic/thermal/mechanical properties, offer a paradigm shift in material science for boosting the rapid development of various sophisticated electronics. Combining with 2D materials, emerging piezotronics and tribotronics can further utilize external mechanical stimuli to modulate their transport properties in an active and direct fashion, delivering more diverse and versatile possibilities in the post-Moore era. Starting with the origin and development of piezotronics and tribotronics with 2D materials, this review provides a comprehensive investigation of their working mechanism, piezotronics in 2D materials, and research progress on piezoelectric nanogenerator (PENG)/triboelectric nanogenerator (TENG) modulated 2D field-effect transistors (FETs) and their broad applications. First, this review focuses on non-centrosymmetric piezoelectric materials and interface engineering to endow 2D materials with piezoelectric properties, and discusses diverse structural designs and applications in environmental/mechanical sensing. Second, the applications of PENG/TENG modulated 2D FETs are discussed regarding mechanical sensing, band structure engineering, artificial synapses, and so on. Finally, the advantages of piezotronics and tribotronics of 2D materials from material to device level are summarized in terms of structural design and functionality. Challenges related to the preparation and processing, reliability and stability of the devices are also pointed out. Synergistic integration of 2D materials with piezo/tribotronics is expected to be a significant complement to current information technology to go beyond Moore's Law, presenting great promise in self-powered smart devices/systems, adaptive human-robot interaction, edge-intelligent artificial prosthesis, etc.

### 1. Introduction - more Moore and beyond the Moore's Law

Moore's Law, which indicates transistors' number on integrated circuits will approximately double every two years, has been a guiding principle for the semiconductor industry since its inception by Gordon Moore in the 1960s.[1,2] This exponential growth is primarily facilitated by the reduction in transistor size, which enhances performance and reduces costs. However, as transistors approach nanoscale dimensions, traditional scaling methods encounter significant physical and technological challenges. Specifically, the escalation in quantum tunneling effects and short-channel effects significantly compromises the performance and reliability of devices.[3–5] To perpetuate Moore's Law and address the issues with the reduction in transistor size, the semiconductor industry has introduced innovative technologies since the 1990s. For instance, high-*k* gate dielectrics have been employed to replace traditional silicon dioxide gate layers. These novel materials

effectively reduce gate leakage currents by increasing the dielectric constant while maintaining a thin oxide layer thickness, thereby enhancing transistor performance. Furthermore, strained silicon technology enhances carrier mobility by modulating the stress state within the silicon lattice, thus improving the switching speed and overall performance of transistors.[4,6] As the 21st century commenced, planar transistor dimensions reached their physical limits, prompting a surge in popularity of three-dimensional transistor architectures such as Fin Field-Effect Transistor (FinFET) and gate-all-around FET.[7–10] These technologies, distinguished by their unique three-dimensional structural designs, effectively manage the short-channel effects, enabling transistors to maintain optimal electrical performance at reduced sizes. They also offer superior gate control capabilities and reduce leakage currents. Technological advancements, including extreme ultraviolet lithography, have surmounted the limitations of traditional lithography techniques, becoming instrumental in further miniaturization of nodes. To enhance

\* Corresponding authors at: Beijing Institute of Nanoenergy and Nanosystems, Chinese Academy of Sciences, Beijing 101400, PR China.

E-mail addresses: [sunqijun@binn.cas.cn](mailto:sunqijun@binn.cas.cn) (Q. Sun), [zhong.wang@mse.gatech.edu](mailto:zhong.wang@mse.gatech.edu) (Z.L. Wang).

<https://doi.org/10.1016/j.mser.2025.100951>

Received 12 September 2024; Received in revised form 9 January 2025; Accepted 12 February 2025

Available online 19 February 2025

0927-796X/© 2025 Elsevier B.V. All rights are reserved, including those for text and data mining, AI training, and similar technologies.

the functional density and overall performance of chips, the semiconductor industry has embraced various innovative packaging techniques, including 2.5-dimensional (2.5D) and three-dimensional (3D) packaging, wafer-scale packaging, and 3D stacking. These technologies optimize the communication speed and energy efficiency between devices.[6,11–14] The broad application of heterogeneous integration technology, which integrates central processing units (CPUs), graphics processing units (GPUs), and artificial intelligence (AI) accelerators on the same chip or chipset, specifically optimizes performance and energy efficiency for specific applications.[15,16] Concurrently, the incorporation of AI and machine learning to optimize design and manufacturing, along with the exploration of emerging computing paradigms (e.g., quantum computation or neuromorphic computation), paves the way beyond the constraints of traditional Moore's Law.[17–21] To address the thermal issues arising from escalating transistor density, advanced heat dissipation techniques have also been developed to ensure consistent system operation.[22–24] These innovations not only perpetuate Moore's Law but also propel semiconductor technology towards higher levels of integration and performance. Presently, leading manufacturers such as TSMC have introduced 3 nm processing technology. However, future node scaling will still present additional technical and economic challenges that may necessitate the exploration of new semiconductor technologies and design approaches. This is crucial to continue driving the industry forward beyond the confines of Moore's Law (Fig. 1).

Typical two-dimensional (2D) materials, including graphene, transition metal disulfides (TMDs), black phosphorus (BP), and hexagonal boron nitride (h-BN), exhibit remarkable potential in the semiconductor industry due to their atomic-level thinness and superior physical properties.[25–28] These materials are fully saturated with surface atoms and lack dangling bonds, enabling seamless integration with existing semiconductor processes via advanced manufacturing techniques such as chemical vapor deposition (CVD).[29–33] Furthermore, the van der Waals (vdW) interfacial properties of 2D materials facilitate the

formation of heterostructures with a broad range of materials possessing different lattice constants, thereby eliminating the need for lattice matching.[28,34–36] In pursuit of the lower limit of size in semiconductor technology, 2D materials have made significant strides in reducing transistor gate lengths, notably MoS<sub>2</sub> FETs, which have evolved from an initial 4 μm gate to 0.34 nm graphene gates.[37,38] The evolution of 2D materials signifies a prospective trajectory beyond the traditional Moore's Law, showcasing remarkable potential and diverse applications in semiconductor technology. Among these, electrolyte gate FETs (EGFETs) leverage the electric double layer (EDL) mechanism and flexible properties of electrolyte materials, rendering them suitable for artificial synapses and electronic skin (e-skin) applications.[39–45] Ferroelectric FETs (FeFETs), on the other hand, facilitate non-volatile storage by employing ferroelectric materials as gate dielectrics, with their rapid switching and high endurance positioning them as candidates for memory applications.[46–49] Van der Waals heterostructure field effect transistors (vdWH-FETs) allow for the combination and modulation of various electronic properties by stacking between 2D materials, without being constrained by lattice constants.[50–54] Floating gate field effect transistors (FGFETs), which use 2D materials as floating gates and regulate the carrier density through the accumulation of charge within the floating gate, are employed for high-density data storage and logic circuits.[55–59] These advancements offer innovative solutions for future electronics.

2D materials are anticipated to transcend the limitations of Moore's Law. Electronic devices are transitioning from mere miniaturization and increased integration towards multifunctionality and diversity, with piezotronics and tribotronics at the forefront of the transformation. 2D materials also greatly expand the potential of piezotronics and tribotronics applications compared to other semiconductor materials due to their rich variety, tunable bandgap, capability for heterostructure construction, and mature fabrication process. The bandgap structure and electronic transport properties of these 2D materials can be modulated by the piezoelectric and triboelectric effects induced by mechanical

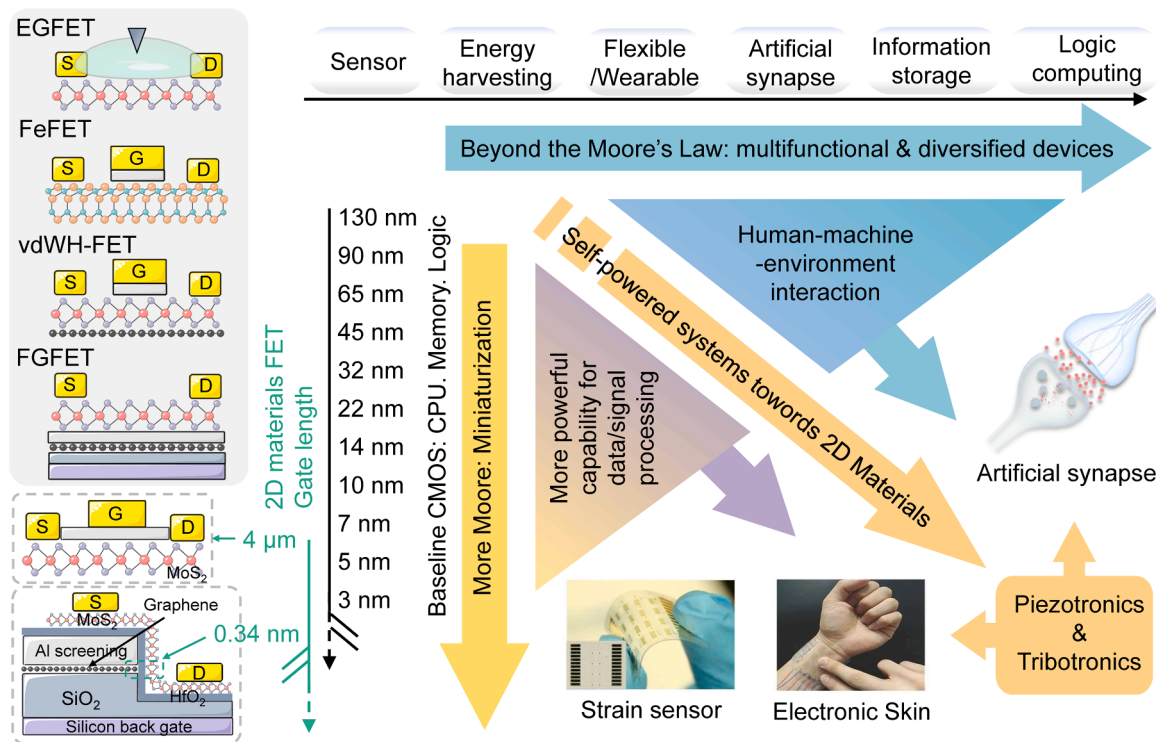


**Fig. 1.** The development prospects of More Moore and beyond the Moore's Law. The vertical coordinate axis represents the continuation of Moore's Law and the development of two-dimensional field-effect transistors (2D FETs). The horizontal coordinate axis represents potential development directions beyond the Moore's Law toward multifunctional and sophisticated devices.

strain, thereby altering their electrical conductivity and semiconductor characteristics.[60–66] This method is extensively employed in self-powered systems that leverage piezotronics and tribotronics, enabling them to generate voltages and currents autonomously without external power sources. This offers innovative design paradigms for self-powered devices and energy-harvesting systems. Furthermore, strain engineering not only paves the way for high-performance electronic and optoelectronic devices but also presents promising avenues in sensor technology,[67–70] energy harvesting,[71–73] flexible/wearable electronics,[39,74,75] artificial synapses,[76–82] information storage,[83–85] and logic computing[78,79,83,86–88]. Self-powered systems play a pivotal role in human-machine-environment interactions. These systems serve not only as energy sources and sensors, capturing information about mechanical stresses and environmental changes, but also enable rapid data processing and storage through their integration. For instance, flexible piezoelectric sensors function as strain sensors to detect minute mechanical changes, while e-skins replicate the sensations of human skin, responding swiftly to variations in touch, pressure, and temperature. Self-powered systems also hold significant potential in the realm of data and information processing. They can expedite data processing and storage and even emulate the synaptic mechanisms of the human brain for intricate signal processing and learning in certain applications. These systems suggest an increasingly critical role for 2D materials in the future development of smart devices and artificial intelligence technologies. Innovative research directions in piezotronics and tribotronics not only allow these systems to operate without external power sources but also facilitate intelligent interactions with humans, machines, and the environment, equipped with powerful data processing capabilities. This transition from 2D nanoscale to interactive system-level applications is anticipated to significantly broaden the application areas of electronic devices and drive future technological advancements.

This review systematically examines the advancements in piezotronics and tribotronics with a focus on 2D materials. The discussion primarily encompasses the working mechanism of piezotronics and tribotronics, their applications in 2D materials, and the research conducted on piezoelectric nanogenerators (PENGs)/triboelectric nanogenerators (TENGS)-modulated 2D FETs. First, the piezotronic properties in 2D materials are introduced and discussed based on material properties such as the symmetry, number of layers, strain modulation, and electronic structure. This review will concentrate on the non-centrosymmetric piezoelectric materials, exemplified by MoS<sub>2</sub>, and interface engineering techniques used to impact piezoelectric properties to ordinary 2D materials like graphene. Potential applications of piezotronics in 2D materials for environmental monitoring, including light, humidity, and temperature, will be explored. Additionally, the use of nanogenerators (NGs) based on piezotronics in 2D materials for mechanical sensing and energy storage will be discussed. Second, the review will delve into the applications of PENG-modulated 2D FETs, particularly in mechanical sensing, band structure engineering and artificial synapses. Finally, we will explore the applications of TENG-modulated 2D FETs in areas such as enhanced photoresponsivity, information storage, binary logic, band structure engineering and artificial synapses. Notably, piezo/tribotronics based on 1D materials, especially 1D piezotronics devices/arrays/systems, have been well summarized in previous literature, which are not the main concern in this review.[60, 89–91] It is believed that the progress in the field of piezotronics and tribotronics of 2D materials suggests high sensitivity and rapid responsiveness to minute mechanical changes, which is expected to drive innovation in interactive and smart devices.

## 2. The development of piezotronics and tribotronics of 2D materials

Piezotronics and tribotronics utilize the piezotronic effect and the triboelectric potential, respectively, to modulate the transport

properties of semiconductors. This allows for a direct and active interaction between various electronics and external environment.[62,66,89, 92–98] Piezotronics applied to 2D materials can be classified into two primary categories. The first category leverages the inherent piezoelectric effect of the 2D material semiconductor to alter the interfacial barrier of the metal-semiconductor contact and the transport properties of the p-n junction region. The second category, which can be considered as a more general and extended concept of conventional piezotronics, employs mechanically induced piezo-potential from PENGs to gate 2D materials-based devices and to modulate the transport properties. Therefore, in addition to the two main branches of piezotronics and tribotronics that have developed toward the mechanical modulation of 2D materials, there are two sub-branches of piezotronics based on 2D materials themselves and PENG-based modulation of 2D FETs (Fig. 2).

Piezotronics, a field that originated from the seminal research conducted by Wang et al. in 2006,[99] employs a conducting atomic force microscopy (AFM) tip to apply pressure to the zinc oxide nanowires (ZnO NWs), realizing effective conversion of the mechanical energy to electrical signals. This process produces a current through the Schottky barrier rectification effect between the tip and the ZnO NW and links an external strain field directly with charge carrier transport properties in the channel, successfully achieving the coupling of piezoelectric characteristics and semiconducting properties. This innovative approach has also paved the way for a new domain of energy harvesting using nanoscale materials.[100] Tribotronics, another field that was pioneered by Zhang et al. in 2014, utilizes triboelectric potentials induced by contact electrification to modulate the electron transport properties in silicon-based FET channels.[101] This method of mechanical modulation bears a resemblance to the gate voltage in conventional FETs. The operational mechanism of NGs in both piezotronics and tribotronics is grounded on Maxwell's displacement current Eq. (1):[31]

$$J_D = \frac{\partial D'}{\partial t} + \frac{\partial P_s}{\partial t} = \epsilon \frac{\partial E}{\partial t} + \frac{\partial P_s}{\partial t} \quad (1)$$

$\partial D'/\partial t$  denotes the displacement current induced by a temporally related electrical field;  $\partial P_s/\partial t$  signifies the current resulting from the movement of altered media, propelled by external forces. This is also the theoretical foundation for the mechanical to electrical energy conversion process.

In the development timeline of piezotronics in 2D materials (Fig. 2, Branch I), the piezoelectric properties of the 2D material MoS<sub>2</sub> were experimentally identified for the first time in 2014, sparking a surge of research in related fields.[102] Presently, advancements in piezotronics within 2D materials have culminated in the creation of diverse structures, encompassing pure 2D structures,[102–104] 1D/2D[105–109] and 2D/2D hybrid structures[110]. These applications leverage the modulation of bandgap structures and electron transport properties of the materials by the piezoelectric potential to modify the materials' responsiveness to light,[67–69,111] humidity[112] and temperature [113]. The majority of these studies focus on MoS<sub>2</sub> devices for environmental sensing. Given this inherent ability to transmute mechanical energy to electrical energy, piezotronics is particularly well-suited for applications as NGs that respond to external mechanical stimuli.[71–73, 114] In the developmental timeline for piezotronics in PENG-modulated 2D FETs (Fig. 2, Branch II), the inherent properties of PENG are leveraged for mechanical sensing applications.[39,115] Drawing upon the diverse structural and functional designs of 2D FETs, piezo-potential powered/modulated heterojunction-based Schottky barristors[116, 117] and artificial synaptic devices[76] can be fabricated and accomplished with PENG active modulation. For TENG, the inherent properties of itself can be used for mechanical sensing applications.[39,115] In the developmental timeline for tribotronics in TENG-modulated 2D FETs (Fig. 2, Branch III), the modulation of the bandgap structure and electron transport properties of materials by triboelectric potentials allow for the adjustment of device photosensitivity[70] and the barriers of channel materials[118,119]. Structural designs based on 2D FETs have

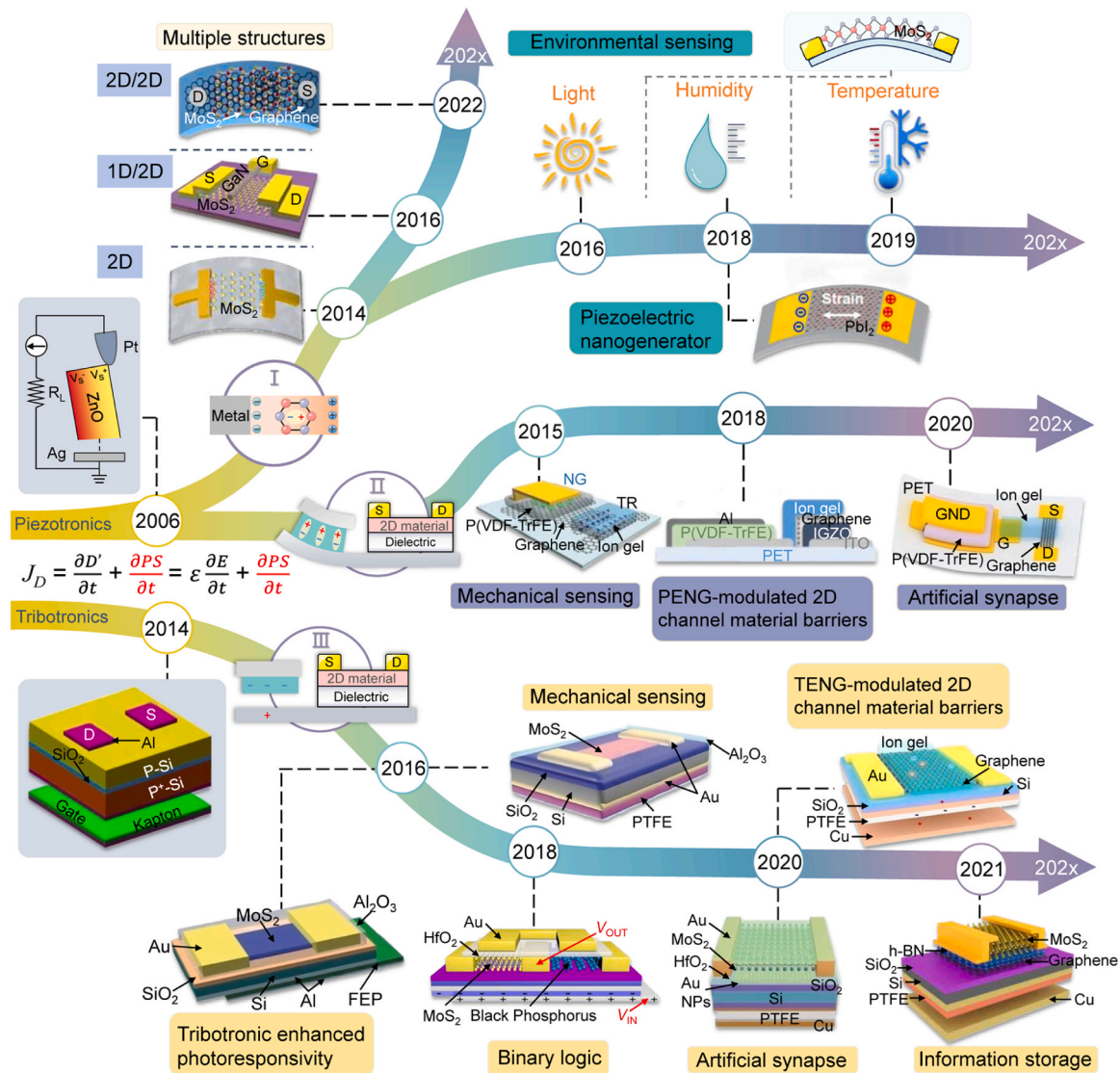


Fig. 2. The development timeline of piezotronics and tribotronics of 2D materials.

been developed for binary logic inverters,[79,83,86–88,120] artificial synaptic devices,[77–82] and information storage devices[83,84], with active regulation achieved through TENG. This review will deliver a detailed overview on the two primary branches of development in piezotronics and tribotronics of 2D materials and related 2D devices.

### 3. Working mechanism of piezotronics and tribotronics

For the first category of 2D materials that are inherently piezoelectric, this effect is not only dependent on the symmetry of the material, but is also influenced by the number of layers, strain modulation, and electronic structure, which together determine the piezoelectric properties of the material. The selection and optimization of proper 2D piezoelectric materials are a crucial step in constructing piezoelectric functional devices. In order to achieve the best piezoelectric effect, the primary consideration when selecting a material is whether its crystal structure is non-centrosymmetric. A non-centrosymmetric structure is necessary for the piezoelectric effect to occur, because only in such a structure can external stresses lead to a charge shift and thus to polarization. It is also important that the electronic structure of the materials has non-zero bandgap[121]. Materials with non-zero bandgap can avoid rapid recombination of electron-hole pairs during polarization generation, thereby maintaining a stable piezoelectric response. The reported

2D monolayer piezoelectric materials can be classified into six categories based on their crystal structures, including TMDCs and Janus TMDCs, II-VI, III-V, III-VI and Janus III-VI, IV-VI and V-V compounds.[64,122] For hexagonal structures such as h-BN and TMDCs ( $\text{MoS}_2$  and  $\text{WS}_2$ ), which possess the  $D_{6h}$  point group, and for III-group monochalcogenides like GaS and InSe, which possess the  $D_{3h}$  point group, upon exfoliation to monolayers, the symmetry reduces to the  $D_{3h}$  point group. These monolayer materials exhibit a honeycomb structure and lack an inversion center.[95,123] The monolayer h-BN consists of a single atomic layer. Monolayer TMDCs contain two chalcogen atoms and one central transition metal atom at different heights. Monolayer III-group monochalcogenides have an X-M-M-X four-atom layer stacking. Monolayer structures of IV-group monochalcogenides like SnSe possess the  $C_{2v}$  point group and exhibit piezoelectricity due to the non-centrosymmetry of their orthogonal structure. In addition, bulk or even-layered  $\text{MoS}_2$  stacked by vdW forces does not exhibit piezoelectricity. However, monolayer or odd-layered  $\text{MoS}_2$  exhibits piezoelectricity because of the absence of a centrosymmetry along the vertical direction.[102]

The standard structure of a 2D material with centrosymmetry, as well as the typical metal-semiconductor-metal (MSM) configuration of the piezotronic device, are depicted in Fig. 3a. The associated energy band alterations are presented in Fig. 3b. In centrosymmetric 2D

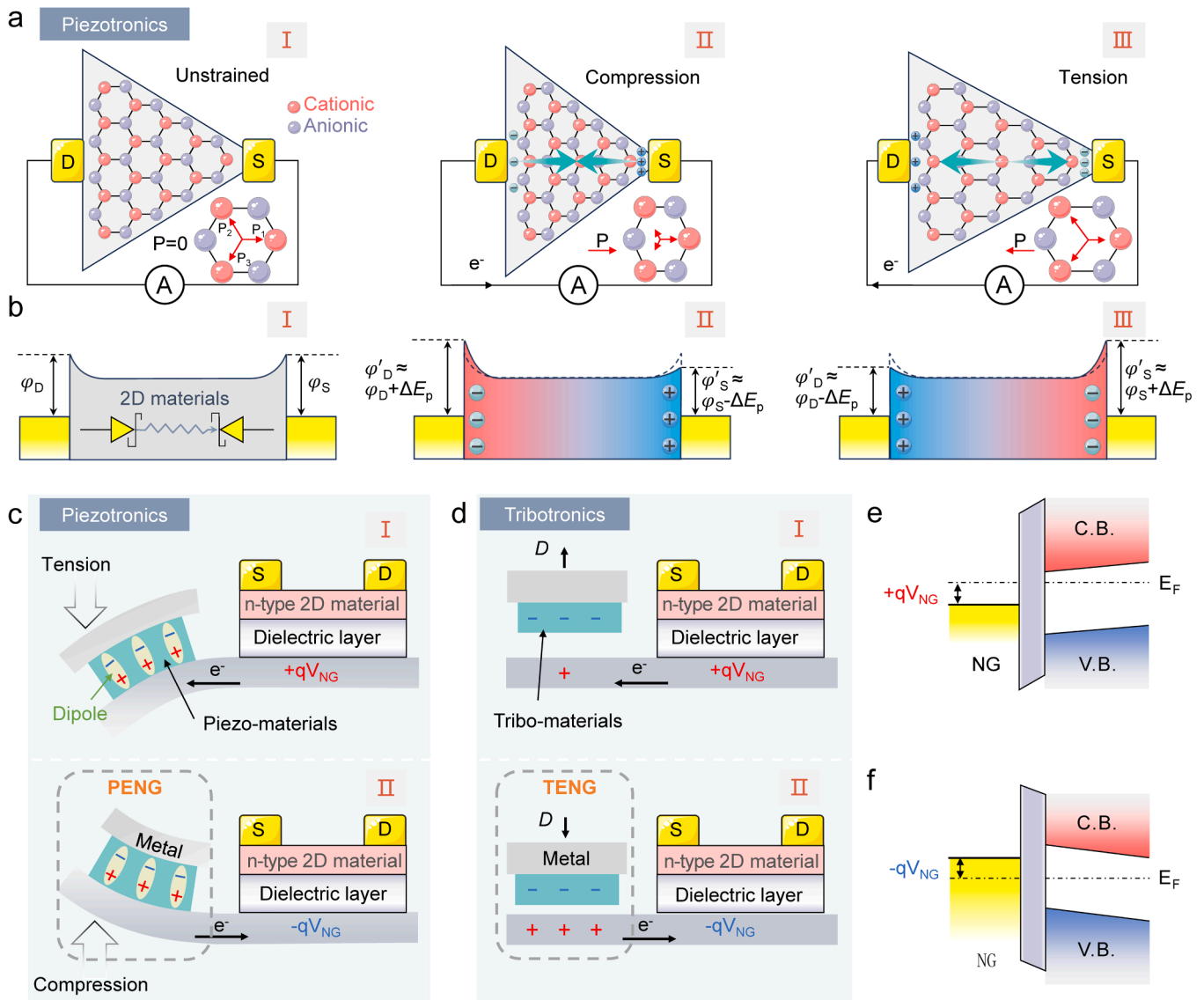


**Fig. 3.** Working mechanism of piezotronics and tribotronics of 2D materials. (a, b) Device structure and energy band changes for piezotronics in 2D materials. (c) Piezotronics of piezoelectric nanogenerator (PENG)-modulated 2D FETs. (d) Tribotronics of triboelectric nanogenerator (TENG)-modulated 2D FETs. (e, f) Schematic energy band diagram of nanogenerator (NG) positive/negative gate voltage modulated 2D FET.

materials, the unit cell typically displays a hexagonal lattice composed of alternating anions and cations, encompassing three dipoles positioned at  $120^\circ$  angles ( $P_1, P_2, P_3$ ). These dipoles possess a total vector sum of zero in the unstrained initial state (State I). At this juncture, the Schottky barrier induced by the work function disparity between metal-semiconductor contact, obstructs the unrestricted flow of electrons. Upon application of compression or tension to the device (State II/III), its electronic transport properties are predominately affected by the combined effects of the piezoelectric and piezoresistive phenomena. [102] The piezoelectric effect modulates the Schottky barrier by inducing a non-uniform charge distribution via strain, while the piezoresistive effect adjusts the overall resistance of the material by modifying its bandgap. The distinct responses of the three dipoles to strain result in directional variations in charge polarization, thereby generating a significant net dipole moment. The macroscopic piezoelectric potential generated by compressive strain is distributed from the drain to the source, while that produced by tensile strain is distributed from the source to the drain. The internal piezoelectric field also induces an asymmetric modulation of the barrier heights at both ends of the device. Specifically, positive charges lower the energy band at the

contact area ( $\phi' \approx \phi - \Delta E_p$ ), while negative charges elevate the band ( $\phi' \approx \phi + \Delta E_p$ ). This leads to uneven changes in the barrier height between the source and drain. Consequently, mechanical strain can function as a gate to tune the internal electrical field in the device, which directly influences the electrons' flow direction through external circuit.

The second category encompasses PENG/TENG-modulated 2D material FETs. Fig. 3c illustrates a typical device structure for piezotronics, using an n-type 2D FET as an example. This design does not necessitate the piezoelectric properties of the 2D material, thereby offering a broader range of channel materials and structural designs. The application of varying strains results in different dipole arrangements within the piezoelectric material, which in turn influences the charge distribution within the bottom gate of the connected FET. Specifically, tensile and compressive strains induce equivalent positive and negative gate electric fields, respectively. Fig. 3d illustrates the standard device structure for tribotronics, where the mechanical displacement ( $D$ ) modulates the electrostatic field equilibrium between the polymer and the FET bottom gate, thereby influencing the dynamic charge distribution within the bottom gate. Elevated and reduced mechanical displacements induce positive and negative gate electric fields, respectively

(depending on the connection strategy). The applied gate electric field from NG undeniably impacts the energy bands and electronic transport properties in the 2D material channel. The equivalent positive gate voltage ( $+qV_{NG}$ ) causes a downward bending of the 2D material's energy bands, resulting in a reduction in the barrier height. This not only enhances electron injection efficiency but also increases the carrier concentration in the channel, thereby boosting the output current (Fig. 3e). Conversely, with a negative gate voltage ( $-qV_{NG}$ ), the barrier height is elevated and the energy band is bent upwards, leading to a decrease in electron concentration in the channel and consequently reducing current (Fig. 3f)

## 4. Piezotronics in 2D materials

### 4.1. Piezotronics in 2D materials

2D materials have garnered lots of attention due to their distinctive electronic and mechanical properties.[124,125] Notably, the piezoelectric nature of these materials presents substantial potential for the advancement of novel nanoelectromechanical systems (NEMS) and sophisticated sensors.[126–128] The piezoelectric property of 2D MoS<sub>2</sub> was initially reported experimentally by Wu et al. in 2014 (Fig. 4a). [102] By applying varying strains (stretch/release) to the MoS<sub>2</sub> device, polarized charges are induced, which facilitate electrons to flow through

the external load to achieve diverse piezoelectric responses. A clear dependence of the piezoelectric charge polarization on the direction of the principal strain applied to 2D materials is observed. As illustrated in Fig. 4b, the same strain applied along the x (“armchair”) and y (“zigzag”) directions of the monolayer MoS<sub>2</sub> yields contrasting outputs. Furthermore, the MSM constructed with MoS<sub>2</sub> demonstrates the current-voltage curve shifts to the left under stretched strain and to the right under compressed strain. This alteration in electrical transport behavior is primarily attributed to two effects: the piezoelectric and piezoresistive effects. The piezoelectric effect modulates the carrier transport by generating polarized charges at the serrated edges of MoS<sub>2</sub>, which directly influence the contact between the metal and MoS<sub>2</sub>. Conversely, the piezoresistive effect regulates the resistance of the entire device through strain-induced bandgap changes. These observations also offer novel methods for modulating nanomaterial properties using varying strain-induced polarization differences (Fig. 4c). It is also pertinent to consider that the number of material layers significantly influences its piezoelectric properties. MoS<sub>2</sub> typically manifests in the prevalent 2H multilayer structure, distinguished by the inverse orientation of the alternating layers. Consequently, when MoS<sub>2</sub>'s layer count is even, centrosymmetry prevents the exhibition of piezoelectric properties and second harmonic generation effects. Conversely, odd-layered MoS<sub>2</sub> displays these characteristics. The results depicted in Fig. 4d confirm that MoS<sub>2</sub> with an odd number of layers demonstrates robust

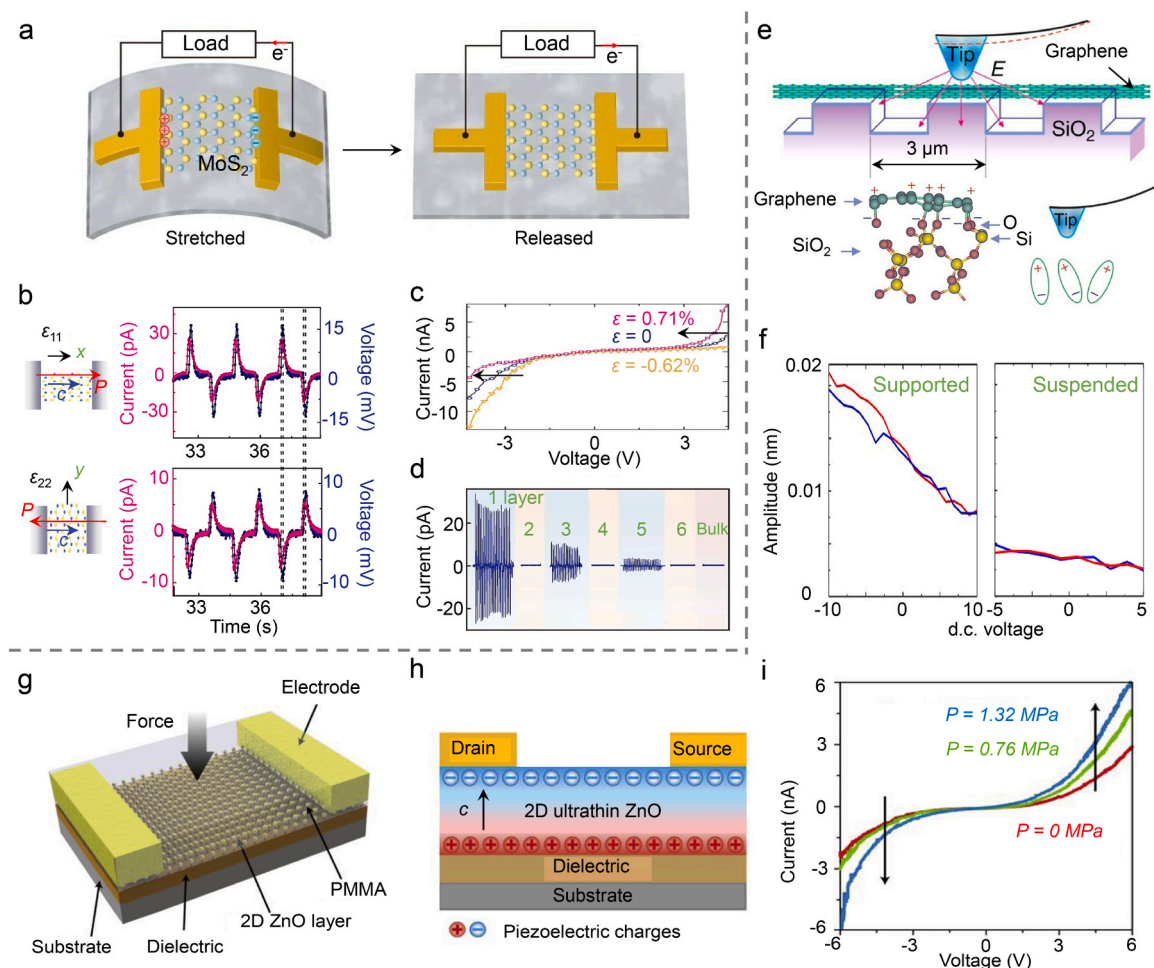


**Fig. 4.** Piezotronics in 2D materials with piezoelectric properties. (a) Piezoelectric properties of 2D MoS<sub>2</sub>. [102] (b) MoS<sub>2</sub> piezoelectric charge polarization depending on the direction of the principal strain. (c) Effect of different strains on the piezoelectric properties of MoS<sub>2</sub>. (d) Effect of the layer number of MoS<sub>2</sub> on the piezoelectric properties. Copyright 2014, Springer Nature. (e) Endowing graphene with piezoelectric properties through interfacial engineering. [103] Copyright 2015, Springer Nature. (f) Piezoresponse voltage spectra of supported and suspended layers of graphene. (g, h) Schematic of device structure and piezoelectric charge distribution of atomically thin ZnO nanosheets. [104] Copyright 2019, Elsevier. (i) Effect of different strains on the piezoelectric properties of ZnO.

intrinsic piezoelectricity due to the disruption of the inversion symmetry. However, as the layer number increases, the piezoelectric properties diminish. In contrast, even-layered MoS<sub>2</sub>, characterized by centrosymmetry and bulk structures, lacks piezoelectricity. These insights are crucial for comprehending the physical properties of MoS<sub>2</sub> and for

designing and implementing MoS<sub>2</sub>-based piezotronic devices.

Through the application of interface engineering, it is feasible to modify non-piezoelectric 2D materials with piezoelectric properties. Rodrigues et al. achieved this by depositing a monolayer graphene onto a SiO<sub>2</sub> grating substrate (Fig. 4e). [103] Graphene, due to its inherently

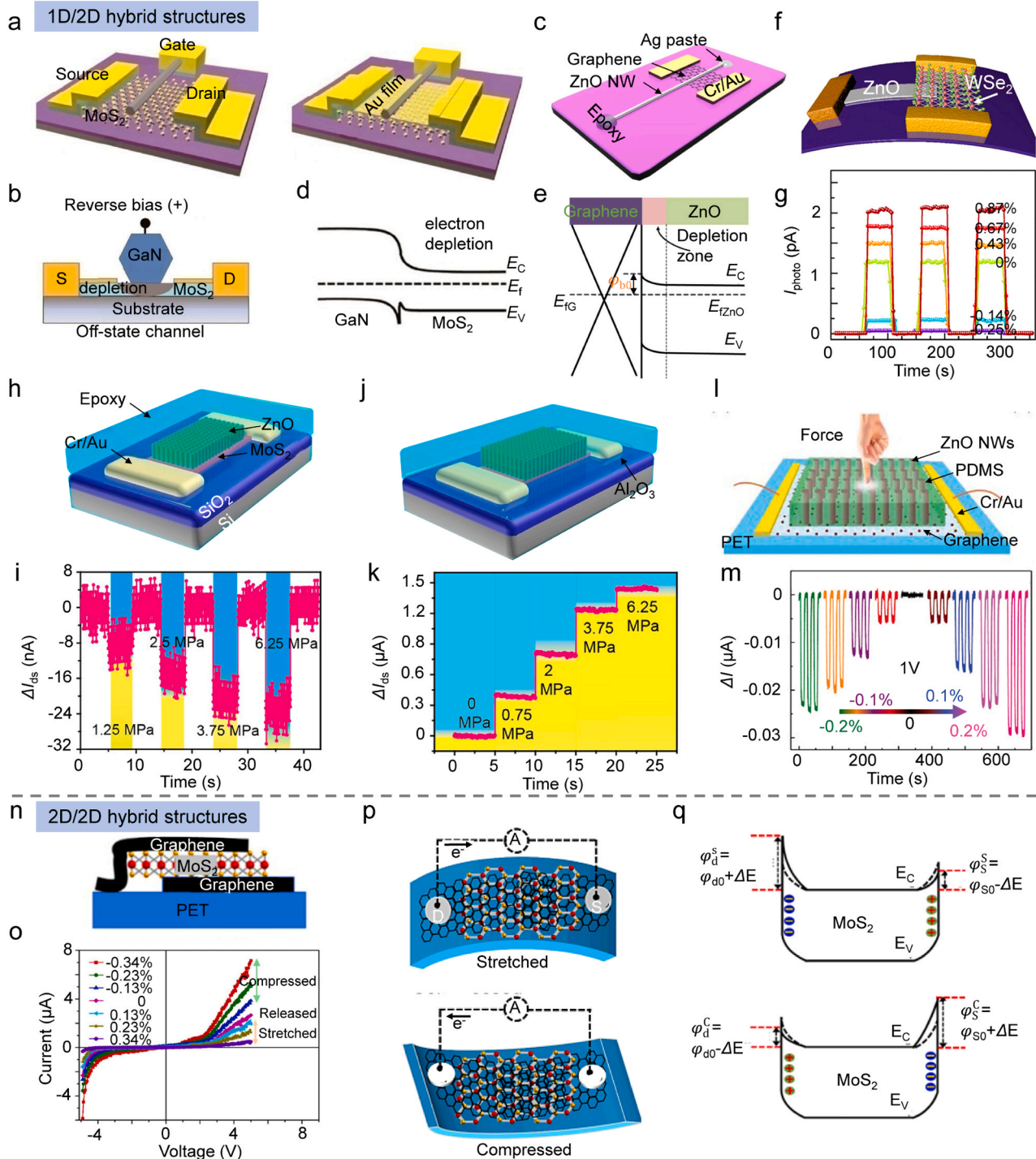


**Fig. 5.** Piezotronics in 1D/2D and 2D/2D hybrid structures. (a, b) Structural schematic and side view of piezotronics of GaN NW/MoS<sub>2</sub> hybrid structure. [105] Copyright 2016, American Chemical Society. (c) Piezotronics of ZnO NW/graphene hybrid structure. [106] (d) Energy band structure of piezotronics of GaN NW/MoS<sub>2</sub> hybrid structure. (e) Energy band structure of piezotronics of ZnO NW/graphene hybrid structure. Copyright 2017, Springer Nature. (f, g) Piezotronics of ZnO/WSe<sub>2</sub> hybrid structure and the effect of mechanical strain on the optoelectronic performance. [107] Copyright 2019, Elsevier. (h, i) Piezotronics of ZnO NW array/MoS<sub>2</sub> hybrid structure and mechanical strain response properties. [108] Copyright 2016, American Chemical Society. (j, k) Piezotronics of ZnO NW arrays/MoS<sub>2</sub> interfaces introduced with Al<sub>2</sub>O<sub>3</sub> and mechanical strain response properties. (l, m) Piezotronics of ZnO NW/graphene hybridized structures and mechanical strain response properties. [109] Copyright 2020, Wiley-VCH. (n, o) Piezotronics of MoS<sub>2</sub>/graphene hybrid structure and mechanical strain response properties. [110] Copyright 2022, Elsevier. (p, q) Device structure and energy band schematic of MoS<sub>2</sub>/graphene piezotronics under different mechanical strains.

centrosymmetric crystal structure, does not exhibit piezoelectricity on its own. However, internal polarization can be induced in graphene through asymmetric strain on the SiO<sub>2</sub> substrate, resulting in a piezoelectric effect. The supported and suspended layers of graphene display distinct chemical structures due to their varying interactions with the SiO<sub>2</sub> substrate. The suspended layer remains unmodified as a monolayer, while the supported layer may form chemical bonds through the oxygen atoms on the substrate. This interaction between carbon and oxygen generates a non-zero net dipole moment and polarization within the structure. The piezoresponse voltage spectra of graphene in the supported and suspended layers are shown in Fig. 4f. The results illustrate that the supported region of graphene exhibits significant piezoelectric activity. When a negative voltage is applied to the probe, the dipole aligns with the normal direction of the substrate, thereby increasing the net polarization. Conversely, a positive bias causes the dipole to deviate from this direction, resulting in a decrease in net polarization.

Research on piezotronics in 1D ZnO NWs has been notably productive over the past two decades.[60,61,99] Recently, Wang et al. pioneered the exploration of 2D piezotronics using atomically thin ZnO nanosheets.[104] This study employed a M-S-M structure encapsulated in poly(methyl methacrylate) (PMMA) to examine the electrical transport behavior of these 2D ZnO nanosheets (Fig. 4g). The strain-induced piezoelectric polarization charge, which is broadly distributed across the surface of the ZnO nanosheets, significantly modifies the distribution and concentration of free carriers within the 2D material. This charge redistribution effectively adjusts the Schottky barrier height of the metal-ZnO interface and the width of conducting channel (Fig. 4h). Consequently, the current demonstrates a consistent increase with escalating compressive stress (Fig. 4i). Furthermore, the author also constructed ultrathin ZnO piezoelectric transistors with ~2 nm channel length based on the vertical structure with strong piezoelectric effect.[129] These researches reveal that an external mechanical stimulus can serve as a direct “gate” control signal to manipulate the electronic behavior of internal crystals via piezoelectric polarization charge, offering a novel modulation strategy for tunable electronics. The evolution from 1D to 2D structures signifies a pivotal paradigm shift in materials science within the realm of nanotechnology.

#### 4.2. Piezotronics in 1D/2D and 2D/2D hybrid structures

In the realm of flexible electronics and optoelectronics, there is a growing interest in directly modulating device performance through piezoelectric effects induced by external mechanical stimuli. These effects control the localized transport of charge carriers. Furthermore, hybrid dimensional vdWH can amalgamate the complementary advantages of materials from different dimensions, thereby enhancing the functionality of these materials and improving the overall performance of the fabricated devices. The piezotronics of 1D/2D hybrid structures, based on the piezoelectric potential of 1D NW, can be used to modulate the channel currents of the 2D materials. Liu et al. constructed a piezotronic device with a GaN NW/MoS<sub>2</sub> hybrid structure.[105] In this device, GaN NW was transferred onto MoS<sub>2</sub> channels, and Au was prepared by a self-alignment process to reduce the access resistance (Figs. 5a, 5b). Liu et al. also constructed a piezotronic device with a ZnO NW/graphene hybrid vdWH (Fig. 5c).[106] As evident from the energy band diagrams plotted in Figs. 5d, 5e, Schottky barriers and depletion regions are readily formed at the 1D/2D material interface, which can effectively decrease the gate leakage current. Moreover, the piezoelectric potential of the 1D NW influences electron transport in the 2D material, enabling not only pressure response but also highly sensitive light detection, a phenomenon known as piezo-phototronics. Du et al. combined 1D ZnO nanoribbons and a 2D WSe<sub>2</sub> layer to modulate the interfacial charge via mechanical strain, thereby influencing the optoelectronic performance of the device (Fig. 5f).[107] A larger tensile strain results in a significant enhancement of photocurrent

characteristics, while a compressive strain leads to a depression of photocurrent (Fig. 5g). The application of tensile strain generates positive piezoelectric polarization charge on the surface of ZnO nanoribbons, which accumulates negative carriers at the 1D/2D interface. This increases the energy band slope of WSe<sub>2</sub> and enhances the efficiency of photogenerated charge carrier to transport, thereby boosting the photocurrent of ZnO/WSe<sub>2</sub>. Conversely, the application of compressive strain generates negative piezoelectric polarization charge from ZnO, which decreases the energy band slope of WSe<sub>2</sub>, impedes carrier transport, and reduces the photoresponsivity. Therefore, by manipulating the type and extent of strain applied to the 1D piezoelectric material, the electronic states and carrier transport paths of the 2D channel material can be effectively controlled. This allows for precise tuning of the photodetector’s performance.

The provision of more active sites to piezotronic devices from NW to NW arrays is feasible. Chen et al. synthesized a 1D/2D hybrid structure of top pressure-gated FET (PGFET) by precisely growing ZnO NW arrays on the MoS<sub>2</sub> device substrate at low temperatures (Fig. 5h).[108] As illustrated in Fig. 5i, when gate strain was gradually applied to the Epoxy package device, the channel current exhibited a negative increase and showed signs of saturation. The effect of a strain of 6.25 MPa was found to be equivalent to that of a -5 V gate voltage. Furthermore, by incorporating an Al<sub>2</sub>O<sub>3</sub> dielectric layer at the 1D/2D interface to form a vertical structure akin to a MOSFET structure (Fig. 5j), the response to pressure was reversed compared to that of Fig. 5h. As shown in Fig. 5k, the channel current demonstrated a positive increment trend with increasing pressure. In the ZnO-MoS<sub>2</sub> combination without Al<sub>2</sub>O<sub>3</sub>, the piezoelectric polarization of the ZnO nanowires directly interacts with the MoS<sub>2</sub>. This direct interaction results in a reduction of electrons in the MoS<sub>2</sub> as these electrons are used to neutralize the positively polarized charges on the ZnO surface. This results in a decrease in the source-drain current, which is represented as a change in the negative current. In contrast, the introduction of Al<sub>2</sub>O<sub>3</sub> enables the piezoelectric polarization effect of ZnO to act on MoS<sub>2</sub> via electrostatic induction through Al<sub>2</sub>O<sub>3</sub>. This results in an accumulation of electrons within the MoS<sub>2</sub> channel, akin to the influence of gate voltage in conventional FETs. This surge in electrons subsequently induces an increased source-drain current, or positive current generation. This transformation underscores how the Al<sub>2</sub>O<sub>3</sub> layer effectively modifies the manner in which the piezoelectric effect regulates the electronic properties of MoS<sub>2</sub>. Consequently, there is a shift in the current response from negative to positive, thereby optimizing device performance. Wang et al. developed a flexible graphene-based device combined with vertically aligned ZnO NW arrays (Fig. 5l).[109] Similarly, the positive piezoelectric polarization charge of ZnO directly impacts the MoS<sub>2</sub>, reducing the interfacial potential. This reduction leads to a decreased number of electrons in the channel, compensating for the positive polarization charge of ZnO. As depicted in Fig. 5m, this results in both tensile and compressive strains causing a change in negative current, with the channel current increasing proportionally with strain.

Piezotronics with 2D/2D hybrid structure utilizes the piezoelectric potential of the 2D material to modulate its channel currents. Puneetha et al. introduced a piezotronic device that incorporates a monolayer MoS<sub>2</sub> continuous thin film and a graphene layer (Fig. 5n).[110] By fine-tuning the charge coupling and electric field screening effects between MoS<sub>2</sub> and graphene, strain-induced adjustments in the device’s electrical properties can be realized. As depicted in Fig. 5o, the output current of the device escalates with increasing strain in compression mode, but diminishes with rising strain in tensile mode. The structure and energy band schematics presented in Figs. 5p and 5q elucidate this behavior. In the stretched mode, a pronounced piezoelectric potential is generated at the source direction, which modifies the Schottky barrier at the drain side, prompting electrons to traverse from the drain to the source. Conversely, when transitioning from stretched mode to compressed mode, the electrons move in the opposite direction. Here, the piezoelectric potential on the drain side is elevated, leading to a more

significant Schottky barrier, and electrons are directed from the source side to the drain direction.

#### 4.3. Mechanical control in 2D piezotronics

The introduction of stress in piezotronic devices can be mechanically controlled and is generally categorized into two primary methods, as illustrated in Fig. 6a. The first method involves applying uniaxial strain to the flexible piezotronic device through stretching or bending. [110, 130–132] This approach offers the advantage of directly modulating the device via mechanical deformation. It is not without drawbacks, including the inevitable substrate strain that can lead to stress concentration and stress softening, thereby diminishing the performance and reliability of electronic or optoelectronic devices. The second method utilizes an AFM probe to apply quantitative stresses. [99, 133–135] This process can realize precise control of the location and strength of the applied stress, making it particularly suitable for micro-nano scale applications where localized fine tuning is necessary. However, this method is limited by the localization of the stress and the potential for non-uniform strain to induce a flexoelectric effect in the material. [136] Furthermore, the complexity of operation and high cost of equipment limit the practical application of applying stress by the AFM probe method. Chi et al. explored a novel piezoelectric and magnetic double-gate semiconductor transistor (PM-FEST) (Fig. 6b). [137] The channel material is  $\alpha$ -In<sub>2</sub>Se<sub>3</sub>, chosen for its high piezoelectric coefficient and ferroelectricity that can be sustained at room temperature, in addition to its unique dipole-locking property. Al<sub>2</sub>O<sub>3</sub> is employed as the gate insulating layer to ensure the electrical stability of the device. Terfenol-D is employed to impart adjustable tensile or compressive

strains on the device in response to an external magnetic field, owing to its exceptional magnetostrictive properties. Consequently, the study is based on a ternary coupling of magnetism, piezoelectricity, and semiconductor property, leading to the concept of Magneto-Ferrotronics (Fig. 6c). This effect facilitates the piezoelectric potential through the strain induced in the magnetostrictive material under a magnetic field, thereby modulating the performance of the ferroelectric semiconductor device. Figs. 6d and 6e illustrate the PM-FEST device's response to varying magnetic field at different polarization directions, demonstrating how the interlocked dipoles ( $P_{IP}$  and  $P_{OOP}$ ) within the ferroelectric semiconductor  $\alpha$ -In<sub>2</sub>Se<sub>3</sub> influence its electrical performance. At a source-drain voltage of  $V_{ds} = -3$  V, the device operates in the  $P_{OOP-up}$  (dipole up polarization) state. As the magnetic field is increased, a trend towards decreased current is observed (Fig. 6f). From an off state to an on state at a magnetic field of 151 mT, the channel current decreases from approximately  $-0.4$  to  $-4.5$  nA (Fig. 6g). Conversely, at  $V_{ds} = 3$  V, the device operates in the  $P_{OOP-down}$  (dipole down polarization) state, with an increasing current trend observed as the magnetic field increases (Fig. 6h). From an off state to an on state at a magnetic field of 183 mT, the channel current escalates from approximately 0.06 to 0.85 nA (Fig. 6i). In the PM-FEST system, a magnetic field is applied to generate mechanical strain in Terfenol-D. This strain subsequently modulates the electrical properties of the ferroelectric semiconductor  $\alpha$ -In<sub>2</sub>Se<sub>3</sub> by altering its piezoelectric potential. This modulation is equivalent to the gating process in conventional FETs, effectively controlling the transport of charge carriers within the semiconductor channel. This mechanism offers a promising technological approach for the creation of non-intrusive or non-contact electronic devices.

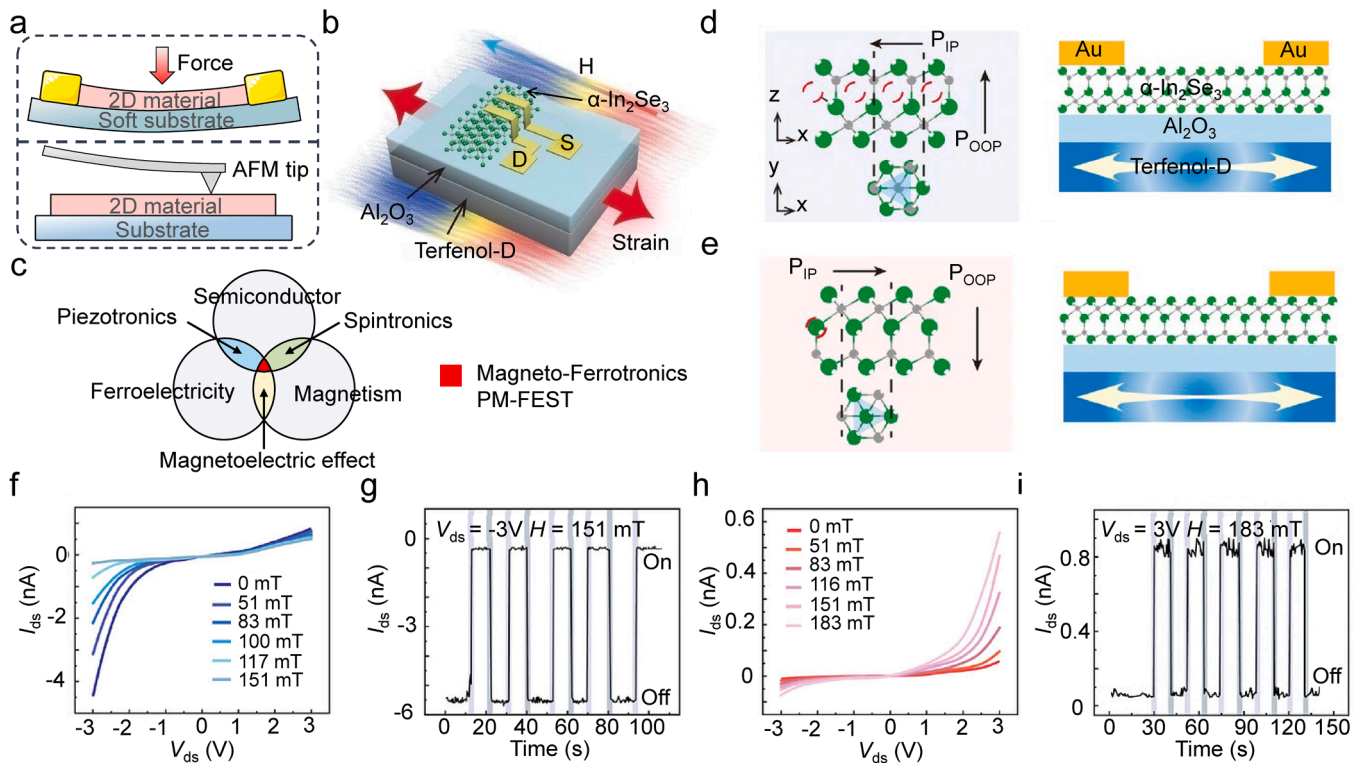


**Fig. 6.** Mechanical control in 2D piezotronics. (a) Two methods of mechanical control of stress introduction in piezotronic devices. Uniaxial strain applied by stretching or bending the flexible substrate of the piezotronic device and quantitative stress applied by an atomic force microscope (AFM) probe. (b) Schematic of piezoelectric and magnetic double-gate ferroelectric semiconductor transistor (PM-FEST). [137] Copyright 2022, Wiley-VCH. (c) Magneto-Ferrotronics based on ternary coupling of magnetism, piezoelectricity and semiconductor property. (d, e) Response of PM-FEST devices to magnetic fields under different polarization directions. The effect of the interlocked dipoles ( $P_{IP}$  and  $P_{OOP}$ ) in the ferroelectric semiconductor  $\alpha$ -In<sub>2</sub>Se<sub>3</sub> on the electrical properties of the device is demonstrated. (f, g) Effect of magnetic field strength on the device being in the  $P_{OOP-up}$  (dipole up polarization) state at  $V_{ds} = -3$  V and the change in channel current from off to on state for the magnetic field. (h, i) Effect of magnetic field strength on the device being in the  $P_{OOP-down}$  (dipole down polarization) state and the change in channel current with the magnetic field from the off state to the on state at  $V_{ds} = -3$  V.

## 5. Applications of piezotronics based on 2D materials

### 5.1. Environmental sensing

Piezo-phototronics, a field rooted in piezotronics, has garnered significant attention due to its ability to precisely modulate the photosensitivity. This is particularly evident in its enhancement of ambient light sensing capability, offering unique advantages. The bandgap structure and internal electric field of the material are manipulated to actively control its optoelectronic properties. The combined effect of light and mechanical strain not only alters the carrier concentration and distribution but also optimizes the charge state of interfacial electrons. This

significantly enhances the photocurrent and device's response speed. The local charge polarization induced by external strain can help to manage the dynamic processes of photogenerated carriers, including their generation, separation, transport, and complexation within the Schottky barrier or p-n structure.[138,139] MoS<sub>2</sub>, a layered TMDC, holds a significant position in optoelectronics research due to its superior photoresponsivity and piezo-phototronic properties. Wu et al. were the first to observe piezo-phototronic effects on monolayer MoS<sub>2</sub>, which they applied to adaptive photo-detection (as shown in the upper right panel of Fig. 7a).[67] They conducted an in-depth exploration of the piezo-phototronic effect of MoS<sub>2</sub>-based photodetectors under mechanical strain (Fig. 7b). In the absence of strain, incident photons excite

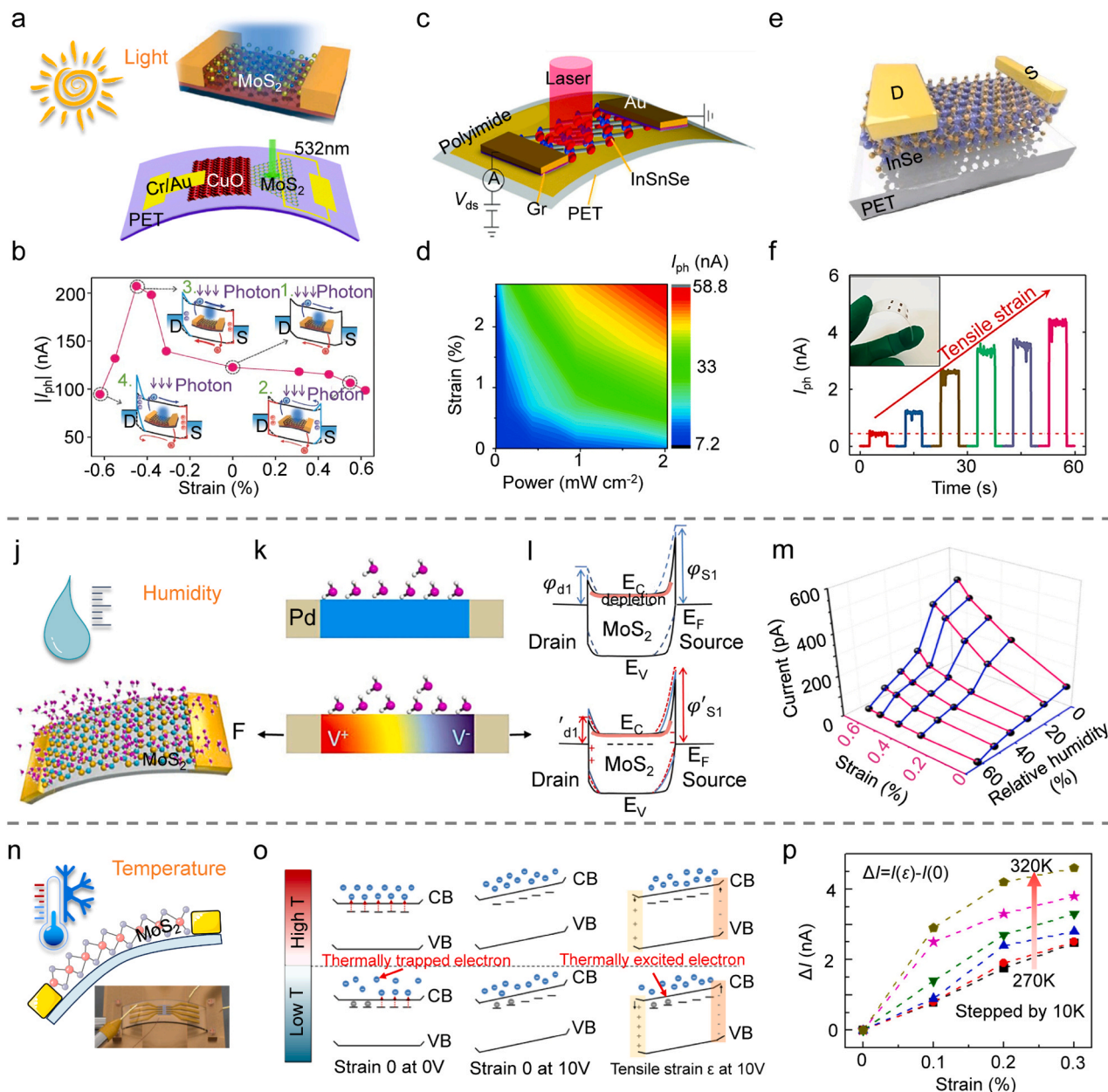


**Fig. 7.** Piezotronics in 2D materials for environmental sensing applications. (a) Light sensing in piezo-phototronics of MoS<sub>2</sub> and CuO/MoS<sub>2</sub> based heterostructures. [67,68] Copyright 2016, Wiley-VCH. Copyright 2017, Royal Society of Chemistry. (b) Working mechanism of piezo-phototronics of MoS<sub>2</sub>. (c, d) Piezo-phototronics of InSnSe and photocurrent variation at different strains and laser power densities.[69] Copyright 2018, Royal Society of Chemistry. (e, f) Piezo-phototronics of InSe and the effect of different strains on the photo-current.[111] Copyright 2019, American Chemical Society. (j) Piezotronics of MoS<sub>2</sub> for humidity sensing.[112] Copyright 2018, American Chemical Society. (k, l) Working mechanism of the effect of the presence or absence of strain on the piezoelectric property of the device with high humidity condition. (m) Effect of different relative humidity and tensile strain on current. (n, o) Temperature sensing and working mechanism of piezotronics of MoS<sub>2</sub>. [113] (p) Effect of different temperature conditions on the output current due to strain. Copyright 2019, Elsevier.

electron-hole pairs in MoS<sub>2</sub>. These carriers are effectively separated and modulated by the built-in and applied electric fields at the Schottky contact, generating photocurrents. This process primarily relies on the effective separation and transport of photo-generated charge carriers within the contact region, a process influenced by the interface barrier. Upon application of mechanical strain, the piezoelectric polarization charge at the MoS<sub>2</sub> edge directly impacts on the metal-MoS<sub>2</sub> interface, altering the distribution and density of free charge carriers near the Schottky barrier. This results in a piezo-phototronic effect that modulates the photoelectric process. The positively polarized charge generated by tensile strain (position 2) diminishes the separation and migration of holes and electrons, elevates the energy barrier for electron transport, and impedes the collection of photogenerated carriers. The application of a small compressive strain (position 3) results in a sloped energy band, which facilitates electron and hole separation in MoS<sub>2</sub>. This separation enhances their transport and thereby boosts the photocurrent. Conversely, an increase in the potential barrier due to larger compressive strain (position 4) inhibits the flow of holes and promotes carrier complexation at the interface. This process also heightens the dark current, consequently diminishing detector performance and reducing the photocurrent. These changes underscore the critical role of piezoelectric polarization in modulating photodetector performance. Furthermore, the screening effect of free carriers can be significantly mitigated by enhancing the crystal quality of MoS<sub>2</sub>. The photovoltaic response can also be markedly improved when tensile strain is applied. [140] In addition to single material of MoS<sub>2</sub>, Zhang et al. leveraged the piezoelectric property of monolayer MoS<sub>2</sub> to modulate the bandgap structure of a heterojunction interface by constructing a CuO/MoS<sub>2</sub> heterostructure flexible photodetector (as depicted in the lower section of Fig. 7a). [68] This approach effectively widened the depletion region, thereby facilitating the efficient photogenerated carriers separation and transport. As a result, there was a significant enhancement in both photocurrent and sensitivity. Other materials such as InSnSe and InSe also exhibit unique piezo-photonic and photovoltaic properties similar to those of MoS<sub>2</sub>. Inbaraj et al. investigated the potential for realizing a piezo-phototronic effect in InSnSe material through the application of mechanical strains, which significantly improved the performance of flexible photodetector (Fig. 7c). [69] InSnSe, characterized by a small number of layer structures, demonstrated a markedly enhanced photocurrent when subjected to bending strain, underscoring its potential for use in flexible photodetection applications. The variation of photocurrent with different strains and laser power densities is shown in Fig. 7d. The contour plot clearly indicates that both bending strain and laser power can significantly enhance the photocurrent. Dai et al. increased the photocurrent by applying tensile strain to InSe, which was achieved through the piezoelectric effect of multilayer  $\gamma$ -InSe (Fig. 7e). [111] Fig. 7f presents the photocurrent response of InSe to varying levels of uniaxial tensile strain under the illumination of the 650 nm light. It is observed that larger strains lead to a significant increase in photocurrent.

In addition to augmenting photosensitivity, Guo et al. engineered an advanced humidity sensor utilizing the piezoelectric effect of monolayer MoS<sub>2</sub> (Fig. 7j). [112] In conditions of high humidity and no strain, a substantial number of water molecules could be adsorbed onto the device surface. This adsorption effectively reduced the conductance of MoS<sub>2</sub> due to the trapped electrons. The accumulation of negative electrons at the Pd-MoS<sub>2</sub> contact interface escalates the Schottky barrier, resulting in a reduction in the sensor's output current under high relative humidity (RH) (Fig. 7k). Conversely, the application of tensile strain at elevated humidity levels, despite generating a positive piezoelectric charge, is partially shielded from the influence of strain-induced polarization charge. This is due to the increased electron accumulation facilitated by water molecule adsorption, which diminishes the modulation of the sensor's performance by the piezoelectric effect less effective at high RH compared to low RH (Fig. 7l). The data presented in Fig. 7m illustrates the impact of varying RH and tensile strain on the

sensor's output current. A reduction in RH and an increase in strain can enhance the output current to a certain degree, thereby affirming the role of the piezoelectric effect in modulating the performance of monolayer MoS<sub>2</sub> humidity sensors.

Sohn et al. conducted a comprehensive investigation on the piezotronic effect of MoS<sub>2</sub> under the influence of different temperatures (Fig. 7n). [113] Fig. 7o illustrates the operational mechanism of the MoS<sub>2</sub> piezotronic effect in relation to temperature variations. In an elevated temperature environment, there is an increase in the number of electrons within the n-type MoS<sub>2</sub> due to the rise in thermally excited electrons. According to the energy band distribution, the likelihood of an electron occupying a specific energy level is contingent upon the Fermi energy and temperature. When subjected to tensile strain, MoS<sub>2</sub> generates piezoelectric charges near the electrode-MoS<sub>2</sub> interface. However, these charges are partially neutralized at higher temperatures due to the increased pressure of thermally excited electrons within MoS<sub>2</sub>, a process known as screening effect. Consequently, the shielding effect of the piezoelectric potential at elevated temperatures fails to significantly alter the Schottky barrier at electrode-MoS<sub>2</sub> contact, resulting in minimal changes in the charge transport behavior of MoS<sub>2</sub> at high temperatures. Conversely, at low temperatures, the number of thermally excited electrons decreases, thereby weakening the screening effect of the strain-induced piezoelectric potential and leading more significant changes in the Schottky barrier. Fig. 7p depicts the variation in current  $\Delta I$  induced by strain under varying temperature conditions, which is defined as the variation in current between the strained  $\epsilon$  and the unstrained state at a 10 V bias. The findings indicate that the current escalates with an increase in strain, with higher temperature resulting in more significant  $\Delta I$  changes. This suggests that the piezoelectric charge modulates the Schottky barrier at the electrode-MoS<sub>2</sub> contact, thereby affecting the charge transport behavior of MoS<sub>2</sub>. This confirms the role of the piezoelectric effect in modulating the performance of monolayer MoS<sub>2</sub> temperature sensors.

Piezotronic effects have shown considerable promise in modulating the photoresponsivity, humidity sensing, and temperature sensing of materials. This has paved the way for advancements in environmental monitoring and the creation of smart devices. By mechanically controlling the electronic structure and internal electric field of materials with precision, piezotronics can not only achieve a highly sensitive response to light signals but also regulate device performance in environments where humidity and temperature fluctuate. This significantly enhances the adaptability and functionality of smart sensors.

## 5.2. Piezoelectric nanogenerator based mechanical sensing and energy storage

Piezotronics, which leverages the internal polarization charge of a material to detect and react to mechanical pressure, presents novel opportunities for sensors and energy harvesting devices that operate without an external power source. 2D materials not only possess a thickness-dependent bandgap and high carrier mobility but also demonstrates significant potential for piezoelectricity and piezotronics applications due to their unique directionality and non-centrosymmetric lattice structures. These non-centrosymmetric lattice structures allow 2D materials to generate electrical energy through mechanical pressure instead of applying any external power supply. This provides new design concepts and implementation pathways for developing self-powered wearable sensors and electronic systems.

Ma et al. conducted a comprehensive investigation into the piezoelectric characteristics of multilayered BP, as depicted in Fig. 8a. [71] BP, a 2D material, exhibits a band gap that varies with thickness and possesses high carrier mobility. Under strain, the non-centrosymmetric lattice structure induces an interlayer charge shift, leading to the creation of a piezoelectric potential difference between electrodes. This facilitates the generation and modulation of the current. Fig. 8b illustrates the piezoelectric output current response in the armchair direction of the

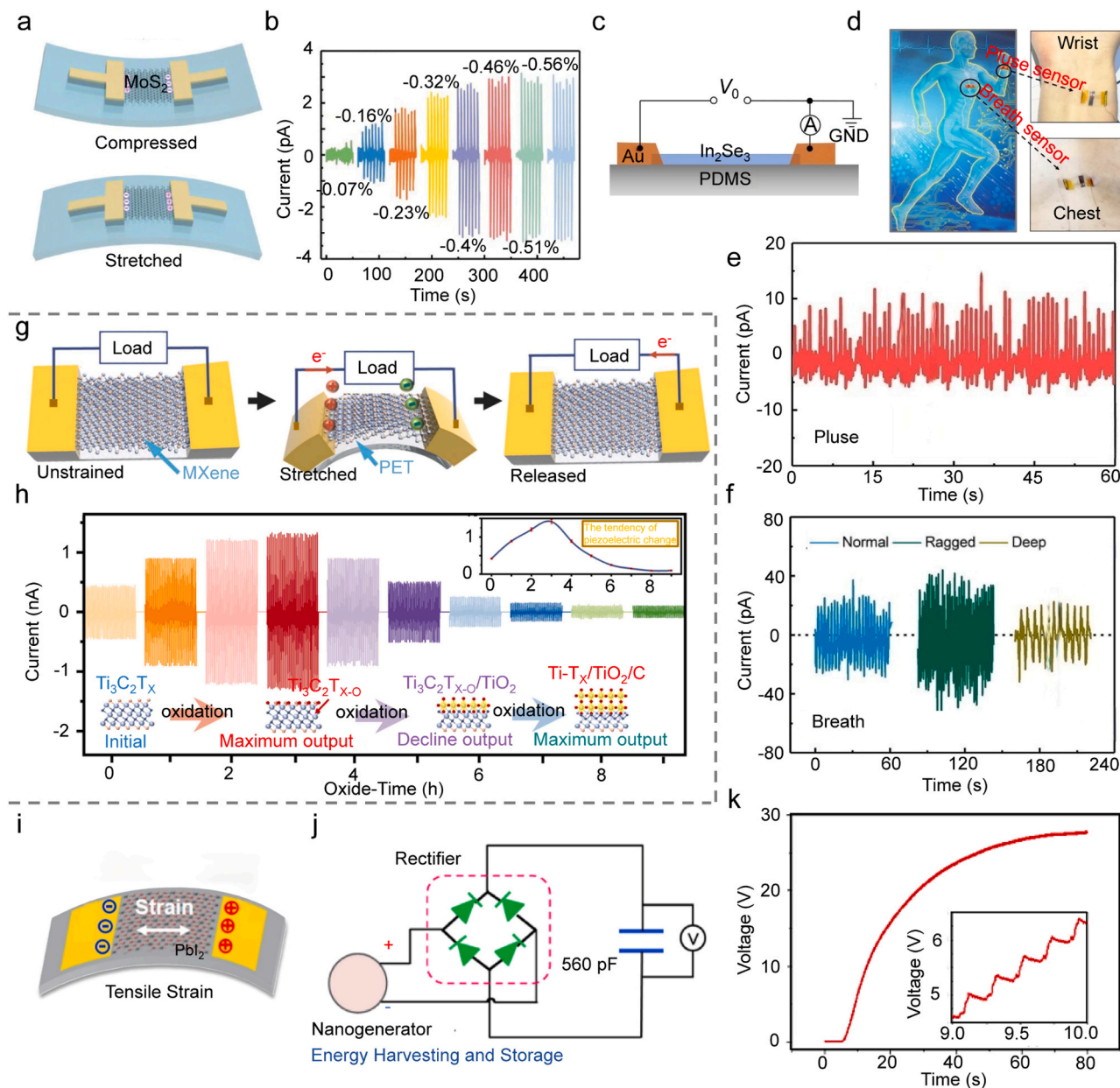


**Fig. 8.** PENG based on piezotronics in 2D materials for mechanical sensing and energy storage applications. (a, b) Multilayer black phosphorus (BP)-based PENG and output currents at different strains.[71] Copyright 2020, Wiley-VCH. (c, d) Multilayer  $\alpha$ - $\text{In}_2\text{Se}_3$ -based PENG and its use for physiological monitoring by attaching to human wrist and chest.[72] (e, f) Real-time monitoring of human pulse and breath data based on PENG sensors. Copyright 2019, American Chemical Society. (g, h) Mechanical sensing of PENG based on monolayer oxidized MXene and the effect of material oxidation on its output current.[114] Copyright 2023, Elsevier. (i) PENG based on  $\text{PbI}_2$  nanosheets.[73] Copyright 2018, Elsevier. (j, k) Schematic of the circuit structure and results of capacitor charging based on PENG for mechanical energy storage.

multilayer black phosphorus structure under periodic strain. The piezoelectric current escalates with an increase in compressive strain, demonstrating an inverse current response upon strain release. By utilizing integrated PENG as the mechanical sensing unit, Dai et al. fabricated a multilayer  $\alpha$ - $\text{In}_2\text{Se}_3$  sensor on polydimethylsiloxane (PDMS) flexible substrate (Fig. 8c).[72] The flexibility and wearability of this structure make it particularly suitable for physiological monitoring against human skin (Fig. 8d). By attaching the sensor to the wrist and chest, human pulse and breathing patterns can be monitored in real time. The sensor recorded a pulse rate of approximately 72 beats per minute as shown in Fig. 8e. Whether monitoring rapid shallow breathing or deep breathing, the device accurately captured the changes in breathing frequency and chest expansion, showing current signals that were synchronized with the respiratory rate as shown in Fig. 8f. These

results not only prove the effectiveness of the sensor in tracking physiological conditions but also show its excellent temporal resolution. The structural features of 2D piezoelectric materials have a significant influence on the output of PENG. Jiang et al. demonstrated the potential of monolayer oxidized MXene for mechanical sensing of NGs and underscored the influence of material oxidation on its piezoelectric properties (Fig. 8g).[114] The current output of oxidized MXene subjected to varying mechanical strains is depicted in Fig. 8h, which emphasizes the crucial role of the oxide layer in amplifying the piezoelectric response of the material. Following a three-hour oxidation process, the piezoelectric device fabricated from MXene achieved its peak output level with the composition of  $\text{Ti}_3\text{C}_2\text{T}_x\text{-o}$ . This discovery offers a novel avenue for 2D materials applied in the area of energy harvesting and sensory technology.

Energy harvesting and energy storage are commonly required to be complementary and hybridized for use. Storing the energy produced by the PENG not only enhances the efficiency of energy utilization but also bolsters system reliability, enabling the device to operate sustainably without continuous mechanical stimulation. Furthermore, energy storage enables the device to execute more complex or energy-intensive tasks even in environments devoid of mechanical activity, such as data processing and information transmission. Consequently, energy storage for PENGs is crucial for optimizing system performance and adapting to

fluctuating environmental conditions, thereby propelling the adaptability of self-powered devices and systems. Song et al. employed  $\text{PbI}_2$  nanosheets for piezoelectric energy harvesting and strain sensation (Fig. 8i). [73] Figs. 8j and 8k further illustrate the schematic circuit structure of this PENG for mechanical energy storage and the results of capacitor charging, respectively. The alternating current signal is converted to direct current by a rectifier bridge and charges a 560 pF capacitor, which can reach a voltage of 27.2 mV after 80 s of charging.

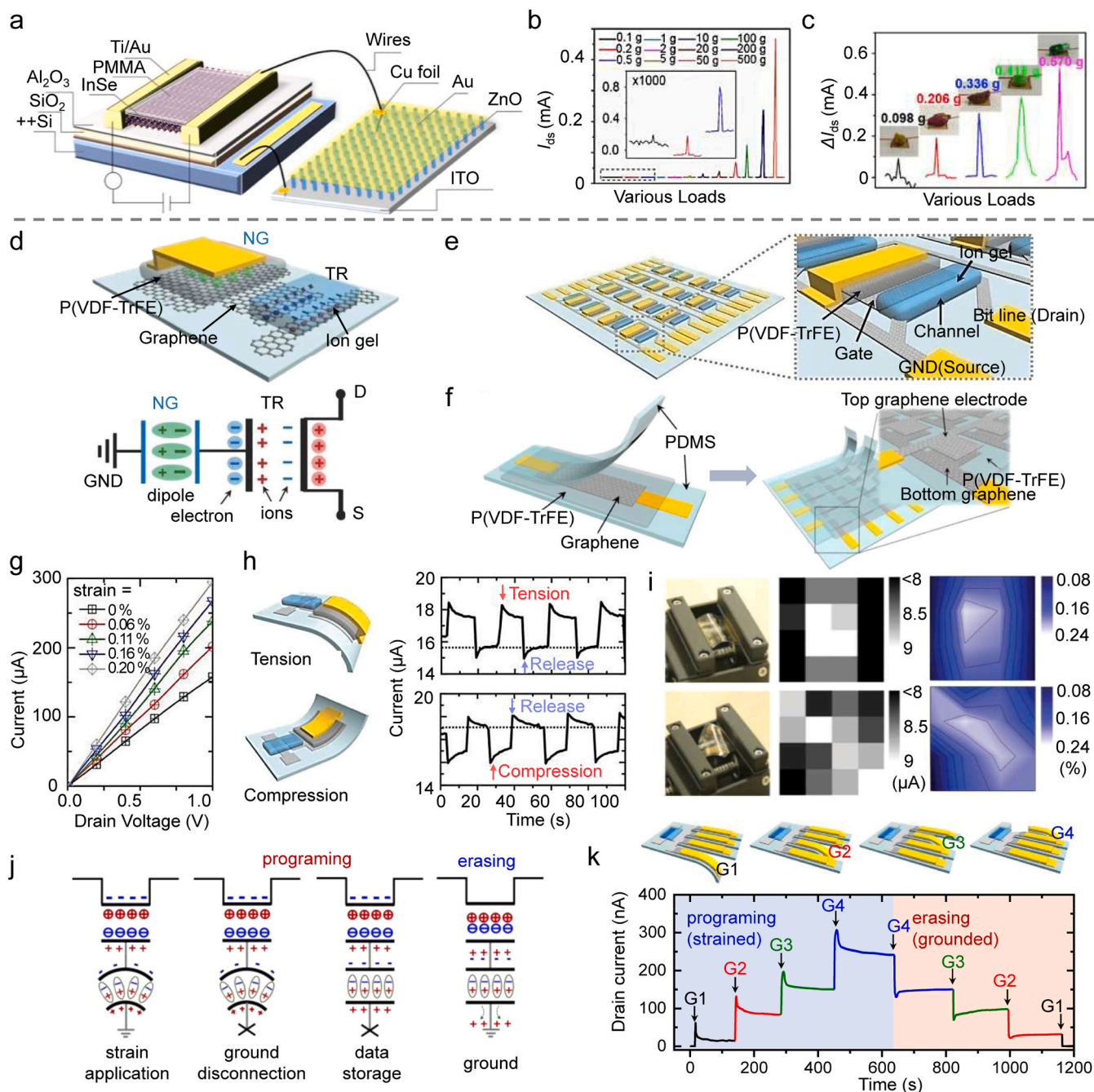


**Fig. 9.** PENG-modulated 2D FET for mechanical sensing applications. (a) PENG based on ZnO NW array to modulate InSe 2D FET. [115] Copyright 2020, Elsevier. (b) Effect of different load masses on PENG-modulated InSe FET. (c) Response of PENG-modulated InSe FET to different weight objects. (d) P(VDF-TrFE) based PENG combined with ion-gel to modulate graphene FET. [39] (e, f) P(VDF-TrFE) and ion-gel allow large area preparation of array structures. [39,40] Copyright 2015, Wiley-VCH. Copyright 2018, American Chemical Society. (g) Current-voltage ( $I$ - $V$ ) characteristics of P(VDF-TrFE) based PENG-modulated graphene FET with different mechanical strains. (h) Effect of different strains on PENG output current. (i) Strain mapping based on a  $4 \times 4$  array. (j) Mechanical stimulation information storage based on the strategy of combining PENG with ion-gel. [141] Copyright 2016, American Chemical Society. (k) Four PENGs coupled to a single ion-gel gate dielectric of IGZO FET for multilevel programming and erasing.

## 6. Applications of PENG-modulated 2D field effect transistors

The integration of PENG and 2D FETs represents a prevailing research trend, offering substantial multifaceted benefits over the reliance on the inherent piezoelectric effect of the 2D material. Primarily, PENG significantly boosts system efficiency due to its superior energy conversion capability. Furthermore, its superior design and integration flexibility facilitates compatibility with versatile electronic and optoelectronic devices. The standalone PENG notably enhances mechanical stability and durability, diminishing dependence on the mechanical properties of the 2D materials. The incorporation of PENG also broadens material selection, encourages the use of additional 2D materials lacking a natural piezoelectric effect, and allows for multi-parameter modulation on semiconductor devices, thereby optimizing the functionality and diversity of the system.

The role of 2D FETs is pivotal in such a system. They not only convert and amplify the minuscule piezoelectric potential signals produced by the PENG into detectable current signals, thereby facilitating an effective conversion from mechanical to electrical energy, but also operate at extremely low voltages, satisfying the demands for low-power operation. Owing to the high electron mobility and sensitivity of 2D materials like graphene and MoS<sub>2</sub>, 2D FETs can respond acutely to minute voltage fluctuations. This not only amplifies the sensitivity of PENG-based systems but also broadens their utility across various applications, including health monitoring, intelligent robots, and environmental surveillance. Furthermore, 2D FETs can be integrated with other electronic or optoelectronic devices on a unified platform to execute more sophisticated logic functions and data processing. This integration further expands the system's application scope and functionality, underscoring the significant potential of this technology in the realm of high-performance electronic/optoelectronic devices.

### 6.1. Mechanical sensing

Mechanical sensing serves as the fundamental function of a PENG, leveraging the piezoelectric potential produced by mechanical stimuli such as pressure and bending to directly modulate the gate voltage of a 2D FET. This enables the transistor's switching and modulation without necessitating an external power supply. Wang et al. constructed their PENG using ZnO NW arrays to modulate an InSe 2D FET, as depicted in Fig. 9a.[115] In this configuration, an array of ZnO nanowires directly interfaces with the back gate of the InSe FET. When subjected to an external force, the ZnO generates a piezoelectric potential that serves as the FET's gate voltage, thereby regulating its drain current. Consequently, alterations in the piezoelectric potential can be directly observed through corresponding changes in the drain current ( $I_D$ ). Fig. 9b illustrates the increase in  $I_D$  correlating with an increase in the piezoelectric potential as load mass applied to the ZnO increases, highlighting the sensor's high sensitivity and responsiveness to gravity variations. Therefore, this device is anticipated to differentiate between objects of varying masses. As illustrated in Fig. 9c, when objects of differing weights exert pressure on the ZnO, their weights are analyzed and identified by measuring the change in  $I_D$ . Given its exceptional sensitivity and accuracy, this piezoelectric sensor holds significant potential for practical applications in gravity sensing.

Sun et al. have effectively employed polyvinylidene fluoride-trifluoroethylene P(VDF-TrFE) in conjunction with ion-gel to modulate 2D FETs in their research, contributing significantly to various works on mechanical sensing applications. The ion-gel's rapid response to external voltage changes and its exceptionally high dielectric constant enable effective transistor modulation even with the lower voltages generated by the PENG. This makes it particularly suited for applications that convert mechanical strain into low-energy electrical inputs. Furthermore, the flexibility and stretchability of the ion-gel allow it to be integrated with flexible PENG and graphene transistors, thereby facilitating the creation of flexible electronic devices.[39] As depicted in

Fig. 9d, this system's PENG generates a piezoelectric potential through its non-centrosymmetric crystal structure when subjected to mechanical pressure, thereby forming an enhanced electric dipole. This will induce piezoelectric potential to regulate the migration of ions within the ion gel to form an electric double layer (EDL), which serves as a surrogate for the gate voltage in conventional FETs. The EDL functions as an ultrathin capacitor at the interface of the ion-gel/transistor's gate. It controls the carrier concentration (either electrons or holes) in the transistor's channel region by modulating the gate potential. This enables rapid response and switching control of the transistor. This technology offers not only a fast response but also extremely low power consumption, presenting an innovative solution for the development of sophisticated sensing devices in low-energy and high-efficiency. Furthermore, P(VDF-TrFE) and ion-gel can be utilized on expansive areas with straightforward masking and lithography techniques to construct array structures (Fig. 9e, f).[39,40] Fig. 9g illustrates the output characteristics of P(VDF-TrFE) based PENG modulated graphene transistors under varying mechanical strains. The conductivity of the graphene transistor escalates with an increase in applied strain, thereby demonstrating its modulability and high sensitivity for practical applications. Moreover, when 0.06 % tensile or 0.06 % compressive strain is applied to the PENG, piezoelectric potentials of opposing signs can be generated, leading to changes in the output current signal in opposite directions (Fig. 9h). This is due to the fact that the direction of the piezoelectric potential alters with strain. Under tensile strain, the piezoelectric potential generated by NG induces an increased number of holes in the channel, while under compressive strain, there is a corresponding decrease number of holes in the channel. This phenomenon is associated with the Dirac voltage of the graphene transistor at approximately 1 V, which serves as the critical voltage point controlling the carrier type transition. Building upon the devices with  $4 \times 4$  arrays, Fig. 9i presents a 2D mapping of the output current distribution from these arrays against the strain distribution under varying mechanical strains. This color-contour map not only offers an intuitive visualization of the pressure position distribution but also highlights the device's capacity to decode intricate external motions through the associated pressure magnitude.

Furthermore, the integration of PENG with ion-gel offers the potential for mechanical stimulus information storage.[141] As illustrated in Fig. 9j, the PENG is first actuated by applying a mechanical strain to generate the required piezoelectric potential. The carriers in the transistor channel are then sustained by disconnecting the NG bottom electrode from the ground, ensuring that the charge carriers in the channel remains stable even after releasing the strain due to the piezoelectric potential preventing holes in the channel from flowing back through the external circuitry to form a stable EDL. Data erasure is achieved by reconnecting the bottom electrode of the PENG connected to ground, which neutralizes the previously induced charge via an external circuit. Sun et al. demonstrated multilevel programming and erasure by using four PENGs coupled to a single ion-gel gated IGZO FET (Fig. 9k). Each NG was capable of signal recording at four different current levels by applying a 0.2 % strain, disconnecting the ground, and performing data storage, respectively. As each NG's electrodes are re-grounded individually, the drain current is progressively reduced. This multi-level storage and erase mechanism is crucial for storage devices requiring multiple mechanical signal recording, highlighting its unique potential for practical applications.

### 6.2. Schottky barrier modulation

The piezoelectric potential of PENGs has been proved to effectively modulate the electronic performance of semiconductor devices. Specifically, the barrier height can be modulated by altering the interface property of the metal-semiconductor contact. This allows for more precise and efficient charge injection and control, which are essential for enhancing the performance and responsiveness of the devices. PENGs

typically require direct contact with semiconductor materials to achieve effective barrier modulation. However, discrepancies in bandgap, work function, and electron affinity between materials can lead to interface mismatch issues.[63] For instance, the insulating nature of the wide bandgap of piezoelectric polymers limits its direct role in energy barrier modulation due to its effect on the modulation of the semiconductor energy bands. Kim et al. effectively addressed this issue by integrating a PENG with a graphene/IGZO vertical Schottky barristor (Fig. 10a). [116] The piezoelectric potential can effectively implement gate modulation via EDL in an ion-gel. The linear energy dispersion and high conductivity of graphene's energy band structure make its work function easily modulated by an electric field. Furthermore, the piezoelectric potential generated by the PENG can dynamically modulate the barrier height under varying strain states, thereby affecting the device's

conductivity and switching characteristics. As illustrated in Figs. 10b and 10c, the device modulates the Schottky barrier at the IGZO/graphene interface via the ion-gel. Under applied pressure, the induced piezoelectric potential shifts the Fermi energy level of graphene upwards or downwards, consequently increasing or decreasing the electron injection barrier from graphene to IGZO. The multilevel modulation of the graphene/IGZO barrier height was successfully accomplished by connecting two PENGs with the graphene gate electrode (Fig. 10d). Upon applying a tensile strain of 0.08 % to one PENG, the resultant positive piezoelectric potential increased the electron count within the graphene and elevated its Fermi energy level. When this same tensile strain is subjected to the second PENG, the corresponding piezoelectric potential further intensifies the accumulation of electrons, prompting the Fermi energy level to continue its upward trajectory (upper part

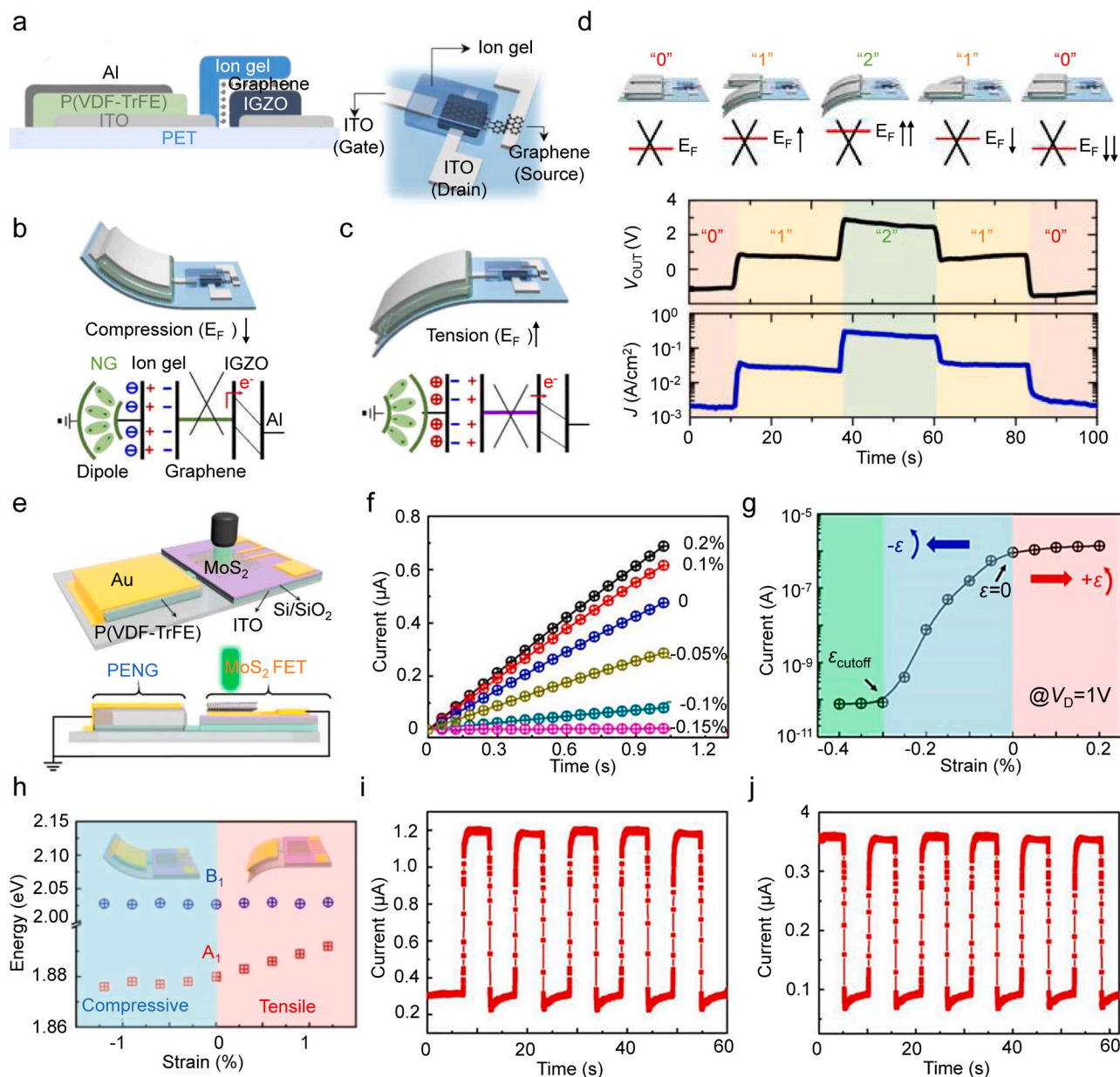


**Fig. 10.** PENG-modulated 2D FETs for band structure engineering applications. (a) Graphene/IGZO vertical Schottky barristor based on P(VDF-TrFE) PENG modulation. [116] Copyright 2018, Elsevier. (b, c) Working mechanism of modulating the Schottky barrier at the graphene/IGZO interface with different mechanical strains. (d) Multi-level modulation of graphene/IGZO barriers realized by two PENGs coupled with ion-gel to graphene electrodes. (e) Static and dynamic barrier modulation of MoS<sub>2</sub> FET based on P(VDF-TrFE) PENG. [117] Copyright 2019, American Chemical Society. (f) Current-voltage (*I*-*V*) characteristics with different strains. (g) Transfer characteristics of the device with different strains. (h) Changes in the peak position of MoS<sub>2</sub> luminescence spectrum with different strains. (i, j) Dynamic electrical response of MoS<sub>2</sub> FETs under tensile and compressive strains.

of Fig. 10d). As the external stress is gradually relieved, the Fermi energy level of graphene decreases in a stepwise manner. The lower part of Fig. 10d illustrates the stepwise change in both the output of the PENG and the current density of the graphene transistor.

2D materials, exemplified by MoS<sub>2</sub>, present several challenges for practical applications in piezoelectric modulation. Firstly, fabricating high-quality single-crystal odd-layer MoS<sub>2</sub> and the establishment of optimal ohmic contacts with metals remain significant obstacles. Secondly, the mechanically-induced piezoresistive and piezoelectric effects in MoS<sub>2</sub> may overlap, leading to alternations in the energy band structure. This could introduce unpredictable variables in the design of precision electronic devices. Accordingly, it is critical to explore a simpler and universally applicable strategy for realizing piezoelectric modulation in 2D semiconductor devices. One such approach is the use of capacitive coupling to circumvent these limitations of MoS<sub>2</sub>. This method not only simplifies the technical process but also effectively avoids application barriers due to material defects. Sun's group employed P(VDF-TrFE) to achieve static and dynamic barrier modulation for MoS<sub>2</sub> FETs (Fig. 10e). [117] In static modulation, the residual polarization of P(VDF-TrFE) influences the Fermi energy level of the

MoS<sub>2</sub> channel through capacitive coupling, thereby altering the initial electrical properties of the channel. In dynamic modulation, the externally applied strain enhances or weakens the piezoelectric potential by adjusting the arrangement of dipoles in P(VDF-TrFE). This, in turn, modulates the energy band in MoS<sub>2</sub> channel and realizes highly sensitive modulation on the current. Fig. 10f illustrates the output characteristics under varying strain conditions. The transfer characteristics of the device, as depicted in Fig. 10g, demonstrate a transition from a very low conductance state ( $10^{-10}$  A) to a relatively high conductance state ( $10^{-6}$  A) under external strain conditions. This transition signifies the highly sensitive modulation of the MoS<sub>2</sub> FET channel's conductance achieved through applied strain. The strain-induced alteration in the piezoelectric potential directly influences the energy band and electron transport properties in MoS<sub>2</sub>. Furthermore, the shift in the peak position of the MoS<sub>2</sub> luminescence spectrum due to different strains can also indicate changes in the device's energy band. As depicted in Fig. 10h, the A<sub>1</sub> exciton peak of the MoS<sub>2</sub> sample undergoes a blueshift as the external strain increases from compression -1.2% to tension 1.2%. The shift is primarily attributed to the accumulation of free electrons, which are induced by the piezoelectric potential. This process diminishes the

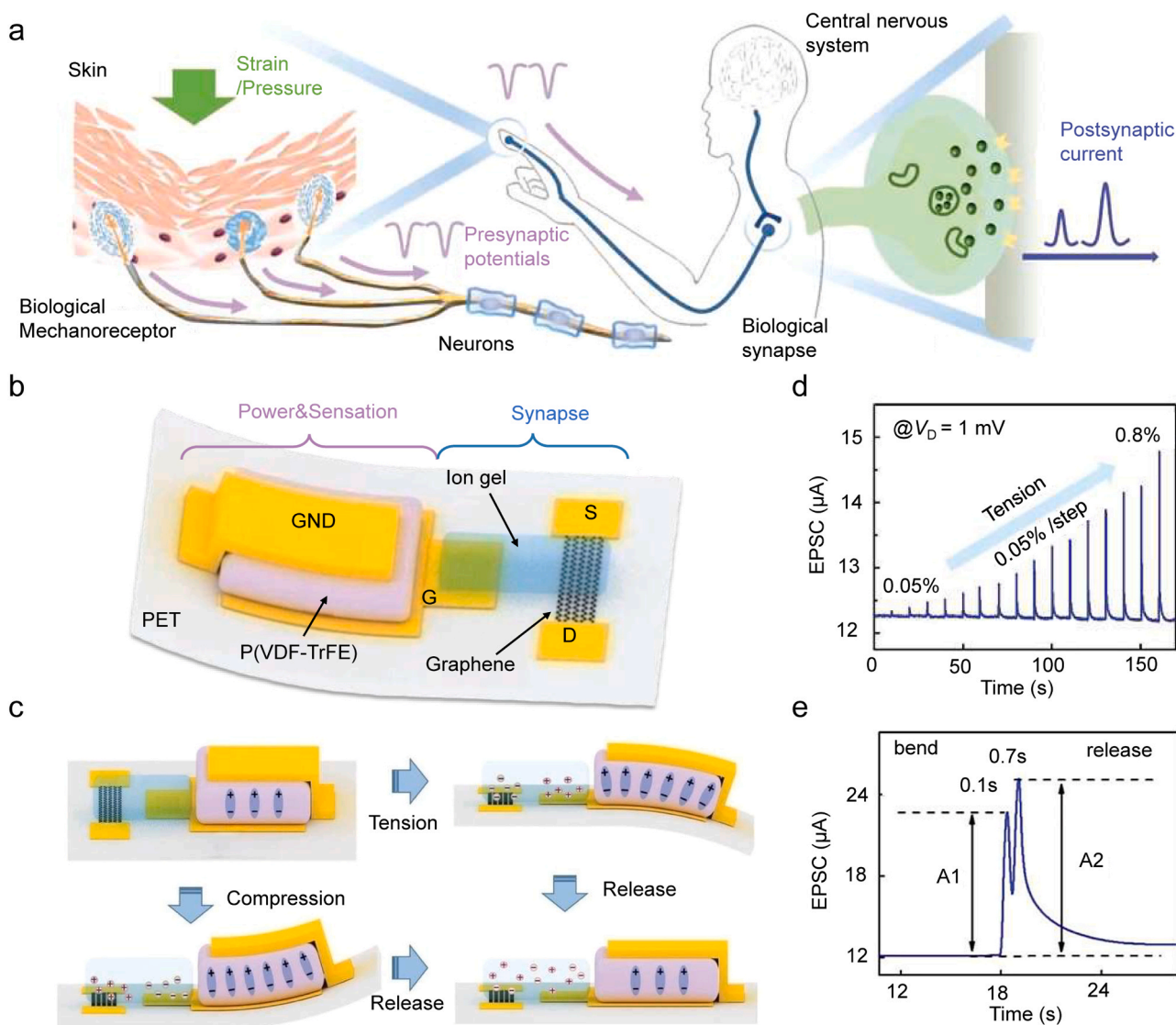


**Fig. 11.** PENG-modulated 2D FET for artificial synapse applications. (a) Schematic diagram of a biological sensing nervous system. [76] The human sensory system consists of three main components: stimulus receptors, afferent nerves and the central nervous system. (b) Artificial sensory synaptic system based on P(VDF-TrFE) based PENG modulated ion-gel gated graphene FET. [76] Copyright 2019, Wiley-VCH. (c) Working mechanism of artificial sensory synapse. (d) Effects of different tensile strains on the excitatory postsynaptic current (EPSC) of the device. (e) Typical short-term plasticity-enhanced paired-pulse facilitation behavior of synapse.

passivation of the MoS<sub>2</sub> surface states, akin to the effect produced by directly applying a positive gate voltage. Conversely, the position of the B<sub>1</sub> peak remains relatively stable under varying strains, which can be ascribed to the lesser impact of the piezoelectric potential on the spin-orbit splitting in the MoS<sub>2</sub> valence band. These findings suggest that the external strain induced piezoelectric potential is comparable to the conventional gate voltage effect in modulating the optoelectronic properties of MoS<sub>2</sub>. Fig. 10i and Fig. 10j illustrate the dynamic electrical response of MoS<sub>2</sub> FETs under the tensile strain (0.1 %) and compressive strain (-0.1 %), respectively. The alteration in strain directly influences the carrier density of the MoS<sub>2</sub> channel, thereby rapidly modulating the current output of the device.

### 6.3. Artificial synapses

Fig. 11a presents a schematic illustration of the biological sensory nervous system.[76] The human sensory system is comprised of three primary components: stimulus receptors, afferent nerves, and the central nervous system. Together, these components form a comprehensive pathway from the perception of the external stimuli to their processing by the brain. Stimulus receptors detect and respond to specific environmental stimuli (e.g., pressure, touch, temperature) and convert these physical or chemical stimuli into electrical signals. Afferent nerves transmit these electrical signals received from the receptors to the central nervous system. The central nervous system serves as the final processing center for sensory information, where incoming signals are further analyzed, integrated, and interpreted to form a perception and awareness of the stimulus. This may result in appropriate response commands. Within the nervous system, the critical link in information transfer occurs in specialized structures known as synapses. Presynapses, are located at the ends of neurons, act as signal transmitters. Upon the arrival of an electrical signal at the presynapse (termed an action potential (AP)), neurotransmitters will be released from synaptic vesicles into the synaptic cleft. These neurotransmitters are subsequently bound to receptors on the postsynapse, instigating either activation or inhibition of the AP from that neuron. This process consequently influences electrical activity of the subsequent neuron. The meticulous chemical-to-electrical signaling mechanism ensures the nervous system's function to efficiently and accurately process complex information.

The design of artificial sensory systems should emulate the intricate biological mechanisms they are intended to mimic. An effective artificial sensory system should possess the capacity to perceive external stimuli with sensitivity, transmit signals swiftly and accurately, and process and integrate information efficiently. Chen et al. have developed a P(VDF-TrFE) based PENG-modulated artificial sensory synaptic system, which includes a PENG as a stimulus receptor and a solid-state electrolyte gated graphene FET as a synapse (Fig. 11b).[76] The synaptic behavior is initiated by mechanical strain on the piezoelectric potential generated by the PENG, which is capacitively coupled to the transistor device through the ion-gel dielectrics. This device replicates the function of a biological synapse, wherein mechanical stress is directly converted into synaptic current, thereby simulating neuronal signal transmission. Fig. 11c provides a detailed explanation of how mechanical strain can be converted into electrical signal via the piezoelectric potential. Upon the application of mechanical tensile strain, the piezoelectric potential generated by the PENG facilitates the formation of the EDL and a negative gate voltage in the ion-gel. This process prompts anion migration to the ion-gel/graphene interface, resulting in a downward shift of the Fermi energy level of graphene. This shift enhances hole transport in the channel, thereby increasing the channel current. Upon release of the strain, the piezoelectric potential dissipates, the ions revert to their original state, and the channel current returns to its baseline level. Conversely, the application of mechanical tensile strain promotes the formation of a positive gate voltage and elevates the Fermi energy level of graphene, thereby enhancing the electron carrier-dominated

transport. Fig. 11d illustrates the effect of varying tensile strains on the postsynaptic current (PSC). The PSC significantly increases with the amplitude of strain, indicating that the synaptic device is sensitive to the corresponding external mechanical stimuli. Furthermore, due to the accumulation properties of ions at the graphene/ion-gel interface under multiple stimuli, the device exhibits the paired-pulse facilitation behavior characteristic of short-term synaptic plasticity (Fig. 11e). This behavior is crucial for the temporal encoding of information.

The integration of PENGs with synaptic transistors has paved the way for a novel, self-powered and low-power operation of synaptic devices. Unlike conventional synaptic devices that depend on external power sources or intricate gate control mechanisms, PENGs efficiently convert mechanical stimuli into electrical signals by directly harnessing the electrical potential produced by mechanical strain, also known as the piezoelectric potential. This triggers a synaptic response. The direct conversion mechanism not only eradicates the need for external energy sources but also significantly diminishes the system's overall energy consumption. Another unique feature of the PENG synaptic system is its capacity to dynamically adjust synaptic weights in real time. This mechanism responds to varying stimuli through mechanical strains, enabling the system to swiftly adapt to environmental changes. This attribute is particularly crucial in applications that demand rapid processing and response to sensory inputs, such as self-powered e-skins, neural interfaces, and intelligent human-computer interaction systems.

## 7. Tribotronics

During the continuous development of PENG, another novel device, TENG, has been pioneered by Wang's research group since 2012.[142] This device leverages the contact/tribo-electrification and electrostatic induction effects between different materials to effectively harvest high-entropy/low-frequency mechanical energy from the environment. This has led to its extensive application in various fields such as self-powered systems, energy harvesting, and sensing technologies. In contrast to traditional FETs that depend on external voltages to control charge carriers, Zhang et al. in 2014 achieved direct regulation of electron transport in FETs by using the TENG generated triboelectric potential as the gate voltage.[101] This breakthrough not only ushered in the field of tribotronics but also demonstrates the potential for direct manipulation of semiconductor devices through mechanical energy, thereby enhancing the energy efficiency of these devices and their interaction with the environment. Tribotronics, which is based on nano-tribology and semiconductor device technology, aims to research and develop novel energy-efficient and systems for human-machine interfaces, electronic skin, smart and wearable sensing applications. By combining tribotronics with optoelectronics, electromagnetics, integrated circuits, and MEMS technologies, it is facile to develop tunable triboelectric functional devices and explore large-scale integration and intelligent interactive technologies.[98,143,144] Furthermore, TENG presents several notable advantages over PENG. Firstly, TENG provides a broader range of material options. Unlike PENGs that depend on specific piezoelectric materials, TENGs can employ a variety of common materials such as metals, polymers, and fur. These materials are not only readily available but also relatively inexpensive. Secondly, TENG is capable of responding to a wider array of mechanical stimuli, including light touch, wind, droplet impact, and human movement. It can effectively convert the stimuli into electricity, thereby demonstrating exceptional flexibility in environmental energy harvesting. Additionally, the triboelectric potential generated by TENG is typically higher than the piezoelectric potential generated by PENG. This characteristic provides superior efficiency and more stable performance in the regulation of electronic devices, particularly in the regulation of electron transport in FETs.

The prototypical tribotronic devices and their corresponding circuits are depicted schematically in Fig. 12a and Fig. 12b,[101] which are composed of a MOSFET with back-gated p-type silicon channel coupled

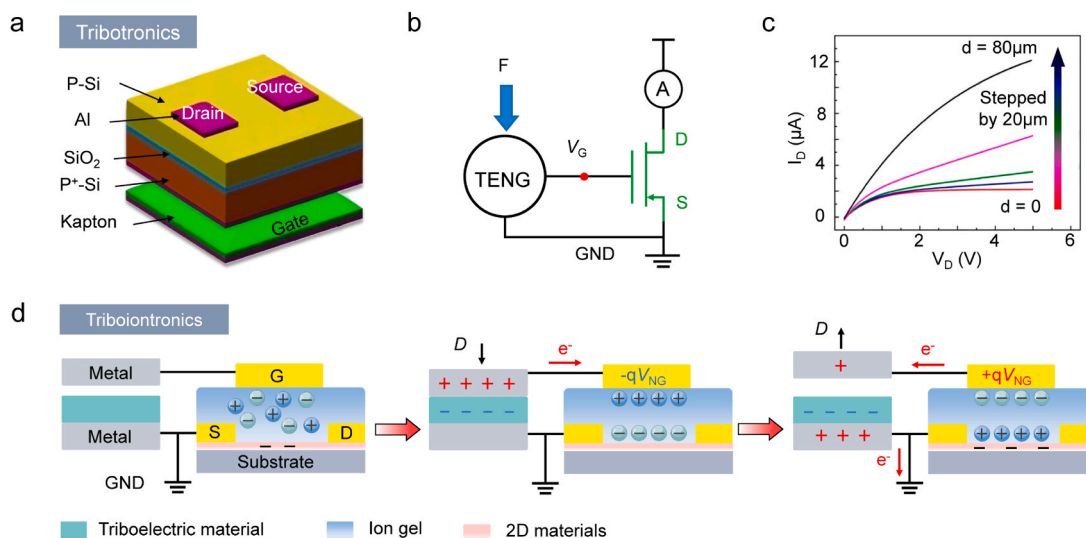


**Fig. 12.** Tribotronics and triboiontronics. (a, b) Schematic diagrams of tribotronic device structure and circuit structure. [101] (c) MOSFET output curve based on TENG displacement modulation. Copyright 2014, American Chemical Society. (d) Working mechanism of triboiontronics.

with a moving layer TENG. The moving layer can be vertically engaged and disengaged from the gate electrode under applied external force, thereby modulating the carrier transport via an internally generated electrostatic potential, even in the absence of an external gate voltage. The output curve of the MOSFET, based on TENG displacement modulation, is illustrated in Fig. 12c. A larger displacement of the TENG results in more triboelectric charges, which is analogous to a larger gate voltage, consequently enhancing the channel current. Tribotronics facilitates more flexible control over the electronic characteristics of the device through mechanical displacement, endowing the device with the capability to interactively respond to external mechanical stimuli.

Triboiontronics, a field that integrates triboelectricity, electrolytes, and semiconductors, merges the principles of triboelectrification with ion-controlled semiconductor devices. [145] The operational mechanism of triboiontronics is depicted in Fig. 12d. When the TENG friction layers come into contact, the upper electrode of the TENG, which is connected to the EGFET gate, accumulates a positive charge due to electrostatic induction. This induces an electron transfer toward the EGFET gate, resulting in a negative triboelectric gate voltage ( $-qV_{NG}$ ) and triggering the formation of EDLs. Conversely, when the TENG friction layers are separated, the negative electric field of the TENG gradually diminishes on the upper electrode. This prompts an electron transfer from the EGFET gate to the TENG upper electrode so as to balance the localized electric field. Consequently, this results in a positive triboelectric gate voltage ( $+qV_{NG}$ ) and stimulates the rearrangement of the electrolyte EDLs. The EDLs play a crucial role as a nanogap capacitor, accounting for the majority of the external gate voltage drop. This results in a significant local electric field driven by a minimal voltage, which efficiently modulates the carriers within the semiconductor channel. Concurrently, EDLs display ion-electron interactions, thereby fostering interdisciplinary research on the manipulation of electronic properties via ion migration and rearrangement. Consequently, triboiontronics is paving new paths in the design and functional realization of electronic devices, with particular relevance to e-skins, artificial synapses, sensors, and more.

## 8. Tunneling triboelectrification for 2D materials

Traditional field effect devices utilize a gate voltage to manipulate charge carriers within a semiconductor channel, which is insulated from the gate by the dielectric layer. However, process compatibility issues significantly constrain the large-scale integration of these devices due to the requirement for different high-quality materials for the gate,

insulator, and channel. Furthermore, tribotronics predominantly depends on the relatively large size of the TENG to modulate the nanoscale FETs, making efficient device integration and minimization challenging due to the size mismatches. It is a crucial challenge in triboiontronics whether the modulation effect persists at the micrometer or nanometer scale. Combining the versatile characterization methods of AFM and Kelvin probe force microscopy (KPFM) allows for a systematic study of the nanoscale-effect of triboelectric modulation on charge transfer and subsequent charge diffusion at the material surface. [146, 147] Bu et al. investigated carrier transport in a transistor with MOSFET-like structure by nanoscale triboelectric modulation based on AFM with a Si probe, as shown in Fig. 13a. [146] The  $\text{SiO}_2$  surface above the channel region was scanned and contacted with the AFM probe during the friction process, and the electrons on the AFM probe could be transferred to the  $\text{SiO}_2$  surface because the effective working function of Si is smaller than that of  $\text{SiO}_2$ . After the contact process, large number of transferred charges accumulated on the top  $\text{SiO}_2$  surface, leading to the formation of an internal electric field in the channel region, which can attract holes in the P-channel (Fig. 13b). And the potential distribution on the top  $\text{SiO}_2$  surface was measured by KPFM, as shown in Fig. 13c. Similarly, Kim et al. investigated a novel method based on AFM for nanoscale tunneling triboelectrification to modulate the electronic properties of 2D materials. [148] As depicted in Fig. 13d, charges are generated through the process of rubbing on graphene and silicon dioxide ( $\text{SiO}_2$ )/silicon (Si) substrates using grounded Pt-coated AFM tips. These triboelectrification induced charges tunnel through the graphene and become trapped at the air- $\text{SiO}_2$  interface, thereby acting as invisible floating gates. The average potential change on the graphene surface before and after rubbing is illustrated in Fig. 13e, demonstrating an increase to 80 mV post-rubbing via the AFM. Furthermore, this tunneling triboelectrification is accompanied by a diffusion of charges on the graphene surface. Fig. 13f illustrates the variation in surface potential following the tunnelling triboelectrification of graphene surfaces with differing numbers of layers. It is evident that the charge diffusion is enhanced with an increased layer of graphene, thereby reducing the localized charge accumulation. In single-layer graphene, the potential change is more pronounced due to its thinner structure and lower charge screening effect. This phenomenon provides significant guidance for a deeper understanding of the application of tunneling triboelectrification technique in modulating the electronic properties of 2D materials. The charge density and polarity of tunneling triboelectrification in graphene can be manipulated by adjusting the AFM tip bias (Fig. 13g). When a negative bias is applied, the KPFM image shows

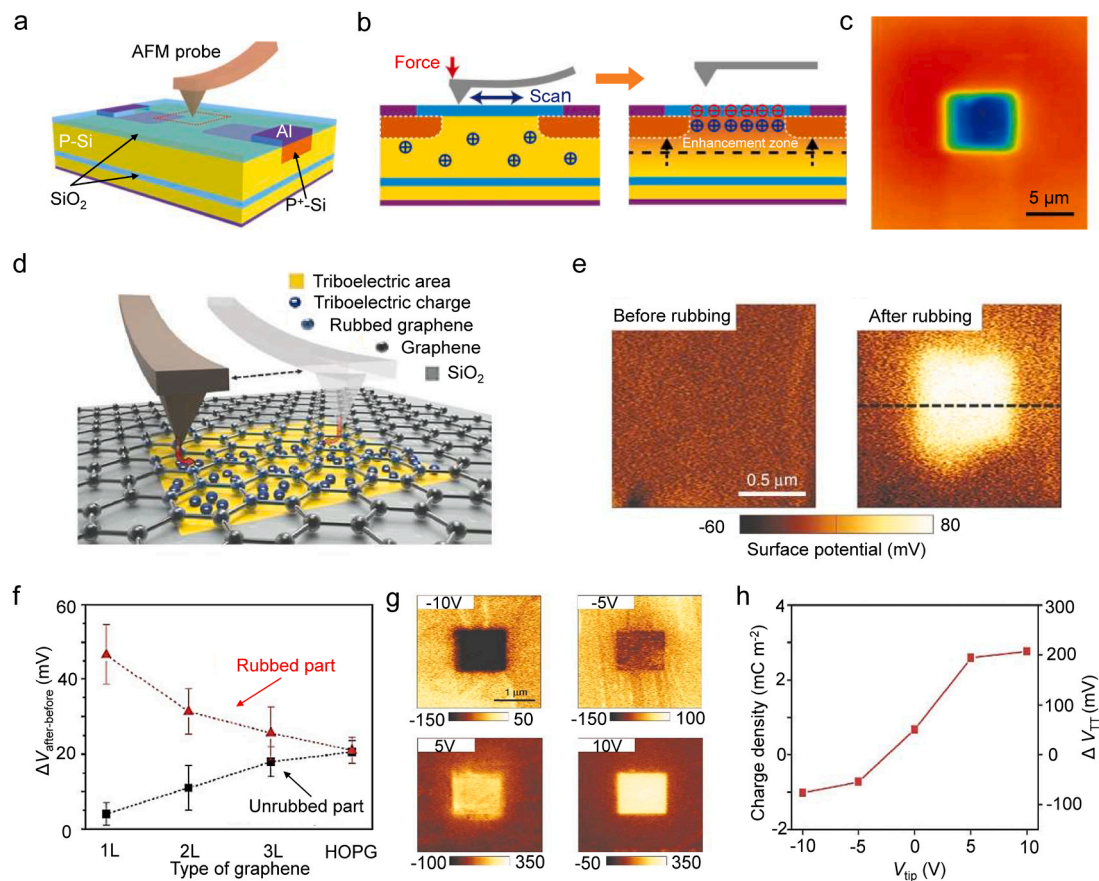


**Fig. 13.** Tunneling triboelectrification to modulate the electronic properties of 2D materials. (a) Schematic of nanoscale triboelectrification modulating carrier transport in a transistor with MOSFET-like structure. [146] Copyright 2020, Springer Nature. (b) Working mechanism of nanoscale triboelectrification. (c) Potential distribution of the top SiO<sub>2</sub> surface measured by KPFM. (d) Modulation of graphene electronic properties by tunneling triboelectrification through AFM tip. [148] Copyright 2017, Springer Nature. These charges will tunnel through the graphene and be trapped at the air-SiO<sub>2</sub> interface, behaving as an invisible floating gate. (e) Change in the average potential of the graphene surface before and after rubbing. (f) Changes in surface potential after tunneling triboelectrification of graphene surfaces with different number of layers. (g) Changing the AFM tip bias regulates the tunneling triboelectrification charge density and polarity in graphene. (h) Relationship between tip bias and surface potential in the rubbing region.

that the trapped negative charge trapped within the rubbing region attracts holes, thereby enhancing the p-type conductivity of graphene. Conversely, a positive bias results in the injection of positive charges and the attraction of electrons, causing graphene to change from p-type to n-type conductivity. The correlation between tip bias and surface potential in the rubbing region, as depicted in Fig. 13h, indicates that the charge density and polarity can be precisely modulated by controlling the bias. A comprehensive understanding of how the tunneling triboelectrification technique controls and manipulates charge on a microscopic scale could potentially pave the way for developing nanoscale tribotronic devices.

## 9. Applications of TENG-modulated 2D field effect transistors

### 9.1. Tribotronic enhanced photoresponsivity

Similar to piezo-phototronics utilizing piezo-potential to enhance the photoresponsivity of optoelectronic FETs, tribotronics possesses the same capability by leveraging the tribo-potential. The bandgap structure of the channel material and the internal electric field are modulated by a TENG in response to external mechanical strain, thereby controlling its photoresponsivity. Pang et al. enhanced this photoresponsivity by combining MoS<sub>2</sub> phototransistors with a sliding-mode TENG (Fig. 14a). [70] This device employs TENG generated electrostatic potential during relative sliding as a substitute for the gate voltage. As the sliding distance increases, so does positive gate voltage generated by the TENG,

leading to an improvement in photoresponsivity. Fig. 14b illustrates that the photoresponsivity of the device significantly increases when the sliding distance is extended from 0 mm to 8 mm at 1 V drain-source bias. Under conditions of 100 mW/cm<sup>2</sup> illumination, the photoresponsivity improves approximately threefold. The energy band diagram depicted in Fig. 14c elucidates the impact on the MoS<sub>2</sub> tribo-phototransistor as a function of varying sliding distances. In the pristine state, devoid of both illumination and sliding, the two TENG friction materials maintain full contact. Consequently, no triboelectric gate voltage is applied to the FETs due to the prevailing local electrostatic equilibrium. However, during the relative displacement of the TENG friction layers, the FEP film accumulates negative charges, while the aluminum film gathers positive charges. This charge disparity induces an intrinsic positive electric field on the MoS<sub>2</sub> material, leading to a downward deflection of its energy bands. This deflection diminishes the potential barrier for electrons transitioning from valence band to conduction band, facilitating the excitation and movement of photogenerated electrons within the conduction band. As a result, there is an enhancement in the induction and separation of photogenerated charge carriers. By modulating the sliding distance, one can adeptly control the magnitude of this internal electric field, thereby fine-tuning both the photocurrent and photoresponsivity of the phototransistor. Such active mechanical modulation offers a versatile and potent approach for crafting innovative photodetectors and sensors.

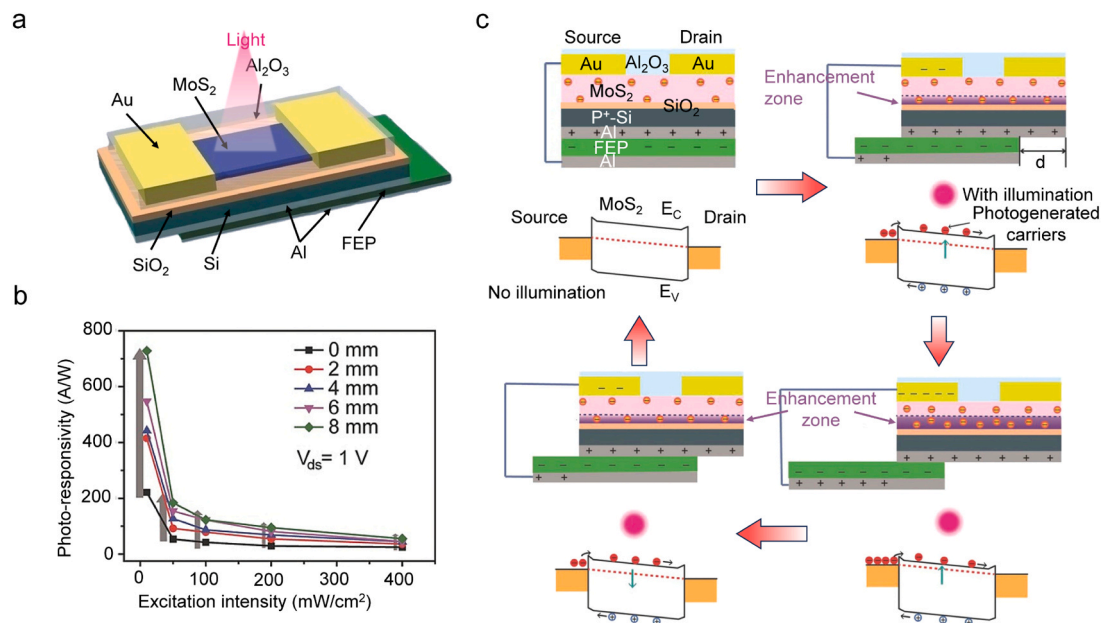


**Fig. 14.** TENG-modulated 2D FETs for enhanced photoresponsivity applications. (a) Enhanced photoresponsivity of MoS<sub>2</sub> phototransistors by sliding mode TENG. [70] Copyright 2016, Wiley-VCH. (b) Effect of different displacements of TENG on the photosensitivity. (c) Working mechanism of the effect on MoS<sub>2</sub> tribo-phototransistor with different sliding distances.

## 9.2. Mechanical sensing

The escalating demand for more interactive and responsive technologies grows in the realms of artificial intelligence systems and human-robotic interfaces has led to the development of tribotronics. This technology harnesses triboelectric charges, generated by mechanical action, to modulate carrier transport within a transistor. This process simplifies device architectures and enhances their robustness. Tribotronics merges mechanical and electronic properties to create highly responsive and energy-efficient interfaces. These are ideally suited for a variety of applications, from interactive mechanical sensors to advanced e-skins for robots that mimic human sensory capabilities. [74,149,150] Notably, tribotronics' unique self-powered mechanism allows it to operate stably without an external power supply, a feature that is particularly advantageous in the circumstance where changing power sources or accessing external power is challenging (e.g., wearable devices and remote monitoring systems). [151–154] Furthermore, its self-powered capability significantly extends the continuous operation and practical applicability of the device, offering an efficient and cost-effective solution for modern sensing technology. These attributes not only reduce operational and maintenance costs but also propel the evolution of sensor technology towards high integration and automation. Xue et al. developed vertically coupled tribotronic transistors, leveraging the single-electrode mode TENG and MoS<sub>2</sub> FET (Fig. 15a), and explored their potential as smart tactile switch (Fig. 15b). [155] A finger touch on the polytetrafluoroethylene (PTFE) film of the TENG induces a mechanical stimulus, leading to a notable modulation in the channel current, achieving an on/off ratio of approximately 16. The switching state is signified by two light-emitting diodes (LEDs), which are effectively activated upon finger contact. Li et al. incorporated InSe tribotronic transistors for tactile switching, utilizing an indium (In) layer both as the surface dopant on the InSe channel and as the protective packaging for the device (Fig. 15d). [156] This device can rapidly transition between its on-state and off-state upon finger touch. Such a feature has been employed to showcase human-machine interfaces, including the transmission of the word "InSe" via Morse code (Fig. 15e). Owing to the charge doping of the In layer, the device boasts a high current on/off ratio of 10<sup>6</sup> at low drain-source biases. It functions as a tactile switch to regulate the LED (Fig. 15f). When the two friction layers

of the TENG are closely aligned, a shift in gate voltage prompts the LED to illuminate swiftly. Conversely, when these friction layers are fully separated, the induced triboelectric potential of the gate reaches its saturation point, resulting in the LEDs being deactivated. If sustained pressure is continuously applied to the Kapton friction layer, the LEDs remain lit for over 300 seconds, underscoring the device's stability and practicality.

Ion-gels have emerged as optimal materials for the creation of flexible e-skins due to their superior material properties. These include high ionic conductivity, excellent mechanical flexibility, and the capacity to form stable EDLs. These characteristics enable ion-gels to effectively regulate the conductivity of semiconductors at low voltages while retaining the flexibility and stability of the overall structure. Furthermore, ion-gels are compatible with lightweight, stretchable substrate materials, making them particularly suitable for use in wearable devices. This compatibility is crucial for integrating mechanical sensing technologies of tribotronics into flexible substrates. The ability of ion-gels to adhere to complex body shapes and maintain functionality even under deformation is essential for continuous and stable monitoring of physiological signals or integration into interactive systems. Khan et al. developed a flexible triboiontronic device, based on single-electrode TENGs with a PDMS friction layer and graphene FET (Fig. 15g, the inset depicts its physical image). [74] This device effectively reflects various mechanical modes such as touch and release through its channel currents (Fig. 15h). The device was prepared as a 3 × 3 flexible array and attached to the wrist to spatially map the intensity and location of the touch stimuli in the form of pixels (Fig. 15i). The inset of the figure illustrates the channel current mapping of the device during two fingers touching. The device's ability to monitor multiple touch points is anticipated by detecting and visualizing complex touch patterns and movements on the sensor surface. Similarly, Meng et al. developed a flexible triboiontronic device based on a single-electrode TENG with a PTFE friction layer and a graphene FET (Fig. 15j). [75] To create a sensitive wearable sensor device, a 1-mm epoxy spacer was prepared at the edge of the PET substrate and applied to the throat to maintain an appropriate contact gap between the ion-gel and the skin (Fig. 15k). With the ion-gel directly facing the skin, vocalization-induced vibrations can be captured sensitively; for instance, the output current exceeds 23 μA during high tones and decreases to approximately 22.2 μA during

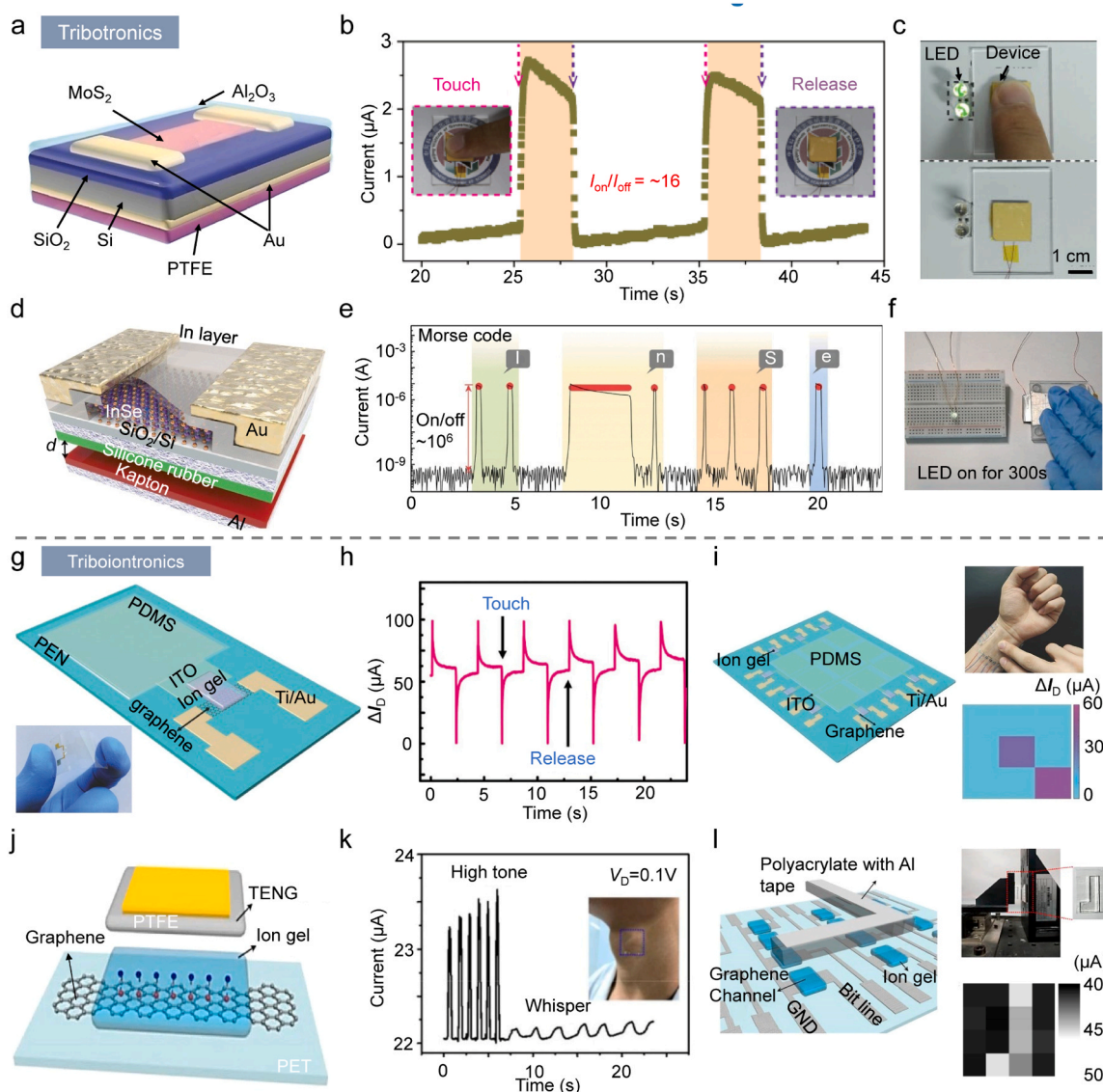


**Fig. 15.** TENG-modulated 2D FETs for mechanical sensing applications. (a) A vertically coupled tribotronic transistor was constructed based on a single-electrode mode TENG and MoS<sub>2</sub> FET. [155] Copyright 2016, Wiley-VCH. (b, c) Application of tribotronics as a smart tactile switch and visualization of the switching state via two light-emitting diodes (LEDs). (d) InSe tribotronic transistor. [156] Copyright 2019, Wiley-VCH. (e, f) Demonstration of tribotronics as a smart tactile switch utilizing Morse code to send the word “InSe” and control the operation of an LED. (g) Flexible triboiontronics device constructed based on PDMS friction layer with single-electrode TENG and graphene FET. [74] Copyright 2017, Wiley-VCH. (h) Channel currents of devices in touch and release mechanical modes. (i) 3 × 3 flexible array device was attached to the wrist to map touch stimuli. (j) Flexible triboiontronics device constructed based on single-electrode TENG with PTFE friction layer and graphene FET. [75] Copyright 2018, American Chemical Society. (k) Flexible tribotronic device is attached to the throat to detect vocalizations. (l) 4 × 4 flexible array device maps the shape of the object with which it is in contact.

whispers. Furthermore, by configuring the device as a 4 × 4 flexible array, the shape of the object in contact with the device can be spatially mapped (Fig. 15l). Additionally, the triboelectric gate voltage is correlated with the distance of contact-separation, thereby allowing the corresponding spacing between the “L” shaped polyacrylates and the arrayed devices to be reflected based on the mapping image.

### 9.3. Information storage

Information storage plays an indispensable role in the evolution of modern society, serving as both the bedrock of scientific and technological advancements and a pivotal catalyst for human civilization’s progress. As science and technology rapidly evolve, semiconductor memory—a fundamental component of information technology—is confronted with the imperative to enhance its performance and

functionality. In this milieu, non-volatile memory has garnered great attention due to its superior electrical characteristics and reliability. Notably, vertically stacked vdWH constructed from 2D materials exhibit promising potential. [157] Furthermore, tribotronics—an emerging field that revolutionizes the design and functional implementation of memory devices by transmuting mechanical energy into gating/modulation/programming/reading voltages via TENG units—has emerged. This technology not only enables data access through conventional electrical means but also allows for the direct recording of data in the FET upon mechanical triggering. Such an approach markedly augments the energy autonomy and interactivity of the memory devices. Tribotronics integrated with 2D vdWH memory devices can not only respond directly to physical touch or motion but also capture external mechanical information, propelling storage technology towards heightened efficiency, reduced power consumption, and enhanced intelligence.

Jia et al. developed a tribotronic memory device based on the FGFET of a graphene/h-BN/MoS<sub>2</sub> vdWH (Fig. 16a).[83] In this configuration, graphene serves as the floating gate layer, h-BN as the tunneling layer, and MoS<sub>2</sub> as the channel layer. When the friction layers of the TENG are in close proximity, the PTFE layer transfers electrons to the Cu layer, causing it to accumulate positive charge. This positive charge induces the electrons in the MoS<sub>2</sub> semiconductor channel to tunnel towards the graphene floating gate layer through the bottom gate, thereby initiating a write operation. Conversely, when the friction layers of the TENG are separated, the electrostatic induction effect leads to reduced positive charge in the Cu layer. The electrons in the graphene floating gate layer return to the MoS<sub>2</sub> channel, facilitating the erase operation. As illustrated in Fig. 16b, positive displacement (+0.2 mm) and negative displacement (-0.2 mm) respectively induced information storage and erasure, maintaining good stability during long cycle tests. Furthermore, the unidirectional multiple displacements based on TENG induce the accumulation of triboelectric gate voltage, enabling multi-bit storage characteristics. As shown in Fig. 16c, with 14 gradual changes in the vertical separation distance from 0.01 mm to 0.25 mm, the device's current varies from 10<sup>-11</sup> A to 10<sup>-6</sup> A. This demonstrates that minor mechanical motions can effectively regulate the storage state. In addition, this type of floating-gate device can further enable an innovative dual-input storage mechanism that combines optical and mechanical inputs, eliminating the need for traditional voltage control. The graphene layer serves as a charge-trapping layer, recording charge changes induced by either optical illumination or mechanical action. Optical illumination triggers the generation of electron-hole pairs within the

MoS<sub>2</sub> layer, which are then captured by the electric field, enabling the optical writing operation.[84]

Wei et al. designed a MoTe<sub>2</sub> tribotronic transistor based on stacked dielectric Al<sub>2</sub>O<sub>3</sub>/HfO<sub>2</sub>/Al<sub>2</sub>O<sub>3</sub>, the structure of which is shown in Fig. 16d.[85] The energy band difference between HfO<sub>2</sub> and Al<sub>2</sub>O<sub>3</sub> forms a deep quantum well within the HfO<sub>2</sub> layer, while Al<sub>2</sub>O<sub>3</sub> layer serves as the barrier layer, effectively preventing the trapped charge from escaping from HfO<sub>2</sub>. Figs. 16e, 16f depict the energy band diagram and charge transfer process of the device in different operating states of TENG. When the triboelectric gate voltage is negative (TENG contact state, D-), holes in the MoTe<sub>2</sub> channel cross the Al<sub>2</sub>O<sub>3</sub> potential barrier and are trapped within the HfO<sub>2</sub> layer. At the same time, the residual electrons in the HfO<sub>2</sub> layer return to the MoTe<sub>2</sub> channel through the field emission effect, leading to an increased channel current. Besides, due to the high energy barrier in the stacked gate, the holes can remain stable in the HfO<sub>2</sub> layer even after the removal of the pulse. When the triboelectric gate voltage is positive (TENG separated state, D+), the trapped holes are repelled back to the MoTe<sub>2</sub> channel, while electrons are injected into the HfO<sub>2</sub> layer through the tunneling effect, leading to a lower channel current threshold. This lays the foundation for a mechanically driven information storage functionality where programming/erasing operations are realized by applying D-/D+ pulses to the memory device. As shown in Fig. 16g, by adjusting the amplitude of the D<sub>PRO</sub> pulse (from -0.04 to -0.16 mm, width = 0.5 s), the drain current of the device varied from 1.7 × 10<sup>-9</sup> to 5.3 × 10<sup>-7</sup> A, creating eight stable and distinguishable current levels (~3 bits), which realized the dynamic multi-level memory function. After 100 cycles of

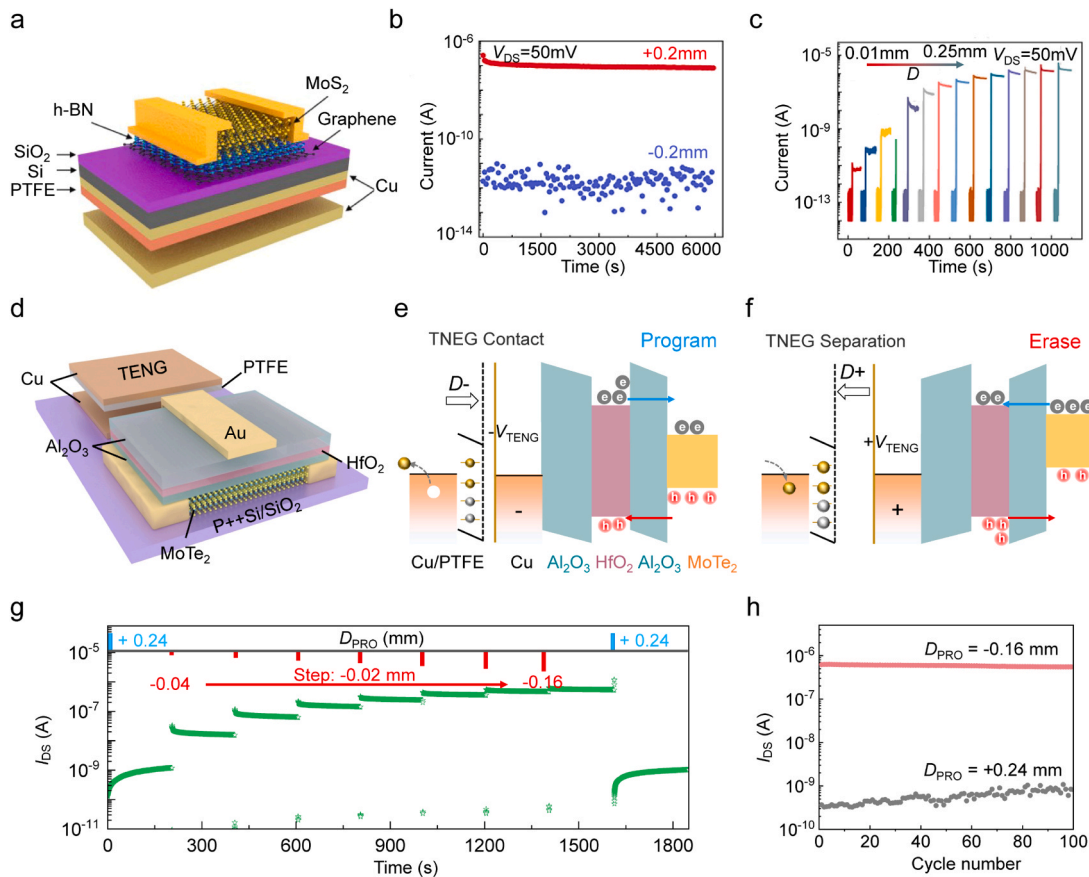


**Fig. 16.** TENG-modulated 2D FETs for information storage applications. (a) Tribotronic memory device is prepared by graphene/h-BN/MoS<sub>2</sub> vdWH FGFET.[83] Copyright 2021, Elsevier. (b) Storage and erasure of information induced by positive displacement (+0.2 mm) and negative displacement (-0.2 mm), respectively. (c) Effect of different displacement distances of TENG on the storage state of the device. (d) Tribotronic memory device is prepared by MoTe<sub>2</sub> FET with stacked dielectric Al<sub>2</sub>O<sub>3</sub>/HfO<sub>2</sub>/Al<sub>2</sub>O<sub>3</sub>. [85] Copyright 2024, Elsevier. (e, f) Energy band structure of the charge trapping mechanism at negative and positive triboelectric gate voltages, respectively. (g) Dynamic multi-level memory function realized by adjusting the amplitude of the D<sub>PRO</sub> pulse (from -0.04 to -0.16 mm, width = 0.5 s). (h) Reliability of the memory device under 100 cyclic programming (D<sub>PRO</sub> = +0.24 mm, width = 0.5 s) and erasing (D<sub>PRO</sub> = 0.16 mm, width = 0.5 s) operations.

programming ( $D_{\text{PRO}} = 0.24$  mm, width = 0.5 s) and erasing ( $D_{\text{PRO}} = 0.16$  mm, width = 0.5 s), the programming/erasing current ratio remained stable (Fig. 16h), verifying the stability and reliability of this tribotronic device for information storage.

#### 9.4. Binary logic gates

Complementary metal-oxide-semiconductor (CMOS) technology is pivotal in the realm of digital circuits, especially in the execution of elementary binary logic ("0" and "1"). This technology employs

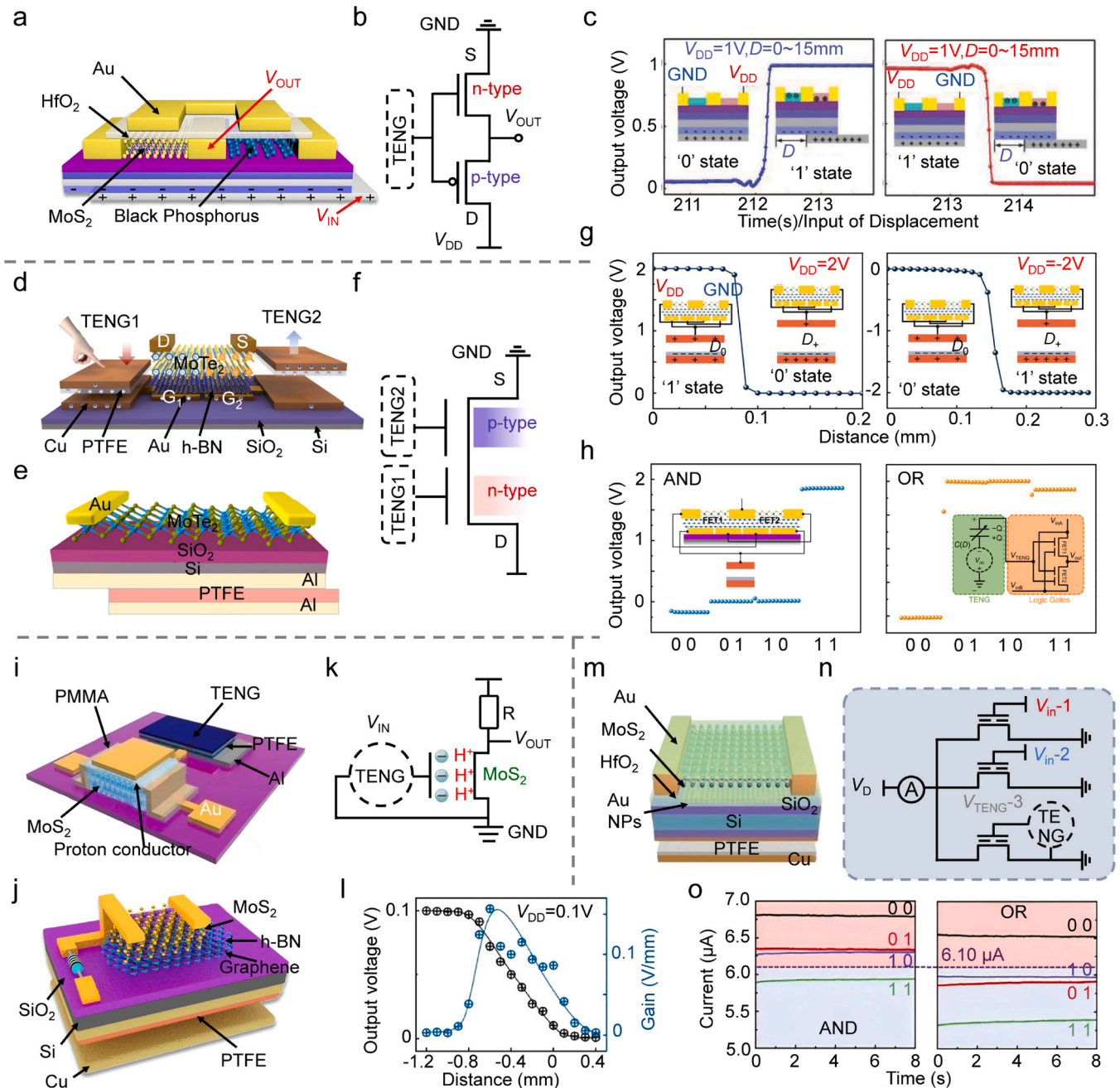


**Fig. 17.** TENG-modulated 2D FET for binary logic applications. (a, b) Schematic diagrams of tribotronic double-gate logic device and complementary inverter structure constructed based on n-type MoS<sub>2</sub> and p-type BP. [86] Copyright 2018, Wiley-VCH. (c) Realization of binary logic state change based on TENG displacement and changing the input direction of  $V_{\text{DD}}$ . The inset shows the working mechanism diagram. (d-f) Schematic of the structure of the tribotronic device and inverter based on bipolar MoTe<sub>2</sub>. [87,88] Copyright 2023, Elsevier. Copyright 2023, Springer Nature. (g) Realization of binary logic state change based on TENG displacement and changing the input direction of  $V_{\text{DD}}$ . The inset shows a diagram of the working mechanism. (h) "AND" and "OR" Boolean logic functions realized by changing circuit connections. The inset shows the device circuit structure and equivalent circuit. (i) Inverter based on proton conductor MoS<sub>2</sub> FET in series with a resistor. [78] Copyright 2020, American Chemical Society. (j) Inverter based on graphene/h-BN/MoS<sub>2</sub> vdWH FGFETs in series with a resistor. [83] Copyright 2021, Elsevier. (k) Equivalent circuit structure of the inverter in series with the resistor. The matching resistance is 10 M $\Omega$ . (l) TENG displacement and logic output voltage. (m, n) FGFET based on Au nanoparticles/HfO<sub>2</sub>/MoS<sub>2</sub> and an artificial neural network structure built based on the three devices. [79] Copyright 2020, Wiley-VCH. These three FGFETs are connected in parallel, two of which serve as inputs for logic operations ( $V_{\text{in-1}}$  and  $V_{\text{in-2}}$ ) by electrical means. The third FGFET modulates the logic gate ( $V_{\text{TENG-3}}$ ) by means of the tribo-potential generated by the TENG. (o) The switching of "AND" or "OR" logic gates is realized by adjusting the modulation voltage of TENG.

complementary n-type and p-type MOSFETs to construct the various logic gates such as “AND”, “OR”, and “NOT”. These gates form the foundation of digital systems and are fundamental to general-purpose computer architectures.[158,159] CMOS technology is highly valued for its energy efficiency, stability, robustness, flexibility, and simplicity of logic operation. In CMOS logic gates, energy consumption primarily occurs during state transitions (from “0” to “1” or “1” to “0”), with virtually no energy consumption in the static state. This characteristic makes CMOS technology ideal for mobile devices and high-performance computing systems.[160,161] Furthermore, the complementary configuration of n-type and p-type transistors ensures the stability and low noise level of the circuits in various logic states, effectively minimizing energy loss and heat generation. This technology not only realizes basic logic gates but also enables that the combination of more complex logic operation units such as adders, counters, and registers, thereby significantly enhancing the functionality and complexity of the circuit. The inverter plays a pivotal role in CMOS technology, serving as a fundamental logic gate that inverts the input signal to produce an output. This is achieved through the use of a single transistor paired with a resistor, thereby enhancing flexibility and functionality for digital circuits. Consequently, the development of basic binary “0” and “1” logic functions via 2D FET-based construction not only lays the groundwork for intricate logic operations but also underpins modern electronic systems capable of processing diverse data sets and executing sophisticated algorithms. By meticulously controlling electron movement within exceedingly thin material layers, 2D FETs deliver superior electrical properties and potential for size reduction, propelling the advancement of microelectronics. Furthermore, the introduction of TENG introduces a novel power source for constructing active logic functions, as well as innovative solutions for information filtering, processing, and the creation of more energy-efficient devices.

Gao et al. developed a tribotronic dual-gate logic device, utilizing n-type MoS<sub>2</sub> and p-type BP (Fig. 17a), to construct a complementary inverter (Fig. 17b).[86] The triboelectric potential of a sliding mode TENG serves as a dynamic gate voltage that fluctuates with mechanical motion, enabling the device to function without the need for an applied gate voltage. The interplay between the triboelectric potential and the semiconductor material of the transistor provides unique control over the device’s logic operation. The TENG generates a triboelectric potential that regulates the carrier concentration in the transistor channel, depleting or accumulating electrons based on the channel’s polarity. As the two transistors are configured in a complementary manner to form an inverter circuit, dynamic changes in the gate voltage of the transistors, induced by changes in the displacement of the TENG, cause one transistor to conduct and the other to cut off, thereby altering the logic output state. Furthermore, a change in the binary logic state can also be achieved by modifying the input direction of V<sub>DD</sub>, as demonstrated in Fig. 17c.

In contrast to constructing a CMOS using ambipolar 2D materials, a unipolar material facilitates a more straightforward preparation process and allows for a more compact structural design. Both Chen et al.[87] and Li et al.[88] conducted logic gate applications based on tribotronics with ambipolar MoTe<sub>2</sub>. The latter utilized a sliding-mode TENG (Fig. 17e), while the former employed a dual-bottom gate and a contact-separation mode TENG to enable more convenient logic input (Fig. 17d). A p-n type CMOS logic circuit is constructed by integrating two TENGs onto the two separate gates of the MoTe<sub>2</sub> FET, which independently and locally configure the MoTe<sub>2</sub> homojunction with differentiated triboelectric potentials (Fig. 17f). The switching of the logic output state can be efficiently achieved by altering the TENG displacement state or the input direction of the V<sub>DD</sub> (Fig. 17h). In the tribotronic logic device based on bipolar MoTe<sub>2</sub> material, logic inputs A and B are connected to the drain of FET1 and the source of FET2, respectively. This configuration enables the realization of two Boolean logic functions: logic “AND” and logic “OR” (Fig. 17h, inset shows the device configuration and equivalent circuit diagram). The execution of these logic

functions is contingent upon the introduction of triboelectric potentials via mechanical displacements, which modulate the doping type of the MoTe<sub>2</sub> channel and consequently its electrical conductivity. In a tribotronic MoTe<sub>2</sub> logic device, the logic inputs “0” and “1” correspond to the input voltages of 0 and 2 V, respectively. During an “AND” logic operation, FET1 and FET2 are adjusted to n-type doping by setting the mechanical displacement  $D = +0.15$  mm. For the logic combination (0, 0), both FETs are inactive, resulting in an output is “0”. In combinations (0, 1) and (1, 0), the output remains “0” as only one FET is active. However, when the input is (1, 1), both FETs conduct, resulting in an output is “1”. For the “OR” logic operation, the displacement is set to  $D = -0.1$  mm, and FET1 and FET2 are set to be p-doped. There is no output for inputs (0, 0). However, at (0, 1), (1, 0) or (1, 1), at least one of the FETs conducts, resulting in an output of “1”. This reflects the characteristics of logic “OR” gates, where the output is a “1” if any of the inputs is a “1”.

The employment of FETs and resistors in series to construct inverters is a prevalent strategy in digital circuit design. Yang et al. investigated a proton conductor MoS<sub>2</sub> FET (Fig. 17i)[78], while Jia et al. examined a graphene/h-BN/MoS<sub>2</sub> vdWH FGFET (Fig. 17j)[83] for their potential use in series with a resistor for inverter applications. The equivalent circuit structure of this inverter, as depicted in Fig. 17k, features a matching resistance of 10 MΩ. A negative tribo-potential induces a negative gate voltage modulation of the proton conductor (logic “0”) when the FET is deactivated. In this state, there is no conductive path between the drain and the source, and the drain terminal is connected via the resistor to the positive bias V<sub>DD</sub> (0.1 V). Consequently, the drain (i.e., the output) manifests as a high voltage level (logic “1”). Conversely, a positive triboelectric potential induces positive gate voltage modulation of the proton conductor (logic “1”) when the FET is activated. This establishes a conductive path between the drain and the source, bringing the drain potential close to the low voltage level. The voltage drop through the resistor reduces the output terminal potential, causing the output terminal to exhibit a low voltage level (logic “0”). The corresponding TENG displacement and logic output voltage are illustrated in Fig. 17l.

In addition, Yang et al. developed a sophisticated artificial neural network utilizing three Au nanoparticle/HfO<sub>2</sub>/MoS<sub>2</sub> FGFETs (device structure schematic depicted in Fig. 17m) to illustrate the neuromorphic AND and OR logic operation functions (Fig. 17n).[79] The three FGFETs are connected in parallel, with two serving as inputs (V<sub>in-1</sub> and V<sub>in-2</sub>) for electrical logic operations, signifying logic “1” and “0” with input voltages of 100 V and -100 V, respectively. The third FGFET modulates the logic gates (V<sub>TENG-3</sub>) via the TENG induced tribo-potential. To ensure precise logic operations execution, the function of “AND” or “OR” logic gates can be alternated by adjusting the modulation voltage produced by the TENG (-100 V or 100 V) with a channel current threshold of 6.1 μA, as shown in Fig. 17o. The capacity of the TENG to enhance the device interaction and control offers a novel approach for constructing more efficient logic devices.

### 9.5. Schottky barrier modulation

TENG has been demonstrated to be effective in optimizing the electronic properties of semiconductor devices. The electrical properties of graphene can be modulated over a wide range due to its zero bandgap property and the fact that the work function can be adjusted across a broad spectrum of Fermi energy levels by an applied electrostatic field. This modulation offers robust technical support for developing high-performance electronic devices. Moreover, the integration of TENG into these systems enables a more flexible and precise modulation of graphene’s electrical properties through its ability to convert mechanical energy into electrical energy. The modulation of TENG’s triboelectric potential provides a unique method for enhancing the performance and expanding the functionality of graphene-based devices, which is particularly suited for addressing the needs of complex and novel interactive and multimodal sensing applications. Zhang et al. introduced

a novel ion-gel capacitively coupled TENG-driven dual-mode FET, comprising a graphene transistor with an ion-gel gate modulation ( $V_{TG}$ ) and an additional triboelectric potential gate modulation ( $V_{BG}$ ) (Fig. 18a).[118] The Fermi energy level of the graphene initially experiences a slight downward shift due to p-type doping by atmospheric oxygen and moisture. Upon separation of the copper electrode is separated from the PTFE, imbalanced triboelectric field induces an equivalent negative  $V_{BG}$ , which in turn leads to further p-type doping in the graphene channel and a subsequent downward shift of the Fermi energy level (Fig. 18b, c). The device's response to varying displacements is depicted in Fig. 18d, e, illustrating the transfer curves and output performance. As the displacement distance increases from 0 to 0.25 mm, there is significant shift in the Dirac point and  $I_D$  of the ion-gel gated

transistor from 0.6 V to 1.4 V and from 0.9 mA to 1.44 mA, respectively (Fig. 18f). This shift underscores the effective regulation of the device barrier by TENG mechanical displacement, suggesting its potential for applications in multiparameter distance sensors.

The zero-bandgap characteristic of graphene restricts its efficacy as a transistor switch. However, the current on/off ratio can be optimized by constructing vdWH with other 2D materials. Furthermore, the Schottky barrier can be precisely controlled by modulating the work function and Fermi energy level of graphene, thereby enhancing the device's performance. Sun's group explored the modulation of the Schottky barrier in vertically stacked graphene/MoS<sub>2</sub> vdWH through mechanical displacement (Fig. 18g).[119] An increase in the triboelectric potential due to the TENG displacement reduces both the height of Schottky

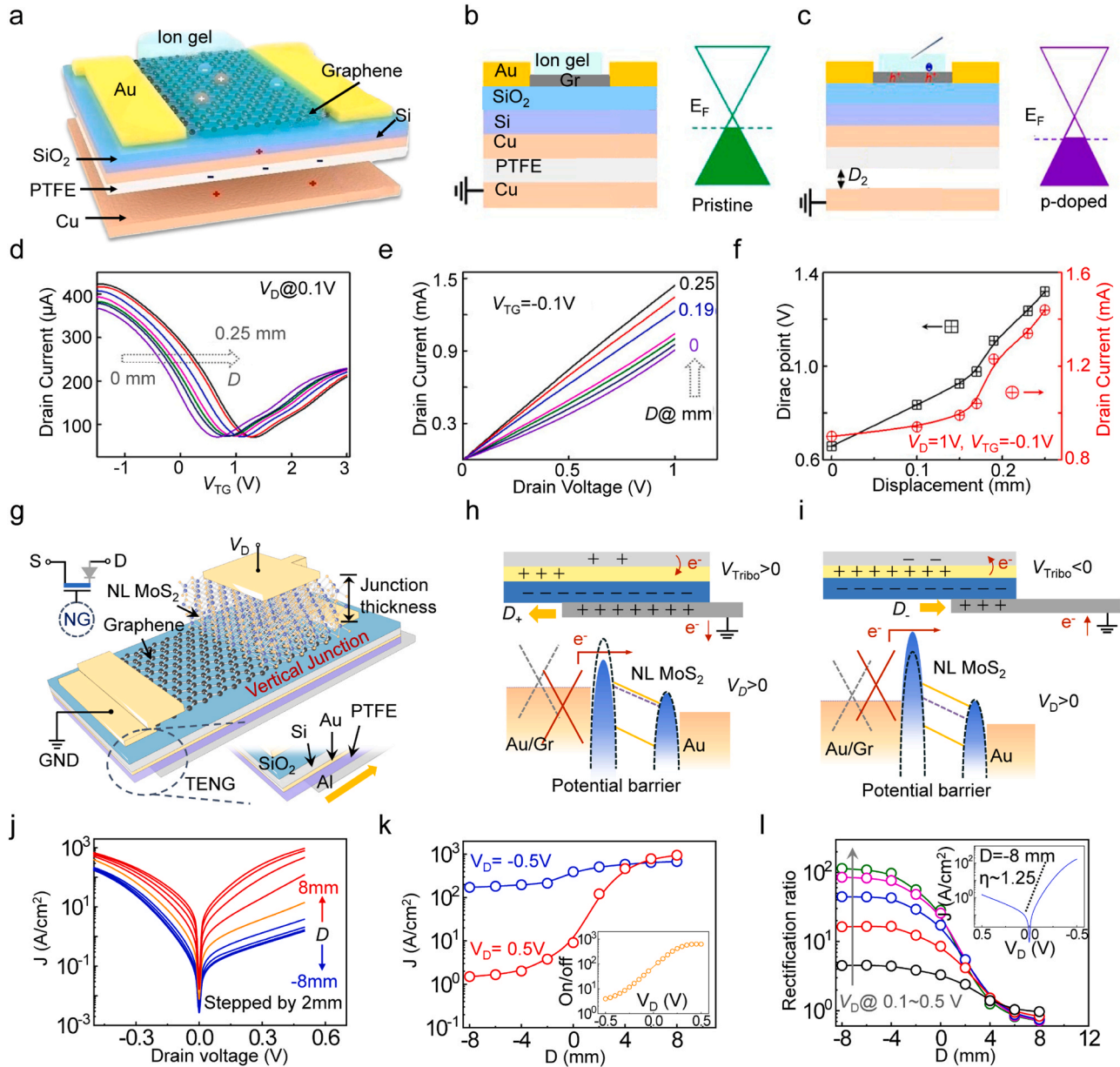


**Fig. 18.** TENG-modulated 2D FETs for band structure engineering applications. (a) Ion-gel capacitively coupled TENG-driven dual-mode graphene FET, including ion-gel gating ( $V_{TG}$ ) and triboelectric potential gating ( $V_{BG}$ ).[118] Copyright 2020, American Chemical Society. (b, c) Working mechanism of the effect of TENG displacement on the fermi energy levels of graphene. (d, e) Transfer and output curves of the device at different TENG displacements. (f) Effect of TENG displacement on the Dirac point and drain current ( $I_D$ ) of ion-gel gated transistor. (g) Vertically stacked graphene/MoS<sub>2</sub> vdWH-FET. [119] Copyright 2024, Wiley-VCH. (h, i) Working mechanism of the effect of mechanical displacement on the graphene/MoS<sub>2</sub> Schottky barrier. (j, k) Output and transfer curves of tribotronic vertical transistors at different TENG displacements. The insets show that the on/off ratios can exceed two orders of magnitude at all positive biases. (l) Displacement dependent rectification ratio. The inset shows the ideal factor  $\eta$  of the diode behavior at  $D = -8$  mm is 1.25.

barrier and the width of depletion layer in the MoS<sub>2</sub> channel, thereby promoting the electron transport properties (Fig. 18h). Conversely, a decrease in triboelectric potential due to a reduction in TENG displacement increases the Schottky barrier height and the depletion layer width in the MoS<sub>2</sub> channel, inhibiting the electron transport

properties (Fig. 18i). Fig. 18j depicts the output characteristics ( $J-V_D$ ) of the tribotronic vertical transistor as a function of varying TENG displacements. As TENG displacement  $D$  increases, there is a corresponding rise in the drain current, which markedly modulates the on/off current, particularly at positive bias. Conversely, the modulation effect is less

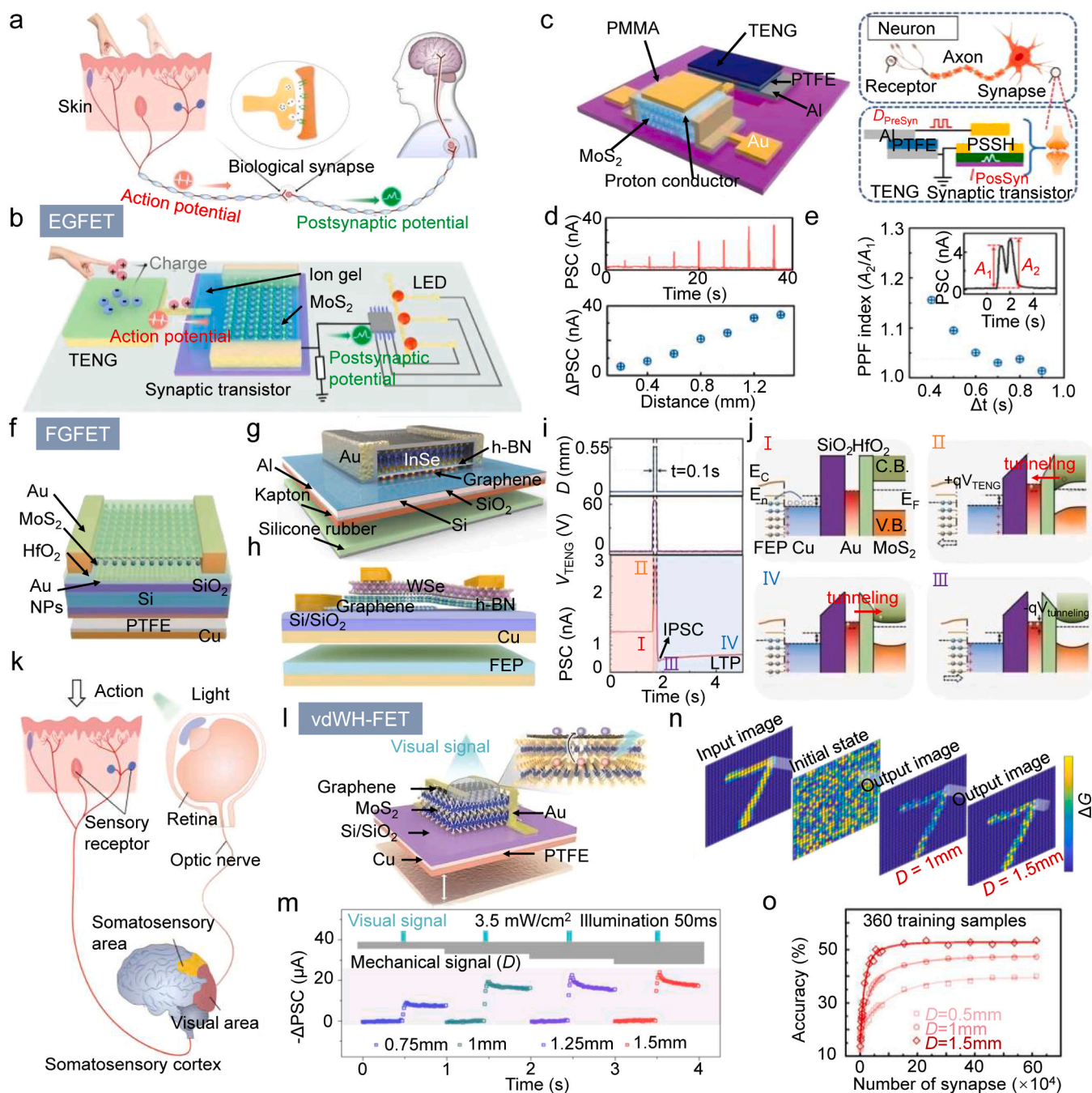


**Fig. 19.** TENG-modulated 2D FET for artificial synapse applications. (a) Schematic diagram of the biosensory nervous system.[77] (b) Artificial sensory neurons based on TENG-modulated MoS<sub>2</sub> EGFET.[77] Copyright 2021, Springer Nature. TENG converts mechanical actions into APs to drive FETs and demonstrates the dynamic logic recognition function for spatiotemporal touch using back-end LEDs. (c) TENG-driven PSSH proton conductor gate-controlled MoS<sub>2</sub> synaptic transistor. [78] TENG mimics receptors and EGFET mimics synapses in biosensory systems. Copyright 2020, American Chemical Society. (d) TENG displacement dependent PSC. (e) Typical synaptic behavior of PPF with short-term plasticity enhancement of the device. (f) Au nanoparticles/HfO<sub>2</sub>/MoS<sub>2</sub> FGFET.[79] Copyright 2020, Wiley-VCH. (g) Graphene/h-BN/InSe FGFET.[80] Copyright 2022, Elsevier. (h) Graphene/h-BN/WSe semi-floating gate FET.[81] Copyright 2022, Elsevier. (i) The variation characteristics of the typical pulse signal of TENG and the typical PSC of the FGFET under mechanical displacement. (j) Corresponding working mechanisms and energy band diagram at the four PSC change stages. (k) Biological neural system for mechano-photonic bimodal perception.[166] Copyright 2022, Elsevier. (l) Mechano-photonic synergistic FET. (m) Effect of mechanical displacement on the photonic PSC. (n) Simulated artificial neural network for image recognition. (o) Effect of mechanical displacement on the accuracy of image recognition.

pronounced at negative bias. This phenomenon can be attributed to that the finite density of states in single-layer graphene and the weak effect of electrostatic screening, which allow the MoS<sub>2</sub> fermi energy levels near the graphene/MoS<sub>2</sub> contact point to be effectively regulated by TENG. However, due to the strong screening effect from the top metal electrode, the MoS<sub>2</sub> Fermi energy levels near the metal/MoS<sub>2</sub> contact cannot be modulated by TENG. These findings suggest that the device has the potential to achieve tunable Schottky diode characteristics through TENG displacement modulation. At a drain voltage of 0.5 V, the device exhibits a current on/off ratio exceeding 600 when the displacement  $D$  fluctuates between  $-8$  mm and 8 mm. This indicates that the external mechanical behavior effectively controls the channel's electrostatic properties, as evidenced by the transfer curve in Fig. 18k. Moreover, the on/off ratios can surpass two orders of magnitude at both positive bias voltages. However, these ratios are significantly diminished at  $V_D = -0.5$  V due to the asymmetry of the source/drain contacts. Fig. 18l provides a summary of the displacement-dependent rectification ratios. The rectification characteristics are more pronounced at negative TENG displacements  $D$ . The ideal factor  $\eta$  of the diode behavior at  $D = -8$  mm is 1.25, as shown in the inset of Fig. 18l.

### 9.6. Artificial synapses

The tactile sensing, a fundamental human functionality, enables recognition of external object characteristics such as shape, temperature, and weight. It plays a crucial role in various aspects including motor coordination, emotional expression, and pain perception. [162–164] External physical stimuli are converted into APs via skin receptors, which are subsequently transmitted to the brain along the nerve fibers and synapses for further processing and interpretation (Fig. 19a). [165,166] In recent years, significant advancements have been achieved in artificial tactile systems, particularly neuromorphic devices based on capacitive, [167] piezoresistive, [165,168] piezoelectric [76,169] and triboelectric technologies [77,79,82]. Notably, TENG technology can directly convert mechanical stimuli into electrical signals with spatio-temporal characteristics, mimicking biological APs. The self-powered feature of TENG significantly reduces device power consumption and effectively replicates basic human neural functions such as the tactile [170–173] and auditory systems [174]. Furthermore, the diverse material options, multiple operating modes, and passive driving characteristics of TENGs greatly enhance their application potential for constructing efficient artificial tactile systems. Currently, the integration of TENG with neuromorphic semiconductor devices (e.g., EGFETs, FGFETs, vdWH-FETs) has primarily led to the development of various tribotronic neuromorphic devices.

Figs. 19b and 19c illustrate triboiontronic neuromorphic devices that utilize the slow migration and redistribution of ions in the EGFET electrolyte in order to emulate changes in PSC. Yu et al. engineered an artificial sensory neuron with a significantly low energy dissipation level of 11.9 fJ. [77] The TENG transduces mechanical actions such as touch, pressure, and displacement into APs. These electrical signals power an ion-gel gated MoS<sub>2</sub> synaptic transistor, demonstrating the dynamic logic recognition functionality for spatiotemporal touch using back-end LEDs (Fig. 19b). Yang et al. created a biocompatible ionic-electronic system. [78] In this system, the TENG simulates receptors and the EGFET simulates synapses within a biosensory system. The horizontally sliding TENG uses the external stimulus to drive the PSSH proton conductor gate-controlled MoS<sub>2</sub> synaptic transistor (Fig. 19c). Fig. 19d depicts the TENG displacement-dependent PSC. With a drain voltage of 0.1 V, a stronger triboelectric potential induces a more significant gate voltage as the TENG displacement increases, leading to an increase in the PSC gain. Two consecutive displacement pulses ( $D = 0.2$  mm,  $\Delta t = 0.4$  s) result in the typical synaptic behavior of PPF, enhancing the short-term plasticity of the device (Fig. 19e).

Fig. 19f-h illustrate neuromorphic devices constructed from tribotronic FGFETs, wherein the channel is continuously modulated by

trapping and detrapping charges via the floating gate layer. The slow leakage of charge in this layer imbues the channel current with non-volatile storage characteristics. For instance, Yang et al. engineered Au nanoparticles/HfO<sub>2</sub>/MoS<sub>2</sub> FGFETs (Fig. 19f); [79] Gao et al. created a graphene/h-BN/InSe FGFET (Fig. 19g); [80] Jia et al. developed graphene/h-BN/WSe semi-floating-gate FETs, which are able to be reconfigured into p-n or n<sup>+</sup>-n junctions through tribo-potential modulation (Fig. 19h). [81] The variation characteristics of the typical pulse signal (pulse width of 0.1 s) of TENG and the typical PSC of the FGFET under mechanical displacement are depicted in Fig. 19i, revealing significant variations in the PSC across four stages. Fig. 19j presents the corresponding operating mechanisms and energy band diagram variations for these four stages. In the initial stage, the FEP and Cu of the TENG come into contact, initiating a charge transfer due to tribo-electrification. However, there is no applied gate voltage to the FGFET, thus maintaining a local electrostatic balance. Consequently, the PSC remains stable at a resting current level of approximately 1.2  $\mu$ A when no external mechanical displacement occurs. In the second stage, the FEP and Cu separate, leading to an equivalent positive triboelectric gate voltage ( $+qV_{\text{TENG}}$ ) being applied to the MoS<sub>2</sub> transistor. This causes a downward bending of the energy band structure and an accumulation of electrons, leading to an instantaneous increase in the PSC to approximately 2.8  $\mu$ A. In the third stage, the FEP and Cu re-establish contact, balancing the localized static charges once again, as if no gate bias is applied to the FGFET. However, the trapped electrons in the floating gate cannot immediately return, creating a negative gate voltage ( $-qV_{\text{tunneling}}$ ). This leads to electron depletion and an upward bending of the energy bands in the MoS<sub>2</sub> channel, resulting in the appearance of inhibitory postsynaptic currents (IPSCs) that are lower than the resting level. In the final stage, the FEP and Cu maintain contact with each other, allowing the electrons in floating gate to gradually tunnel backwards and reduce the equivalent  $-qV_{\text{tunneling}}$ . This reduces electron depletion and the corresponding upward bending of the energy bands. The PSC gradually returns to its resting level, a process characterized as long-term plasticity.

Tribotronic neuromorphic devices have demonstrated considerable potential in replicating biological tactile sensory systems. However, the complexity of human sensory system makes it challenging to interact effectively with the real world in real time using a single sensory function. The integration of TENG with semiconductor devices that possess sensory functions allows these neuromorphic devices to perform multimodal sensing. For instance, they can mimic the visual system by responding to external light stimuli through FETs. [78,82,175,176] Furthermore, analyzing the correlation between biomechanical motion and visual information is a fundamental perception and recognition function of the human brain. It is crucial for simulating artificial intelligence in order to acquire somatosensory and visual data (Fig. 19k). [166] Therefore, it is particularly important to employ mechano-photonic synergy to update synaptic weights for multimodal plasticity in interactive neuromorphic devices. These multimodal systems are capable of constructing more complex and energy-efficient artificial sensory networks that achieve pattern recognition and decision processing capabilities comparable to those of the human brain. Yu et al. engineered mechano-photonic synergistic bimodal vdWH-FETs, wherein the triboelectric potential generated by the TENG prompts a redistribution of charge within the graphene/MoS<sub>2</sub> vdWH, thereby modulating the behavior of the photosynaptic synapses (Fig. 19l). [82] The negative triboelectric potential causes a bending in the energy band between MoS<sub>2</sub> and graphene, which subsequently impacts the photocurrent. Concurrently, the electron-hole pairs in MoS<sub>2</sub> are redistributed in response to light. This results in photogenerated electrons being injected into graphene, resulting in an increased resistance and consequently affecting the PSC. As illustrated in Fig. 19m, larger mechanical displacements ranging from 0.75 to 1.5 mm result in an increase in the photonic PSC from 9 to 24  $\mu$ A. This suggests that mechanical displacements effectively modulate the plasticity of photonic synapse. The

device was further employed to simulate artificial neural network recognition of the image “7” to validate the mechano-photonic synergy (Fig. 19n). As the displacement escalates from 1 to 1.5 mm, there is a significant increment in the  $\Delta G$  value of the pixel, thereby enhancing the prominence of digital features. This indicates that adjusting the mechanical displacement optimizes the synaptic weights of the artificial neural network, thereby improving image recognition efficiency. As demonstrated in Fig. 19o, increasing the displacement from 0.5 to 1.5 mm elevates the maximum accuracy of image recognition from 37 % to 54 %. This confirms that larger displacements can enhance the learning and processing capabilities of visual perception, thereby increasing recognition accuracy.

## 10. Statistics of PENG/TENG modulated 2D FETs

In Table 1, an in-depth statistical analysis of 2D FETs modulated by PENG and TENG is presented. In recent years, the research focus has gradually shifted from piezotronics to tribotronics, which has been gaining increasing attention due to its unique advantages. In terms of NG dielectric, specific material systems are assigned to PENG and TENG. Commonly used materials for PENGs include P(VDF-TrFE) and ZnO NWs, which are considered well-suited for high-sensitivity sensor applications because of their excellent piezoelectric properties. In contrast, TENG's dielectric materials are more diverse, including FEP, PTFE, silicone rubber, etc. These materials are relatively easy to prepare, reducing the complexity of fabricating tribotronic devices.

In terms of signal output, the output of PENG varies across studies, whereas the signal of TENG is significantly stronger and is able to directly drive semiconductor devices, making tribotronics more adaptable and practical than piezotronics. The output of PENG is typically in the range of a few volts and often needs to be combined with ion-gel to construct an EGFET to reduce the driving gate voltage of 2D FET. TENG usually does not require the property of an additional gate dielectric layer, which simplifies the device structure design and allows direct modulation of many types of FETs, including vdWH-FET and FGFET. Consequently, tribotronics has been widely used in the fields of mechanical sensing, information storage, and artificial synapses.

In terms of mechanical variables, PENG's applications typically involve strain ( $\epsilon$ ) and stress ( $\sigma$ ), making them suitable for fixed-position sensors and micro-actuators. While TENG's applications are mainly operated through displacement ( $D$ ) and are suitable for direct-touch application scenarios, which can respond to various mechanical stimuli and show a wider range of applicability. In terms of performance parameters, for piezotronics, the main parameters are the sensitivity associated with the change in 2D FET channel current due to strain or stress of the PENG, which can be expressed by the equations  $\partial I_{ds}/(I_0 \partial \epsilon)$  and  $\partial I_{ds}/\partial \sigma$ , respectively. For tribotronics, the main parameters are the tribotronic transconductance ( $g_t = \partial I_{ds}/\partial D$ ) and the tribotronic sub-threshold swing ( $SS_t = \partial D/\partial \log(I_{ds})$ ), which characterize the channel current change induced by the TENG displacement and TENG displacement required for one order of magnitude channel current change, respectively. These parameters provide a reference for optimizing the performance of devices based on piezotronics and tribotronics.

## 11. Summary and perspective

This review has provided a comprehensive discussion on piezotronics and tribotronics based on 2D materials, with a particular focus on the promising applications that arise from the introduction of mechanical strain modulation into these materials. Fig. 20 further encapsulates the advantages and challenges associated with piezotronics and tribotronics in relation to 2D materials. The potential benefits of the device, ranging from material level to system level, are outlined in terms of design and functionality. Concurrently, the challenges related to the preparation process, reliability, and stability are also presented in

Fig. 20.

Firstly, the advantages of 2D materials are manifold. At the material level, these offer a broad spectrum of options due to their unique electronic, mechanical, and chemical properties that are intrinsically linked to the structure of 2D materials. For instance, 2D ferroelectric materials can display inherent polarization without necessitating an external electric field, making them useful in non-volatile memory devices and sensor applications. Ambipolar 2D materials, which possess two distinct polar properties, can be modulated by external factors of electric field and mechanical strain. This allows for the design and optimization of innovative electronic/optoelectronic devices. Furthermore, the surfaces of 2D materials can be readily modified through chemical or physical means, further enhancing the properties of the materials and establishing a foundation for designing high-performance devices. In the case of TENGs, a diverse array of materials is available, including fur, silk, plastics, and more. Depending on the specific application scenarios, specific triboelectric materials, such as cellulose, silk protein, and rice paper, can be selected for the development of biodegradable TENGs.

Device-level advantages of 2D materials are primarily concerned with their unique characteristics that can be leveraged for device fabrication and performance modulation. These benefits are derived from the inherent properties of these materials and are actualized through meticulous engineering. Firstly, 2D materials offer a broad spectrum of design possibilities for various transistor structures, thereby providing an extensive array of construction options for electronic and optoelectronic devices. For instance, 2D FGFETs, which have a fixed charge storage layer, are particularly advantageous in memory and logic circuit applications. On the other hand, 2D EGFETs employ an electrolyte material as the gate dielectric, enabling the regulation of the charge concentration in the channel region at low voltages. Furthermore, 2D materials exhibit superior mechanical properties, making it possible to integrate EGFETs into flexible or wearable electronic devices. The fabrication process of these devices is facilitated by the ease of processing of 2D materials, allowing for customization using standard semiconductor process technologies. Notably, piezotronics and tribotronics do not require a traditional gate bias, a feature that reduces energy consumption while enhancing device functionality.

At the system level, piezotronics and tribotronics integration with 2D materials offers notable benefits. NGs are adept at efficiently transforming low-frequency and high-entropy mechanical energy into electrical energy. This capability is crucial for harnessing micro-vibrations and environmental mechanical energy sources such as human motion, machine vibrations, and wind power. Such a micro-energy harvesting approach eliminates the need for centralized energy conversion facilities, enabling direct energy extraction in the user's immediate surroundings, thus enhancing local energy efficiency. The synergistic coupling of piezoelectric/triboelectric potentials with 2D semiconductor devices introduces an innovative mechanical sensing and response mechanism. This allows for direct interaction with external mechanical stimuli, translating mechanical pressures, vibrations, and other behaviors into gate voltage signals that modulate the FET. Such direct gate voltage modulation based on external mechanical inputs notably diminishes device power consumption, ensuring efficient operation. Furthermore, by integrating the nanogenerator's responsiveness to external mechanical stimuli with the 2D FET's sensitivity to light, heat, chemicals, electromagnetism, etc., the system can be multi-parametrically modulated and respond in diverse modes. This flexibility surpasses the constraints of singular functionality, ensuring robust adaptability and reliability in intricate application scenarios while paving the way for the design of highly integrated and intelligent sensors.

The challenges associated with 2D materials and device processing are multifaceted. The primary technical obstacles lie in how to prepare high-quality 2D materials, which necessitates stringent control over crystal quality, size uniformity, and the number of layers. This synthesis process demands precise regulation of growth conditions, including

**Table 1**  
PENG/TENG modulated 2D FETs.

Modulate type	Year	NG dielectric	Channel	dielectric	Mechanical variation	Equivalent $V_G$	$V_{DS}$	Channel current variation	Performance parameters	Applications	Ref.
PENG	2015	P(VDF-TrFE)	Graphene	Ion-gel	Strian = 0.20 %	0.3 V	1 V	75 $\mu$ A	Sensitivity = 389	Mechanical sensing	[39]
	2016	ZnO NW	MoS <sub>2</sub>	Al <sub>2</sub> O <sub>3</sub>	Pressure = 6.25 MPa	-5 V	1 V	1.4 $\mu$ A		Mechanical sensing	[108]
		GaN NW	MoS <sub>2</sub>	SiO <sub>2</sub>	Strian = 0.18 %		1 V	0.265 $\mu$ A/ $\mu$ m		Enhancing photoresponsivity	[105]
	2017	P(VDF-TrFE)	IGZO	Ion-gel	Strian = 0.2 %	0.5 V	2 V	0.13 $\mu$ A	Sensitivity = 5202	Information storage	[141]
		ZnO NW	Graphene		Strian = 0.44 %		0.1 V	75 $\mu$ A		Enhancing photoresponsivity	[106]
	2018	P(VDF-TrFE)	IGZO/Graphene	Ion-gel	Strian = 0.16 %	~2 V	1 V	0.8 A/cm <sup>2</sup>		Modulating barriers	[116]
	2019	P(VDF-TrFE)	Graphene	Ion-gel	Strian = 0.8 %	~-1.6 V	1 mV	0.25 $\mu$ A	Sensitivity = 193	Artificial synapses	[76]
		P(VDF-TrFE)	MoS <sub>2</sub>	Al <sub>2</sub> O <sub>3</sub>	Strian = 0.2 %	~-8.3 V	1 V	0.225 $\mu$ A	Sensitivity = 4800	Modulating barriers	[117]
	2020	ZnO	InSe	SiO <sub>2</sub>	Pressure = 500 g	1 V	1 V	0.43 A		Mechanical sensing	[115]
		ZnO	Graphene		Pressure = 110 kPa		1 V	0.14 $\mu$ A	Pressure Sensitivity = 1.7 nA/KPa	Mechanical sensing	[109]
TENG	2016	FEP	MoS <sub>2</sub>	SiO <sub>2</sub>	$D = 8$ mm	10 V	1 V	2.12 $\mu$ A		Enhancing photoresponsivity	[70]
		PTFE	MoS <sub>2</sub>	SiO <sub>2</sub>	$D = 30$ mm	1 V	2 V	14 $\mu$ A	$g_t = 5.9$ $\mu$ A/mm	Mechanical sensing	[155]
	2017	PDMS	Graphene	Ion-gel	Pressure = 14 N		0.5 V	15 $\mu$ A	2 %/kPa	Mechanical sensing	[74]
	2018	PTFE	MoS <sub>2</sub> , Black Phosphorus	HfO <sub>2</sub>	$D = 30$ mm		0.1 V	1 pA	$g_t = 0.18$ $\mu$ A/mm	Binary logic	[86]
		PTFE	Graphene	Ion-gel	$D = 1$ mm	0.47 V	0.1 V	6 $\mu$ A	$SS_t = 1.57$ mm/dec $g_t = 7.4$ $\mu$ A/mm	Mechanical sensing	[75]
	2019	Silicone rubber	InSe	SiO <sub>2</sub>	$D = 30$ mm	86 V	0.1 V	10 $\mu$ A	$g_t = 143$ $\mu$ A/mm	Mechanical sensing	[156]
		Kapton	MoS <sub>2</sub>	SiO <sub>2</sub>	$D = 160$ $\mu$ m	0.35 V	0.1 V	2.9 $\mu$ A	$g_t = 20$ $\mu$ m/dec	Binary logic	[145]
	2020	PTFE	MoS <sub>2</sub>	PSSH	$D = 1.4$ mm	1 V	0.1 V	81 nA	$g_t = -0.16$ $\mu$ A/mm $SS_t = 89$ $\mu$ m/dec	Artificial synapses	[78]
		FEP	MoS <sub>2</sub> /HfO <sub>2</sub> /Au	SiO <sub>2</sub>	$D = 0.7$ mm	90 V	0.1 V	0.76 $\mu$ A		Artificial synapses	[79]
		PTFE	Graphene	Ion-gel	$D = 0.3$ mm	7 V	0.1 V	54 $\mu$ A	$g_t = 216$ $\mu$ A/mm $SS_t = 0.67$ mm/dec	Modulating barriers	[118]
		2021	PTFE	MoS <sub>2</sub> /h-BN/Graphene	SiO <sub>2</sub>	$D = 0.2$ mm	50 V	50 mV	1 $\mu$ A	$g_t = 1$ $\mu$ A/mm	Binary logic
		PETF	Graphene	Ion-gel	$D = 120$ $\mu$ m	0.8 V	0.1 V	135.5 nA	$SS_t = 40$ $\mu$ m/dec	Artificial synapses	[77]
		PTFE	MoS <sub>2</sub> /Graphene	SiO <sub>2</sub>	$D = 1$ mm	-40 V	1 V	35 $\mu$ A	$g_t = 80$ $\mu$ A/mm	Artificial synapses	[82]
		PTFE	MoS <sub>2</sub> /Al <sub>2</sub> O <sub>3</sub> /Graphene	SiO <sub>2</sub>	$D = 0.65$ mm	90 V	1 V	1 $\mu$ A		Information storage	[84]
	2022	Silicon rubber	InSe/h-BN/Graphene	SiO <sub>2</sub>	$D = 0.7$ mm	70 V	0.5 V	54 $\mu$ A	$g_t = 3.17$ $\mu$ A/mm	Information storage	[80]
		Kapton	WSe <sub>2</sub> /h-BN/Graphene	SiO <sub>2</sub>	$D = 30$ $\mu$ m	66 V		1 nA	$g_t = -37.4$ nA/mm	Artificial synapses	[81]
	2023	PTFE	MoTe <sub>2</sub>	h-BN	$D = 120$ $\mu$ m	3.75 V	1 V	13 $\mu$ A ( p type ) 92 nA ( n type )		Binary logic	[87]
		PTFE	MoTe <sub>2</sub>	SiO <sub>2</sub>	$D = 12$ mm	40 V	0.1 V	0.2 nA(p type) 100 nA ( n type )	$g_t = -0.386$ nA/mm ( p type ) $g_t = 9.84$ nA/mm ( n type )	Binary logic	[88]
	2024	PTFE	Graphene/MoS <sub>2</sub>	SiO <sub>2</sub>	$D = 8$ mm	60 V	0.5 V	999 A/cm <sup>2</sup>	$g_t = 1.485$ $\mu$ A/mm $SS_t = 12.666$ mm/dec	Modulating barriers	[119]
PTFE		MoTe <sub>2</sub>	Al <sub>2</sub> O <sub>3</sub> /HfO <sub>2</sub> /Al <sub>2</sub> O <sub>3</sub>	$D = 0.24$ mm	19.6 V	30 mV	1 $\mu$ A	$g_t = 2.5$ $\mu$ A/mm	Information storage	[85]	

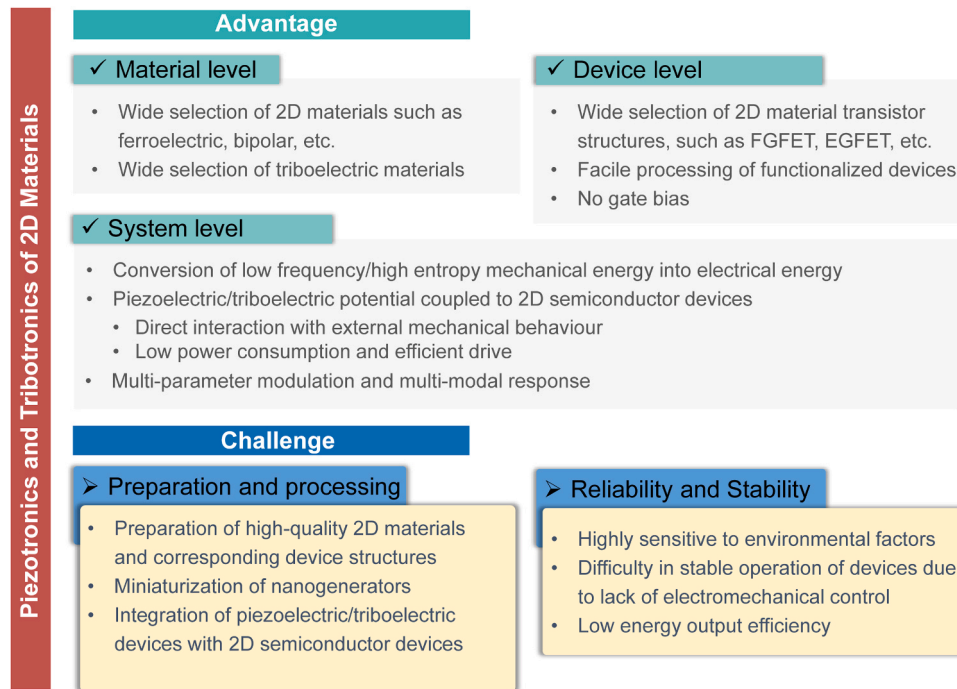


Fig. 20. Advantages and challenges of piezotronics and tribotronics of 2D materials.

temperature, pressure, and chemical environment. However, defects such as vacancies, doping, and grain boundaries inevitably arise during synthesis, significantly impacting the material's electrical conductivity, optical absorption, and mechanical properties. Furthermore, the processing of 2D devices presents its own set of challenges. These include ensuring compatibility with micro-nano processing techniques, preventing damage to the material during transfer, and maintaining interfacial quality through meticulous interface engineering. A common theme among these challenges is the need for precision and minimal damage in processing methods. Additionally, a deep understanding on the unique properties of 2D materials is essential. Each step from material synthesis to device integration must be carefully designed and precisely controlled to ensure that the final device's performance and reliability meet the high standards required for practical applications. Secondly, to enhance integration with 2D FETs, there is a necessity for the miniaturization of NGs. This is crucial to maintain the mechanical-electrical conversion efficiency while still effectively driving 2D FETs. Given their thin-layer structure and surface effect, 2D FETs are highly sensitive to input signals. This necessitates that the NGs must provide sufficient energy to ensure reliable turn-on and turn-off of the transistors. However, the energy generated by miniaturized NGs may not be adequate to directly drive 2D FETs. Therefore, strategies for energy storage and management, such as integrated supercapacitors, must be considered. Additionally, high-efficiency energy harvesting circuits should be employed to accumulate and enhance the output, although this often results in reduced efficiency. Finally, integrating piezoelectric or triboelectric materials with 2D semiconductor devices presents a significant challenge due to the interface between two materials with vastly different scales or properties. Piezoelectric or triboelectric materials typically generate energy at the macroscopic scale, whereas 2D FETs operate at the atomic or molecular level. This requires efficient energy transfer and signaling connectivity between the two materials.

Finally, the reliability and stability of these devices present significant challenges. Firstly, systems incorporating NGs are highly sensitive to environmental conditions during their operation. Minor vibrations and human electrostatic fields can significantly impact the output performance of the TENG, leading to signal fluctuations. The resultant instability and decreased long-term reliability due to these

environmental variables pose a substantial challenge for application scenarios that require stable modulation of 2D FETs in varying environments. Secondly, most current NGs rely on the precise control by electric motors, resulting in the electrical signals that are often unstable and highly volatile. This instability is particularly problematic when attempting to modulate 2D FETs, as it leads to unpredictable responses from the 2D FET, affecting both the accuracy of the device and its reliability in practical applications. Thirdly, PENGs face particular challenges in terms of energy output efficiency. Smaller output signals are insufficient to drive standard 2D FETs. To overcome this challenge, innovative structures and materials are required to enable low-voltage driving. One potential solution is EGFET, which can enhance energy output efficiency and improve the signal transmission by reducing the operating voltage. However, EGFETs have notable shortcomings in terms of long-term operational stability.

In conclusion, the study of piezotronics and tribotronics of 2D materials incorporates multiple disciplines such as materials science, physics and engineering, providing new opportunities to go beyond the Moore's Law. The efficient conversion of mechanical energy into electrical energy, along with the direct interaction between mechanical behaviors and various electronic properties, reveals substantial potential in applications such as information devices, sensors, and self-powered systems. 2D materials can also significantly enhance the sensitivity and responsiveness of sensors to minute physical changes, thereby offering substantial benefits for low-power consuming devices and smart sensing networks. Further research will concentrate on overcoming existing challenges such as improving device reliability, optimizing stability control systems, and enhancing their compatibility with current silicon-based technologies. Through interdisciplinary research and innovative engineering, these technologies are anticipated to provide a new platform for future energy conversion and smart materials, heralding a new era in wireless sensing and autonomous energy systems.

#### CRediT authorship contribution statement

**Sun Qijun:** Writing – review & editing, Writing – original draft, Validation, Supervision, Funding acquisition, Conceptualization. **Wang**

**Zhong Lin:** Writing – review & editing, Validation, Supervision, Conceptualization. **Wang Yifei:** Writing – original draft, Methodology, Investigation, Formal analysis.

### Declaration of Competing Interest

The authors declare that they have no known competing financial interests or personal relationships that could have appeared to influence the work reported in this paper

### Acknowledgements

This work is supported by the National Natural Science Foundation of China (52073031), the National Key Research and Development Program of China (2023YFB3208102, 2021YFB3200304), Beijing Nova Program (Z191100001119047), and the “Hundred Talents Program” of the Chinese Academy of Sciences.

### Data Availability

Data will be made available on request.

### References

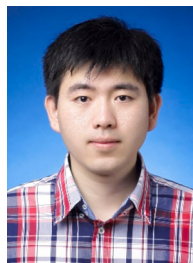
- [1] M.M. Waldrop, *Nature* 530 (2016) 144–147.
- [2] J.S. Clarke, *Nat. Electron.* 6 (2023) 332.
- [3] M. Lundstrom, *Science* 299 (2003) 210–211.
- [4] D. Akinwande, C. Huyghebaert, C.H. Wang, M.I. Serna, S. Goossens, L.J. Li, H. P. Wong, F.H.L. Koppens, *Nature* 573 (2019) 507–518.
- [5] S. Das, A. Sebastian, E. Pop, C.J. McClellan, A.D. Franklin, T. Grasser, T. Knobloch, Y. Illarionov, A.V. Penumatcha, J. Appenzeller, Z. Chen, W. Zhu, I. Asselberghs, L.J. Li, U.E. Avci, N. Bhat, T.D. Anthopoulos, R. Singh, *Nat. Electron.* 4 (2021) 786–799.
- [6] W. Cao, H. Bu, M. Vinet, M. Cao, S. Takagi, S. Hwang, T. Ghani, K. Banerjee, *Nature* 620 (2023) 501–515.
- [7] J. Tang, Q. Wang, Z. Wei, C. Shen, X. Lu, S. Wang, Y. Zhao, J. Liu, N. Li, Y. Chu, J. Tian, F. Wu, W. Yang, C. He, R. Yang, D. Shi, K. Watanabe, T. Taniguchi, G. Zhang, *Adv. Electron. Mater.* 6 (2020) 2000550.
- [8] M.L. Chen, X. Sun, H. Liu, H. Wang, Q. Zhu, S. Wang, H. Du, B. Dong, J. Zhang, Y. Sun, S. Qiu, T. Alava, S. Liu, D.M. Sun, Z. Han, *Nat. Commun.* 11 (2020) 1205.
- [9] P. Lu, B. Colombeau, S. Hung, W. Li, X. Duan, Y. Li, E.M. Bazizi, S. Natarajan, J.C. S. Woo, *IEEE Trans. Electron Devices* 68 (2021) 1352–1357.
- [10] Y. Shen, Z. Dong, Y. Sun, H. Guo, F. Wu, X. Li, J. Tang, J. Liu, X. Wu, H. Tian, T. L. Ren, *Adv. Mater.* 34 (2022) 2201916.
- [11] B. Noia, K. Chakrabarty, E.J. Marinissen, *J. Electron. Test.* 28 (2011) 103–120.
- [12] M. Lapisa, M. Antelius, A. Tocchio, H. Sohlström, G. Stemme, F. Niklaus, *Sens. Actuators A: Phys.* 201 (2013) 154–163.
- [13] Y. Liu, C. Yao, F. Sun, H. Fang, *Microelectron. Reliab.* 125 (2021) 114343.
- [14] M.D.A. Kabir, D. Petranovic, Y. Peng, Coupling extraction and optimization for heterogeneous 2.5D chiplet-package co-design, *Proc. 39th Int. Conf. Comput.-Aided Des.* (2020) 1–8.
- [15] Y. Zheng, B. He, T. Li, *Appl. Sci.* 12 (2022) 6616.
- [16] Y. Huang, H. Zhang, X. Shao, X. Li, H. Ji, *Future Gener. Comput. Syst.* 140 (2023) 79–90.
- [17] L. Sun, Y. Zhang, G. Han, G. Hwang, J. Jiang, B. Joo, K. Watanabe, T. Taniguchi, Y. Kim, W.J. Yu, B. Kong, R. Zhao, H. Yang, *Nat. Commun.* 10 (2019) 3161.
- [18] D. Silver, A. Huang, C.J. Maddison, A. Guez, L. Sifre, G. van den Driessche, J. Schrittwieser, I. Antonoglou, V. Panneershelvam, M. Lanctot, S. Dieleman, D. Grewe, J. Nham, N. Kalchbrenner, I. Sutskever, T. Lillicrap, M. Leach, K. Kavukcuoglu, T. Graepel, D. Hassabis, *Nature* 529 (2016) 484–489.
- [19] M.F. Gonzalez-Zalba, S. de Franceschi, E. Charbon, T. Meunier, M. Vinet, A. S. Dzurak, *Nat. Electron.* 4 (2021) 872–884.
- [20] C.H. Yang, R.C.C. Leon, J.C.C. Hwang, A. Saraiva, T. Tantt, W. Huang, J. Camirand Lemyre, K.W. Chan, K.Y. Tan, F.E. Hudson, K.M. Itoh, A. Morello, M. Pioro-Ladriere, A. Laucht, A.S. Dzurak, *Nature* 580 (2020) 350–354.
- [21] J. Park, A. Kumar, Y. Zhou, S. Oh, J.-H. Kim, Y. Shi, S. Jain, G. Hota, E. Qiu, A. L. Nagle, I.K. Schuller, C.D. Schuman, G. Cauwenberghs, D. Kuzum, *Nat. Commun.* 15 (2024) 3492.
- [22] C.R. King, Jr., J. Zaveri, M.S. Bakir, J.D. Meindl, *Ieee, Electrical and Fluidic C4 Interconnections for Inter-layer Liquid Cooling of 3D ICs, 60th Electronic Components and Technology Conference, Las Vegas, NV, 2010*, pp. 1674–1681.
- [23] H. Wei, T.F. Wu, D. Sekar, B. Cronquist, R.F. Pease, S. Mitra, *Ieee, Cooling Three-Dimensional Integrated Circuits using Power Delivery Networks, IEEE International Electron Devices Meeting (IEDM), San Francisco, CA, 2012*.
- [24] S. Wang, Y. Yin, C. Hu, P. Rezai, *Micromachines* 9 (2018) 287.
- [25] A.C. Ferrari, *Solid State Commun.* 143 (2007) 47–57.
- [26] A.H. Castro Neto, F. Guinea, N.M.R. Peres, K.S. Novoselov, A.K. Geim, *Rev. Mod. Phys.* 81 (2009) 109–162.
- [27] S.Z. Butler, S.M. Hollen, L. Cao, Y. Cui, J.A. Gupta, H.R. Gutierrez, T.F. Heinz, S. S. Hong, J. Huang, A.F. Ismach, E. Johnston-Halperin, M. Kuno, V.V. Plashnitsa, R.D. Robinson, R.S. Ruoff, S. Salahuddin, J. Shan, L. Shi, M.G. Spencer, M. Terrones, W. Windl, J.E. Goldberger, *ACS Nano* 7 (2013) 2898–2926.
- [28] K.S. Novoselov, A. Mishchenko, A. Carvalho, A.H. Castro Neto, *Science* 353 (2016) 461.
- [29] X. Ling, W. Fang, Y.-H. Lee, P.T. Araujo, X. Zhang, J.F. Rodriguez-Nieva, Y. Lin, J. Zhang, J. Kong, M.S. Dresselhaus, *Nano Lett.* 14 (2014) 3033–3040.
- [30] J. Zhao, Q. Deng, A. Bachmatiuk, G. Sandeep, A. Popov, J. Eckert, M. H. Ruemmel, *Science* 343 (2014) 1228–1232.
- [31] J. Wang, H. Fang, X. Wang, X. Chen, W. Lu, W. Hu, *Small* 13 (2017) 1700933.
- [32] J. Yao, Z. Zheng, G. Yang, *Adv. Funct. Mater.* 27 (2017) 1701823.
- [33] Y. Zhao, K. Xu, F. Pan, C. Zhou, F. Zhou, Y. Chai, *Adv. Funct. Mater.* 27 (2017) 1603484.
- [34] D. Jariwala, T.J. Marks, M.C. Hersam, *Nat. Mater.* 16 (2017) 170–181.
- [35] D. Zhong, K.L. Seyler, X. Linpeng, R. Cheng, N. Sivadas, B. Huang, E. Schmidgall, T. Taniguchi, K. Watanabe, M.A. McGuire, W. Yao, D. Xiao, K.-M.C. Fu, X. Xu, *Sci. Adv.* 3 (2017) e1603113.
- [36] C. Gong, X. Zhang, *Science* 363 (2019) 706–717.
- [37] B. Radisavljevic, A. Radenovic, J. Brivio, V. Giacometti, A. Kis, *Nat. Nanotechnol.* 6 (2011) 147–150.
- [38] F. Wu, H. Tian, Y. Shen, Z. Hou, J. Ren, G. Gou, Y. Sun, Y. Yang, T. Ren, *Nature* 603 (2022) 259–264.
- [39] Q. Sun, W. Seung, B.J. Kim, S. Seo, S.-W. Kim, J.H. Cho, *Adv. Mater.* 27 (2015) 3411–3417.
- [40] Q. Zhang, T. Jiang, D. Ho, S. Qin, X. Yang, J.H. Cho, Q. Sun, Z.L. Wang, *ACS Nano* 12 (2018) 254–262.
- [41] J. Du, C. Ge, H. Riahi, E. Guo, M. He, C. Wang, G. Yang, K. Jin, *Adv. Electron. Mater.* 6 (2020) 1901408.
- [42] J. Jiang, J. Guo, X. Wan, Y. Yang, H. Xie, D. Niu, J. Yang, J. He, Y. Gao, Q. Wan, *Small* 13 (2017) 1700933.
- [43] D. Xie, W. Hu, J. Jiang, *Org. Electron.* 63 (2018) 120–128.
- [44] B. Yao, J. Li, X. Chen, M. Yu, Z. Zhang, Y. Li, T. Lu, J. Zhang, *Adv. Funct. Mater.* 31 (2021) 2100069.
- [45] K. Xu, S.K. Fullerton-Shirey, *J. Phys.: Mater.* 3 (2020) 032001.
- [46] H. Xiang, Y.C. Chien, L. Li, H. Zheng, S. Li, N.T. Duong, Y. Shi, K.W. Ang, *Adv. Funct. Mater.* 33 (2023) 2304657.
- [47] S. Zhang, Y. Liu, J. Zhou, M. Ma, A. Gao, B. Zheng, L. Li, X. Su, G. Han, J. Zhang, Y. Shi, X. Wang, Y. Hao, *Nanoscale Res. Lett.* 15 (2020) 157.
- [48] S. Wan, Y. Li, W. Li, X. Mao, C. Wang, C. Chen, J. Dong, A. Nie, J. Xiang, Z. Liu, W. Zhu, H. Zeng, *Adv. Funct. Mater.* 29 (2019) 1808606.
- [49] J. Wang, W. Hu, *Chin. Phys. B* 26 (2017) 037106.
- [50] X. Xu, L. Yang, Q. Gao, X. Jiang, D. Li, B. Cui, D. Liu, *J. Phys. Chem. C* 127 (2023) 7878–7886.
- [51] D. Xiang, Y. Cao, K. Wang, Z. Han, T. Liu, W. Chen, *Nanotechnology* 33 (2022) 175201.
- [52] L.D.V. Sangani, S. Mandal, S. Ghosh, K. Watanabe, T. Taniguchi, M.M. Deshmukh, *Nano Lett.* 22 (2022) 3612–3619.
- [53] L. Ren, Z. Li, Y. Lv, X. Li, D. Zhang, W. Li, L. Liu, L. Kong, X. Duan, X. Wang, A. Pan, L. Liao, Y. Liu, *Appl. Phys. Lett.* 120 (2022) 053107.
- [54] J. Wang, X. Zhao, G. Hu, J. Ren, X. Yuan, *Nanomaterials* 11 (2021) 3338.
- [55] H. Wang, H. Guo, R. Guzman, N. Jiazila, K. Wu, A. Wang, X. Liu, L. Liu, L. Wu, J. Chen, Q. Huan, W. Zhou, H. Yang, S.T. Pantelides, L. Bao, H.-J. Gao, *Adv. Mater.* (2024) 2311652.
- [56] H. Cho, D. Lee, K. Ko, D.-Y. Lin, H. Lee, S. Park, B. Park, B.C. Jang, D.-H. Lim, J. Suh, *ACS Nano* 17 (2023) 7384–7393.
- [57] H. Wu, Y. Cui, J. Xu, Z. Yan, Z. Xie, Y. Hu, S. Zhu, *Nano Lett.* 22 (2022) 2328–2333.
- [58] T. Sasaki, K. Ueno, T. Taniguchi, K. Watanabe, T. Nishimura, K. Nagashio, *ACS Nano* 15 (2021) 6658–6668.
- [59] G. Migliato Marega, Y. Zhao, A. Avsar, Z. Wang, M. Tripathi, A. Radenovic, A. Kis, *Nature* 587 (2020) 72–77.
- [60] Z.L. Wang, W. Wu, *Natl. Sci. Rev.* 1 (2014) 62–90.
- [61] W. Wu, Z.L. Wang, *Nat. Rev. Mater.* 1 (2016) 16031.
- [62] W. Hu, C. Zhang, Z.L. Wang, *Nanotechnology* 30 (2019) 042001.
- [63] J. Yu, X. Yang, Q. Sun, *Adv. Intell. Syst.* 2 (2020) 1900175.
- [64] Q. Zhang, S. Zuo, P. Chen, C. Pan, *Infomat* 3 (2021) 987–1007.
- [65] Z. Huo, J. Yu, Y. Li, Z.L. Wang, Q. Sun, *J. Phys. Energy* 5 (2023) 012002.
- [66] L. Wang, Z.L. Wang, *Nano Today* 37 (2021) 101108.
- [67] W. Wu, L. Wang, R. Yu, Y. Liu, S.-H. Wei, J. Hone, Z.L. Wang, *Adv. Mater.* 28 (2016) 8463–8468.
- [68] K. Zhang, M. Peng, W. Wu, J. Guo, G. Gao, Y. Liu, J. Kou, R. Wen, Y. Lei, A. Yu, Y. Zhang, J. Zhai, Z.L. Wang, *Mater. Horiz.* 4 (2017) 274–280.
- [69] C.R.P. Inbaraj, R.J. Mathew, G. Haider, T.P. Chen, R.K. Ulaganathan, R. Sankar, K.P. Bera, Y.M. Liao, M. Kataria, H.I. Lin, F.C. Chou, Y.T. Chen, C.H. Lee, Y. F. Chen, *Nanoscale* 10 (2018) 18642–18650.
- [70] Y. Pang, F. Xue, L. Wang, J. Chen, J. Luo, T. Jiang, C. Zhang, Z.L. Wang, *Adv. Sci.* 3 (2016) 1500419.
- [71] W. Ma, J. Lu, B. Wan, D. Peng, Q. Xu, G. Hu, Y. Peng, C. Pan, Z.L. Wang, *Adv. Mater.* 32 (2020) 1905795.
- [72] M. Dai, Z. Wang, F. Wang, Y. Qiu, J. Zhang, C.Y. Xu, T. Zhai, W. Cao, Y. Fu, D. Jia, Y. Zhou, P.A. Hu, *Nano Lett.* 19 (2019) 5410–5416.
- [73] H. Song, I. Karakurt, M. Wei, N. Liu, Y. Chu, J. Zhong, L. Lin, *Nano Energy* 49 (2018) 7–13.
- [74] U. Khan, T.H. Kim, H. Ryu, W. Seung, S.W. Kim, *Adv. Mater.* 29 (2017) 1603544.

- [75] Y. Meng, J. Zhao, X. Zhu, C. Zhao, S. Qin, J.H. Cho, C. Zhang, Q. Sun, Z.L. Wang, *ACS Nano* 12 (2018) 9381.
- [76] Y. Chen, G. Gao, J. Zhao, H. Zhang, J. Yu, X. Yang, Q. Zhang, W. Zhang, S. Xu, J. Sun, Y. Meng, Q. Sun, *Adv. Funct. Mater.* 29 (2019) 1900959.
- [77] J. Yu, G. Gao, J. Huang, X. Yang, J. Han, H. Zhang, Y. Chen, C. Zhao, Q. Sun, Z. L. Wang, *Nat. Commun.* 12 (2021) 1581.
- [78] X. Yang, J. Han, J. Yu, Y. Chen, H. Zhang, M. Ding, C. Jia, J. Sun, Q. Sun, Z. L. Wang, *Acs Nano* 14 (2020) 8668–8677.
- [79] X. Yang, J. Yu, J. Zhao, Y. Chen, G. Gao, Y. Wang, Q. Sun, Z.L. Wang, *Adv. Funct. Mater.* 30 (2020) 2002506.
- [80] C. Gao, Q. Nie, C.-Y. Lin, F. Huang, L. Wang, W. Xia, X. Wang, Z. Hu, M. Li, H.-W. Lu, Y.-C. Lai, Y.-F. Lin, J. Chu, W. Li, *Nano Energy* 91 (2022) 106659.
- [81] M. Jia, P. Guo, W. Wang, A. Yu, Y. Zhang, Z.L. Wang, J. Zhai, *Sci. Bull.* 67 (2022) 803–812.
- [82] J. Yu, X. Yang, G. Gao, Y. Xiong, Y. Wang, J. Han, Y. Chen, H. Zhang, Q. Sun, Z. L. Wang, *Sci. Adv.* 7 (2021) eabd9117.
- [83] M. Jia, J. Yu, Y. Liu, P. Guo, Y. Lei, W. Wang, A. Yu, Y. Zhu, Q. Sun, J. Zhai, Z. L. Wang, *Nano Energy* 83 (2021) 105785.
- [84] J. Zhao, Z. Wei, X. Yang, G. Zhang, Z. Wang, *Nano Energy* 82 (2021) 105692.
- [85] Y. Wei, J. Yu, Y. Li, Y. Wang, Z. Huo, L. Cheng, D. Yue, K. Zhang, J. Gong, J. Wang, Z.L. Wang, Q. Sun, *Nano Energy* 126 (2024) 109622.
- [86] G. Gao, B. Wan, X. Liu, Q. Sun, X. Yang, L. Wang, C. Pan, Z.L. Wang, *Adv. Mater.* 30 (2018) 1705088.
- [87] L. Cheng, J. Yu, Y. Wei, Z. Feng, Y. Li, Y. Wang, N. Xu, Z.L. Wang, Q. Sun, *Nano Energy* 114 (2023) 108632.
- [88] Y. Li, J. Yu, Y. Wei, Y. Wang, L. Cheng, Z. Feng, Y. Yang, Z.L. Wang, Q. Sun, *Nano Res.* 16 (2023) 11907–11913.
- [89] Z.L. Wang, *Adv. Mater.* 24 (2012) 4632–4646.
- [90] L. Zhu, Z.L. Wang, *Appl. Phys. Lett.* 122 (2023) 250501.
- [91] R. Ghosh, *Nano Energy* 113 (2023) 108606.
- [92] Z.L. Wang, *J. Phys. Chem. Lett.* 1 (2010) 1388–1393.
- [93] Y. Zhang, Y. Liu, Z.L. Wang, *Adv. Mater.* 23 (2011) 3004–3013.
- [94] C. Zhang, Z.L. Wang, *Nano Today* 11 (2016) 521–536.
- [95] J. Kou, Y. Liu, Y. Zhu, J. Zhai, *J. Phys. D: Appl. Phys.* 51 (2018) 493002.
- [96] P. Lin, C. Pan, Z.L. Wang, *Mater. Today Nano* 4 (2018) 17–31.
- [97] Z.L. Wang, *Mrs Bull.* 48 (2023) 1014–1025.
- [98] C. Zhang, J. Zhao, Z. Zhang, T. Bu, G. Liu, X. Fu, *Int. J. Extrem. Manuf.* 5 (2023) 042002.
- [99] Z.L. Wang, *J. Song, Science* 312 (2006) 242–246.
- [100] X. Lin, Z. Feng, Y. Xiong, W. Sun, W. Yao, Y. Wei, Z.L. Wang, Q. Sun, *Int. J. Extrem. Manuf.* 6 (2024) 032011.
- [101] C. Zhang, W. Tang, L. Zhang, C. Han, Z.L. Wang, *ACS Nano* 8 (2014) 8702–8709.
- [102] W. Wu, L. Wang, Y. Li, F. Zhang, L. Lin, S. Niu, D. Chenet, X. Zhang, Y. Hao, T. F. Heinz, J. Hone, Z.L. Wang, *Nature* 514 (2014) 470–474.
- [103] G.D.C. Rodrigues, P. Zelenovskiy, K. Romanuk, S. Luchkin, Y. Kopelevich, A. Kholkin, *Nat. Commun.* 6 (2015) 7572.
- [104] L. Wang, S. Liu, Z. Zhang, X. Feng, L. Zhu, H. Guo, W. Ding, L. Chen, Y. Qin, Z. L. Wang, *Nano Energy* 60 (2019) 724–733.
- [105] X. Liu, X. Yang, G. Gao, Z. Yang, H. Liu, Q. Li, Z. Lou, G. Shen, L. Liao, C. Pan, Z. Lin Wang, *ACS Nano* 10 (2016) 7451–7457.
- [106] S. Liu, Q. Liao, Z. Zhang, X. Zhang, S. Lu, L. Zhou, M. Hong, Z. Kang, Y. Zhang, *Nano Res.* 10 (2017) 3476–3485.
- [107] J. Du, Q. Liao, M. Hong, B. Liu, X. Zhang, H. Yu, J. Xiao, L. Gao, F. Gao, Z. Kang, Z. Zhang, Y. Zhang, *Nano Energy* 58 (2019) 85–93.
- [108] L. Chen, F. Xue, X. Li, X. Huang, L. Wang, J. Kou, Z.L. Wang, *Acs Nano* 10 (2016) 1546–1551.
- [109] Y. Wang, L. Zhu, C. Du, *Adv. Mater. Interfaces* 7 (2020) 1901932.
- [110] P. Puneetha, S.P.R. Mallem, K.S. Im, S.J. An, D.Y. Lee, H. Park, K.I. Park, J. Shim, *Nano Energy* 103 (2022) 107863.
- [111] M. Dai, H. Chen, F. Wang, Y. Hu, S. Wei, J. Zhang, Z. Wang, T. Zhai, P. Hu, *Acs Nano* 13 (2019) 7291–7299.
- [112] J. Guo, R. Wen, Y. Liu, K. Zhang, J. Kou, J. Zhai, Z.L. Wang, *Acs Appl. Mater. Interfaces* 10 (2018) 8110–8116.
- [113] A. Sohn, S. Choi, S.A. Han, T.-H. Kim, J.H. Kim, Y. Kim, S.W. Kim, *Nano Energy* 58 (2019) 811–816.
- [114] C. Jiang, L. Zeng, D. Tan, P. Yan, N. Sun, Q. Guo, Z. Zhang, Z. Tao, C. Fang, R. Ji, H. Sun, R. Xu, *Nano Energy* 114 (2023) 108670.
- [115] F. Wang, J. Jiang, Q. Liu, Y. Zhang, J. Wang, S. Wang, L. Han, H. Liu, Y. Sang, *Nano Energy* 70 (2020) 104457.
- [116] S. Kim, Y.J. Choi, H.J. Woo, Q. Sun, S. Lee, M.S. Kang, Y.J. Song, Z.L. Wang, J. H. Cho, *Nano Energy* 50 (2018) 598–605.
- [117] J. Zhao, Z. Wei, Q. Zhang, H. Yu, S. Wang, X. Yang, G. Gao, S. Qin, G. Zhang, Q. Sun, Z.L. Wang, *Acs Nano* 13 (2019) 582–590.
- [118] H. Zhang, J. Yu, X. Yang, G. Gao, S. Qin, J. Sun, M. Ding, C. Jia, Q. Sun, Wang, *ACS Nano* 14 (2020) 3461.
- [119] Y. Wang, X. Lin, G. Gao, J. Yu, Y. Wei, J. Gong, J. Sun, Z.L. Wang, Q. Sun, *Adv. Funct. Mater.* (2024) 2313210.
- [120] X. Yang, J. Han, J. Yu, Y. Chen, H. Zhang, M. Ding, C. Jia, J. Sun, Q. Sun, Z. L. Wang, *Acs Nano* 14 (2020) 8668–8677.
- [121] G. Cheon, K.N. Duerloo, A.D. Sendek, C. Porter, Y. Chen, E.J. Reed, *Nano Lett.* 17 (2017) 1915–1923.
- [122] M.N. Blonsky, H.L. Zhuang, A.K. Singh, R.G. Hennig, *ACS Nano* 9 (2015) 9885–9891.
- [123] H. Zhu, Y. Wang, J. Xiao, M. Liu, S. Xiong, Z.J. Wong, Z. Ye, Y. Ye, X. Yin, X. Zhang, *Nat. Nanotechnol.* 10 (2015) 151–155.
- [124] C. Lee, X. Wei, J.W. Kysar, J. Hone, *Science* 321 (2008) 385–388.
- [125] J. Zhang, S.A. Meguid, *Semicond. Sci. Technol.* 32 (2017) 043006.
- [126] P.F. Ferrari, S. Kim, A.M. van der Zande, *Appl. Phys. Rev.* 10 (2023) 031302.
- [127] P. Zhang, Y. Jia, M. Xie, Z. Liu, S. Shen, J. Wei, R. Yang, *Acs Nano* 16 (2022) 2261–2270.
- [128] Z. Wang, P.X.L. Feng, *Appl. Phys. Lett.* 104 (2014) 103109.
- [129] L. Wang, S. Liu, G. Gao, Y. Pang, X. Yin, X. Feng, L. Zhu, Y. Bai, L. Chen, T. Xiao, X. Wang, Y. Qin, Z.L. Wang, *ACS Nano* 12 (2018) 4903–4908.
- [130] P. Puneetha, S.P.R. Mallem, P. Bathalavaram, J.-H. Lee, J. Shim, *Nano Energy* 84 (2021) 105923.
- [131] P. Puneetha, S.P.R. Mallem, Y.-W. Lee, J. Shim, *ACS Appl. Mater.* 12 (2020) 36660–36669.
- [132] J.M. Wu, K.-H. Chen, Y. Zhang, Z.L. Wang, *Rsc Adv.* 3 (2013) 25184–25189.
- [133] D.J. Bayerl, X. Wang, *Adv. Funct. Mater.* 22 (2012) 652–660.
- [134] W. Guo, Y. Yang, J. Liu, Y. Zhang, *Phys. Chem. Chem. Phys.* 12 (2010) 14868–14872.
- [135] Y. Yang, J.J. Qi, Y.S. Gu, X.Q. Wang, Y. Zhang, *Phys. Status Solidi-Rapid Res. Lett.* 3 (2009) 269–271.
- [136] L. Wang, S. Liu, X. Feng, C. Zhang, L. Zhu, J. Zhai, Y. Qin, Z.L. Wang, *Nat. Nanotechnol.* 15 (2020) 661–667.
- [137] M. Chi, Y. Zhao, X. Zhang, M. Jia, A. Yu, Z.L. Wang, J. Zhai, *Adv. Funct. Mater.* (2023) 2307901.
- [138] Z.L. Wang, R. Yang, J. Zhou, Y. Qin, C. Xu, Y. Hu, S. Xu, *Mater. Sci. Eng. R.-Rep.* 70 (2010) 320–329.
- [139] Z.L. Wang, *Nano Today* 5 (2010) 540–552.
- [140] P. Lin, L. Zhu, D. Li, Z.L. Wang, *J. Mater. Chem. C* 7 (2019) 14731–14738.
- [141] Q. Sun, D.H. Ho, Y. Choi, C. Pan, D.H. Kim, Z.L. Wang, J.H. Cho, *ACS Nano* 10 (2016) 11037–11043.
- [142] F. Fan, Z. Tian, Z. Lin Wang, *Nano Energy* 1 (2012) 328–334.
- [143] W. Ding, A.C. Wang, C. Wu, H. Guo, Z.L. Wang, *Adv. Mater. Technol.* 4 (2019) 1800487.
- [144] C. Zhang, T. Bu, J. Zhao, G. Liu, H. Yang, Z.L. Wang, *Adv. Funct. Mater.* 29 (2019) 1808114.
- [145] G. Gao, J. Yu, X. Yang, Y. Pang, J. Zhao, C. Pan, Q. Sun, Z.L. Wang, *Adv. Mater.* 31 (2019) 1806905.
- [146] T. Bu, L. Xu, Z. Yang, X. Yang, G. Liu, Y. Cao, C. Zhang, Z.L. Wang, *Nat. Commun.* 11 (2020) 1054.
- [147] Y. Liu, G. Liu, T. Bu, C. Zhang, *Mater. Today Energy* 20 (2021) 100686.
- [148] S. Kim, T.Y. Kim, K.H. Lee, T.-H. Kim, F.A. Cimini, S.K. Kim, R. Hinchet, S.-W. Kim, C. Falconi, *Nat. Commun.* 8 (2017) 15891.
- [149] Z. Huo, Y. Peng, Y. Zhang, G. Gao, B. Wan, W. Wu, Z. Yang, X. Wang, C. Pan, *Adv. Mater. Interfaces* 5 (2018) 1801061.
- [150] Z.W. Yang, Y. Pang, L. Zhang, C. Lu, J. Chen, T. Zhou, C. Zhang, Z.L. Wang, *Acs Nano* 10 (2016) 10912–10920.
- [151] G. Zhu, Y.S. Zhou, P. Bai, X.S. Meng, Q. Jing, J. Chen, Z.L. Wang, *Adv. Mater.* 26 (2014) 3788–3796.
- [152] Y. Yang, Z.H. Lin, T. Hou, F. Zhang, Z.L. Wang, *Nano Res.* 5 (2012) 888–895.
- [153] J. Qian, X. Jing, *Nano Energy* 52 (2018) 78–87.
- [154] H. Zhang, J. Wang, Y. Xie, G. Yao, Z. Yan, L. Huang, S. Chen, T. Pan, L. Wang, Y. Su, W. Yang, Y. Lin, *Acs Appl. Mater. Interfaces* 8 (2016) 32649–32654.
- [155] F. Xue, L. Chen, L. Wang, Y. Pang, J. Chen, C. Zhang, Z.L. Wang, *Adv. Funct. Mater.* 26 (2016) 2104–2109.
- [156] M. Li, F.S. Yang, Y.C. Hsiao, C.Y. Lin, H.M. Wu, S.H. Yang, H.R. Li, C.H. Lien, C. H. Ho, H.J. Liu, W. Li, Y.F. Lin, Y.C. Lai, *Adv. Funct. Mater.* 29 (2019) 1809119.
- [157] P. Singh, S. Baek, H.H. Yoo, J. Niu, J.-H. Park, S. Lee, *Acs Nano* 16 (2022) 5418–5426.
- [158] H. Jeong, L. Shi, *J. Phys. D: Appl. Phys.* 52 (2019) 023003.
- [159] Y. Wang, Q. Sun, J. Yu, N. Xu, Y. Wei, J.H. Cho, Z.L. Wang, *Adv. Funct. Mater.* 33 (2023) 2305791.
- [160] J. Pu, K. Funahashi, C. Chen, M. Li, L. Li, T. Takenobu, *Adv. Mater.* 28 (2016) 4111–4119.
- [161] A.J. Cho, K.C. Park, J.Y. Kwon, *Nanoscale Res Lett.* 10 (2015) 115.
- [162] K.O. Johnson, *Curr. Opin. Neurobiol.* 11 (2001) 455–461.
- [163] A. Handler, D.D. Gin, *Nat. Rev. Neurosci.* 22 (2021) 521–537.
- [164] S. Chun, J.S. Kim, Y. Yoo, Y. Choi, S.J. Jung, D. Jang, G. Lee, K.I. Song, K.S. Nam, I. Youn, D. Son, C. Pang, Y. Jeong, H. Jung, Y.J. Kim, B.-D. Choi, J. Kim, S.P. Kim, W. Park, S. Park, *Nat. Electron.* 4 (2021) 429–438.
- [165] C. Wan, G. Chen, Y. Fu, M. Wang, N. Matsuhisa, S. Pan, L. Pan, H. Yang, Q. Wan, L. Zhu, X. Chen, *Adv. Mater.* 30 (2018) 1801291.
- [166] J. Yu, Y. Wang, S. Qin, G. Gao, C. Xu, Z. Lin Wang, Q. Sun, *Mater. Today* 60 (2022) 158–182.
- [167] S.H. Kim, G.W. Baek, J. Yoon, S. Seo, J. Park, D. Hahm, J.H. Chang, D. Seong, H. Seo, S. Oh, K. Kim, H. Jung, Y. Oh, H.W. Baac, B. Alimkhanuly, W.K. Bae, S. Lee, M. Lee, J. Kwak, J.-H. Park, D. Son, *Adv. Mater.* 33 (2021) 2104690.
- [168] Y. Kim, A. Chortos, W. Xu, Y. Liu, J.Y. Oh, D. Son, J. Kang, A.M. Foudeh, C. Zhu, Y. Lee, S. Niu, J. Liu, R. Pfattner, Z. Bao, T.W. Lee, *Science* 360 (2018) 998–1003.
- [169] H.Q. Huynh, T.Q. Trung, A. Bag, T.D. Do, M.J. Sultan, M. Kim, N.E. Lee, *Adv. Funct. Mater.* 33 (2023) 2303535.
- [170] J. Polena, D. Afzal, J.H.L. Ngai, Y. Li, *Chemosensors* 10 (2021) 12.
- [171] L. Shan, Y. Liu, X. Zhang, E. Li, R. Yu, Q. Lian, X. Chen, H. Chen, T. Guo, *Nano Energy* 88 (2021) 106283.
- [172] L. Li, J. Li, D. Jiang, W. Fu, W. Zhu, J. Zhang, *IEEE Electron Device Lett.* 42 (2021) 1002–1005.
- [173] L. Chen, C. Wen, S.-L. Zhang, Z.L. Wang, Z.-B. Zhang, *Nano Energy* 82 (2021) 105680.

- [174] Y. Liu, E. Li, X. Wang, Q. Chen, Y. Zhou, Y. Hu, G. Chen, H. Chen, T. Guo, *Nano Energy* 78 (2020) 105403.
- [175] X. Wu, E. Li, Y. Liu, W. Lin, R. Yu, G. Chen, Y. Hu, H. Chen, T. Guo, *Nano Energy* 85 (2021) 106000.
- [176] F. Tan, Y. Xiong, J. Yu, Y. Wang, Y. Li, Y. Wei, J. Sun, X. Xie, Q. Sun, Z.L. Wang, *Nano Energy* 90 (2021) 106617.



**Dr. Yifei Wang** received his Ph.D. degree in 2024 from Beijing Institute of Nanoenergy and Nanosystems (CAS), University of Chinese Academy of Sciences. He is currently a postdoctoral fellow with the Department of Applied Physics, The Hong Kong Polytechnic University. His research interests are focused on self-powered sensors and triboelectricity activated neuromorphic devices.



**Prof. Qijun Sun** has joined Beijing Institute of Nanoenergy and Nanosystems (CAS) since 2016, as the principal investigator of Functional Soft Electronics Lab. The main research interests of his group include triboiontronic devices, mechanoplastic neuromorphic transistors, artificial synaptic devices electronic skin, 2D materials based flexible semiconductor devices, human-machine interactive systems and micro-nano fabrication, aiming to develop advanced systems for human health monitoring and human-robotic interface.



**Prof. Zhong Lin Wang** received his Ph. D from Arizona State University in physics. He now is the Hightower Chair in Materials Science and Engineering, Regents' Professor, Engineering Distinguished Professor and Director, Center for Nanostructure Characterization, at Georgia Tech. Dr. Wang has made original and innovative contributions to the synthesis, discovery, characterization and understanding of fundamental physical properties of oxide nanobelts and nanowires, as well as applications of nanowires in energy sciences, electronics, optoelectronics and biological science. He pioneered the field of piezotronics and piezo-phototronics by introducing piezoelectric potential gated charge transport process in fabricating new electronic and optoelectronic devices.